Functional Characterization of Cancer- and RASopathies-associated SHP2 and BRAF Mutations

Dissertation

zur Erlangung des akademischen Grades
doctor rerum naturalium
(Dr. rer. nat.)
im Fach Biologie/ Molekularbiologie

eingereicht an der
Lebenswissenschaftlichen Fakultät
der Humboldt–Universität zu Berlin

von

M. Sc. Paula Andrea Medina-Pérez

Präsident der Humboldt–Universität zu Berlin
Prof. Dr. Jan–Hendrik Olbertz

Dekan der Lebenswissenschaftlichen Fakultät
Prof. Dr. Richard Lucius

Gutachter:
1. Prof. Dr. Reinhold Schäfer
2. Prof. Dr. Hanspeter Herzel
3. Prof. Dr. Holger Sültmann

Tag der mündlichen Prüfung: 12.03.2015

Abstract

Deregulation of the Ras/MAPK signaling is implicated in a wide variety of human diseases, including developmental disorders and cancer. In the last years, a group of developmental disorders, characterized by an overlapping phenotype in patients, was clustered under the term RASopathies. These disorders result from germline mutations in genes encoding key components of the Ras/MAPK signaling cascade. Although the incidence of solid tumors in patients suffering from these disorders is rather low, reports on different forms of leukemia have considerably increased.

In this work, a group of mutations in the genes SHP2/*PTPN11* and BRAF, both key regulators of the MAPK signaling pathway and implicated in RASopathies and cancer, were selected for expression in well-established cell systems for a comprehensive molecular and phenotypic characterization using high-throughput approaches and functional assays. Synthetic cDNA sequences carrying the SHP2 mutations T42A, E76D, I282V (Noonan syndrome-associated), E76G, E76K, E139D (Noonan- and leukemia-associated), T468M (LEOPARD syndrome -associated) and the BRAF mutations Q257R, S467A, L485F and K499E (cardio-facio-cutaneous syndrome-associated) were shuttled into the modified lentiviral vector pCDH-EF1-IRES-GFP. The non-tumorigenic human cell lines MCF10A, BJ-ELB and HA1EB and the rat preneoplastic 208F fibroblasts were transduced with recombinant lentiviral particles carrying either SHP2 or BRAF mutations to identify their potential roles in neoplastic transformation. MCF10A and BJ-ELB cells overexpressing SHP2 mutations displayed a growth arrest morphology, while BRAF mutations induced cell proliferation and a transformation phenotype. In contrast, both SHP2 and BRAF mutations promoted a spindle-like cell morphology, cell proliferation, density- and anchorage-independent growth in 208F rat fibroblasts. These results suggested that RASopathies-associated mutations in SHP2 and BRAF confer a transformation phenotype *in vitro* similar to the classical H-Ras and BRAF oncogenes. To further investigate whether mutations in SHP2 contribute to tumor growth *in vivo*, 208F cells expressing either SHP2 wild-type, E76G or T468M mutations were subcutaneously injected in nude mice. Interestingly, cells harboring mutations on SHP2, as well as overexpressing wild-type SHP2, promoted tumor growth.

Reverse-phase protein array (RPPA) and immunoblot assays revealed that RASopathies-associated mutant SHP2 and BRAF proteins constitutively activate the Ras/MAPK signaling pathway in a moderate manner compared to the oncogenic BRAF V600E. Furthermore, to identify modifications in the protein interaction mechanisms of SHP2 mutant proteins, tandem affinity purification (TAP) and yeast-two-hybrid assays were performed using the isogenic dox-inducible HEK-TREx cell system. E76G and T42A SHP2 mutant proteins showed an increased binding strength to GAB1 compared to the wild-type protein. Finally, to investigate the impact of these mutations on gene transcription, a microarray analysis of mRNA from HEK-TREx cells expressing mutant transgenes was conducted. A gene cluster was found to be commonly regulated in both RASopathies-associated BRAF and the oncogenic V600E mutation. This is the first report on transcriptome analysis of RASopathies-associated mutations.

The findings of this study might be useful for a better understanding of the downstream mechanisms of RASopathies-related signaling pathways and their involvement in cancer progression. Moreover, new candidate therapeutic targets for the effective treatment of patients suffering from Ras/MAPK pathway-associated developmental disorders could be evaluated in the future.

Acknowledgments

This work could not be possible without the encouragement and collaboration of many people. I am especially grateful to my supervisor Prof. Reinhold Schäfer for his guidance and valuable advices. I also want to thank Prof. Christine Sers, for the constructive discussions on science and the struggles of the scientific career.

I want to thank the collaborators of the MUTANOM Consortium, specially to Prof. Holger Sültmann and Dr. Julia Starmann from the German Cancer Research Center (DKFZ) for the RPPA analysis, Dr. Gerard Joberty from Cellzome, Dr. Artur Muryadan and PD. Dr. Bodo Lange from the Max Planck Institute for Molecular Genetics for the TAP purification and mass spectrometry and Dr. Sean-Patrick Riechers from the Max-Delbrück Center (MDC) for the yeast-two-hybrid assay. Thanks to Maria Stecklum and Dr. Jens Hoffmann from the Experimental Pharmacology and Oncology (EPO) GmbH, who provided the *in vivo* experiments in nude mice.

I am thankful to Bertram Klinger and Dr. Karsten Jürchott for the valuable discussions and clear explanations on bioinformatics and the microarray analysis.

I also would like to thank Sabine Bobbe, Conny Gieseler and Kerstin Möhr for their technical help in minipreps, platting cells and southern blot preparations. A special thank to Jana Keil, who had always time for explaining new methods and answering all type of technical and do-you-know-where-is-it questions.

I am very greatul to all members of Molecular Tumor Pathology Lab, for their helpful comments and suggestions on my results. Thanks to Stephanie Seibt, Shila Mang-Fatehi, Sha Liu, Natalia Kuhn, Christina Kuznia, Dirk Schumacher, Felix Bormann and other members of the lab for the nice working atmosphere and support. Thanks to Dr. Torben Redmer for the german style corrections.

A big thank to my family and friends, particularly my mother, who despite the physical distance was always present and motivate me not to give up, and my sister, who cheered me up in the difficult moments.

Finally, my deeply gratitude goes to my Husband Manuel Góngora, for his constant support, love, motivation and infinite patience during this time. Also to our Son Miguel Angel, who confront me with my ability to explain him cancer biology in the most simple way.

Contents

List of Figures

List of Tables

1 INTRODUCTION

1.1 The Ras/MAPK signaling pathway

The Ras/mitogen-activated protein kinases (MAPK) pathway is among the most wide-ranging regulatory mechanisms of signal transduction in the eukaryotic organisms. The MAPK pathway has been associated with diverse biological processes varying from development, cell growth, proliferation, differentiation, migration and apoptosis. Therefore, it is not surprising that deregulation of the MAPK pathway plays also a central role in many cancer types, not only because its extensive capability to crosstalk with other signaling pathways, but also because many of its core components are encoded by oncogenes frequently found mutated, including the small GTPase Ras and RAF proteins and the receptor tyrosine kinase epidermal growth factor receptor (EGFR).
This signaling cascade becomes activated when extracellular growth factors or cytokines bind to the corresponding receptors, commonly receptor tyrosine kinases (RTK). (fig. 1.1). After ligand binding, activation of the receptor leads to the recruitment of adaptor proteins to the cytosolic membrane, which in turn, transduce the extracellular signal stimulus to intracellular components (Lemmon and Schlessinger, 2010).

1.1.1 Post-translational regulation of the MAPK signaling pathway by protein tyrosine phosphatases

There are a variety of molecular mechanisms that regulate the activation of core components of the MAPK pathway. Ras proteins, for example, undergo palmitoylation and farnesylation to enable membrane association under normal physiological conditions (for review, see Roberts and Der, 2007). Also SUMOylation of MEK1 and MEK2 proteins has been reported to act as a negative modulation mechanism to downregulate the MAPK pathway (Kubota et al., 2011). Nevertheless, phosphorylation of protein kinases is the most well elucidated post-translational modification (PTM) that acts as a positive regulator of this signaling cascade. Equivalently, dephosphorylation by protein phosphatases has gained strength as a key regulation event that influences not only protein activation, but also localization and stability.
Protein phosphatases are derived from different ancestors and are classified in mainly two groups: protein serine/threonine phosphatases and protein tyrosine phosphatases (PTPs). To date, 107 members of the human PTP superfamily have been identified to share the common cysteine-dependent signature motif HC(X)5R to remove a phosphate group from the substrate (Tonks, 2006). According to its structural homology and

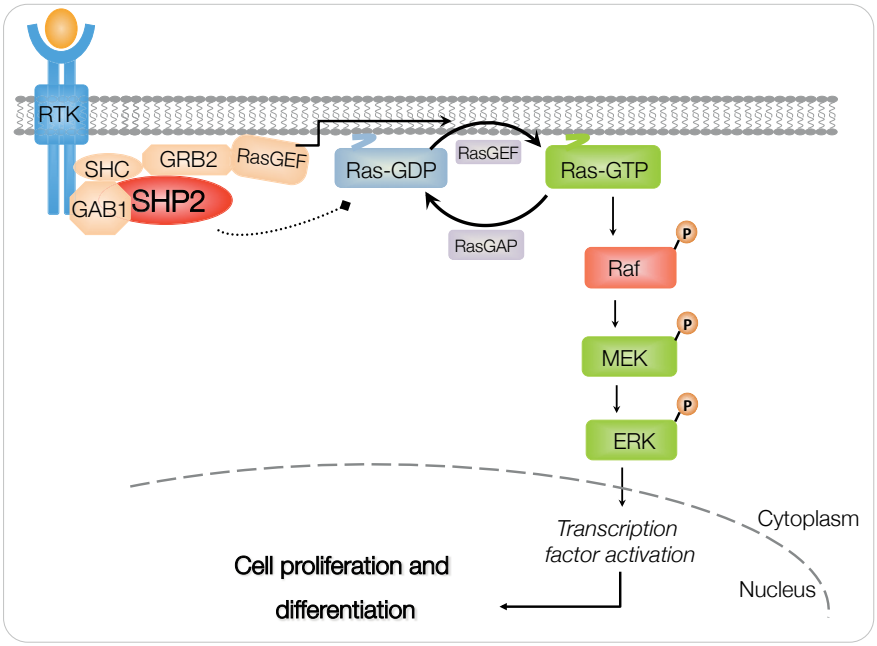

Figure 1.1: The Ras/MAPK signaling pathway. Extracellular growth factors or cytokines binds to receptor tyrosine kinases (RTKs), leading to its dimerization and cross-phosphorylation of tyrosine residues. Phosphorylation of the RTK leads to the recruitment of adaptor proteins such growth-factor receptor bound protein 2 (GRB2), which binds to the guanine nucleotide exchange factor (RasGEF) Son Of Sevenless (SOS). SOS activates Ras by binding to Ras-GDP complexes and promotes the exchange of GDP (guanosine diphosphate) to GTP (guanosine triphosphate). Next, Activated Ras (Ras-GTP) binds the serine/threonine kinase RAF, which then activates a phosphorylation cascade of MEK and ERK proteins that are translocated to the nucleus and activate transcription factors. Modified from Lemmon and Schlessinger (2010); Ahearn et al. (2012).

substrate specificity, the PTP family is subdivided in four classes: phosphotyrosine-specific phosphatases, dual-specificity phosphatases, cdc25 phosphatases and low molecular PTPs.

1.1.2 The protein tyrosine phosphatase SHP2

Mammalian SHP2 (also known as SH-PTP2, SH-PTP3, PTP2C, PTP1D and Syp) is an ubiquitously expressed non-transmembrane protein-tyrosine phosphatase that belongs to the phosphotyrosine-specific phosphatases and is encoded by the gene *PTPN11* in the human chromosome 12q24. It shares homologues in *Drosophila* (Corkscrew) and *C. elegans* (Ptp2). SHP2 was identified by R. M. Freeman et al. (1992), shortly after corkscrew (csw) (Perkins et al., 1992).

1.1.2.1 SHP2 protein activation

SHP2 contains two tandemly arranged src-homology 2 region domains (SH2 domains), followed by a catalytic phosphatase domain (PTP domain), two tyrosine residues at the C-terminus and a proline-rich sequence. The crystal structure revealed an autoinhibitory mechanism of the catalytic site that regulates its basal state (Hof et al., 1998). SHP2 activity is suppressed by intramolecular interactions between residues in the backside loop of the N-terminal SH2 domain (N-SH2) and the catalytic surface of the PTP domain (fig. 1.2). Upon growth factor or cytokine stimulation, SHP2 is recruited, via its SH2 domains,

to phosphorylated tyrosine residues on RTKs, cytokine receptors, and/or scaffolding adaptors, such as insulin receptor substrate, fibroblast growth factor receptor substrate, or GRB2-associated binding (GAB) proteins. Phosphotyrosyl (pY) peptide binding to the N-SH2 domain disrupts the autoinhibitory interaction leading to an equilibrium shift and hence to an open conformation of the PTP domain and its catalytic activation (Ahmad et al., 1993; R. M. Freeman et al., 1992).

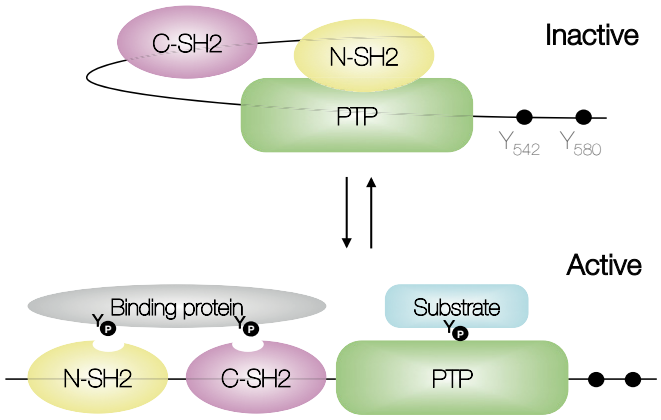

Figure 1.2: Activation of the protein tyrosine phosphatase SHP2. SHP2 is conformed by two src-homology 2 domains (N-SH2 and C-SH2), a protein tyrosine phosphatase domain (PTP) and two C-tail tyrosine residues (Y542 and Y580). SHP2 is kept in a closed conformation by the interaction of N-SH2 and the PTP domains that blocks the catalytic site. Upon binding of phosphotyrosine proteins (pY) to SH2 domains, the PTP domain is exposed, so substrates can bind the active site. Adapted from Grossmann et al. (2010); Qiu et al. (2014).

Bennett et al. (1994) identified SHP2 as a positive regulator of the platelet-derived growth factor receptor β (PDGFR) by binding GRB2 and the PDGF receptor directly. Additionally, SHP2 has been found to act as a modulator upstream of the Ras/MAPK signaling cascade by regulating Sprouty activity through tyrosine dephosphorylation. This results in dissociation of Sprouty proteins from GRB2, enabling the positive regulation of ERK activation (Hanafusa et al., 2004; Jarvis et al., 2006). Additionally, SHP2 binding to c-Met-activated GAB1 leads to c-Met specific signaling activation (Schaeper et al., 2000)

1.1.2.2 Biological relevance of SHP2

Due to its ubiquitous expression and its cell-type specific signaling outcome, SHP2 acts as a positive regulator in many signaling cascades that includes the Jak/STAT, the NFkB and the Ras/MAPK pathway (Grossmann et al., 2010). Therefore, it is not surprising that SHP2 plays a central role in a broad spectrum of cellular processes such as cell proliferation, differentiation and embryonic development. For example, Saxton et al. (1997) demonstrated that Shp2 is essential during gastrulation in the organization of axial mesoderm. They generated a mouse model by introducing an internal deletion of residues 46-110 in the N-terminal SH2-domain and found that mice homozygous for the mutant allele died *in utero* at mid-gestation. The mutant embryos showed uncompleted

turning, recognized by the disorganized neuroectoderm, and perturbed development of the vascular system. These observations were later confirmed in tissue-specific null mutations by different groups (Kontaridis et al., 2008; Princen et al., 2009).
Additionally, SHP2 is required for branching morphogenesis of the kidney in mammals (Schaeper et al., 2000; Willecke et al., 2011) and the development and maintenance of the nervous system (Grossmann et al., 2010). It also regulates cell fate during cardiomyogenesis and angiogenesis (Mannell et al., 2008). Recently, SHP2 has been also found to influence the differentiation of goblet and paneth cells in the murine intestine by controlling of the canonical Wnt/β-catenin signaling pathway (Heuberger et al., 2014).

1.1.2.3 Role of SHP2 in cancer

According to the Catalogue of Somatic Mutations in Cancer (COSMIC), there are 142 mutations in the *PTPN11* gene associated with cancer. Most of them are located in the N-SH2 domain, followed by mutations encoding for the terminal tail of the PTP domain. These somatic mutations are frequently associated with hematopoietic malignancies, from which approximately 35% are related with juvenile myelomonocytic leukemia (JMML) and in a lower incidence, with acute myeloid leukemia (AML), chronic myelomonocytic leukemia (CMML), myelodysplastic syndrome (MDS), and B-acute lymphoblastic leukemia (B-ALL) (Forbes et al., 2008; Grossmann et al., 2010).
To date, 65 substitution mutations in 21 amino acid positions of the N-SH2 domain have been reported, being the position Glu76 the most frequently mutated aminoacid. The E76K mutation alone has been reported in 85 cancer samples, most of them related with different forms of leukemia, but also in single cases of lung and colon cancer. Two additional amino acids, Ala72 (A72) and Asp61 (D61), are also frequently mutated.
The PTP domain has as well a relative high incidence of mutations (70 substitution mutations in 38 positions). Only the position Gly503 (G503) accounts for 36 reported cancer samples closely followed by Ser502 (19 counts). On the other hand, the C-SH2 domain shows a relative low mutation frequency (16 substitution mutations) compared to the N-SH2 domain, being mutations in the position Glu139 (E139) the most common.

SHP2 and *H. pylori*-CagA

Epidemiological studies have demonstrated that there is a strong correlation between increased SHP2 protein expression and gastric carcinogenesis in patients infected with *Helicobacter pylori* CagA-positive strains. *H. pylori* CagA is a 120-145 KDa protein and a tyrosine-phosphorylated by Src family protein-tyrosine kinase. CagA was first identified as a virulence factor of *H. pylori* (CagA positive strains) and associated with peptic ulcers. Additionally, infections with cagA-positive *H. pylori* strains are strongly associated with gastric adenocarcinoma (Hatakeyama, 2006b; Kim et al., 2010; Jiang et al., 2013). Not only the increased expression of SHP2 but also the activation of the IL6/gp130/STAT3 signaling pathway has been shown to be implicated in the development of gastric cancer (Lee et al., 2010). The interaction of the phosphorylated CagA protein with SHP2 triggers its activation and posterior inactivation of the focal adhesion kinase (FAK) by

dephosphorylation, promoting an elongated host-cell shape termed the "hummingbird phenotype" and increased cell motility (Higashi et al., 2002; Tsutsumi et al., 2006). Moreover, the effector protein CagA may also modulate a similar cell motility response by targeting the c-Met receptor, which in turn, recruits the adapter proteins GAB1 and SHP2 in epithelial cells (Churin et al., 2003).

1.1.3 Post-translational regulation of the MAPK signaling pathway by the protein kinase BRAF

BRAF, encoded in the human chromosome 7q34, is a serine/threonine protein kinase that belongs to the RAF family, key regulators of the MAPK pathway. Somatic mutations in this gene are associated with 8% of all human cancers, including colorectal cancer, malignant melanoma, thyroid carcinoma and non-Hodgkin lymphoma (Davies et al., 2002). Recent studies associate germline mutations in *BRAF* with developmental disorders, such as the cardio-facio-cutaneous syndrome (CFC syndrome).
BRAF protein consists of three conserved regions, which share the following domains with other RAF proteins: two regulatory CR1 and CR2 domains and a CR3 region that contains a motif called the negative-charge regulatory region (N-region), a glycine-rich loop, a catalytic loop and the activation domain or kinase domain (Sithanandam et al., 1990; Wellbrock and Marais, 2005). The most frequently somatic point mutation found in cancer is V600E (>90%) is located in the activation segment of the kinase domain (CR3). As a consequence, the V600E mutation derives in a BRAF protein with an elevated kinase activity.

BRAF Activation

There are three Raf paralogs in humans (A-Raf, B-Raf and C-Raf) coding for Raf proteins that are activated after extracellular stimuli and by binding of Ras-GTP to the cysteine-rich domain located in the CR1 region (fig. 2.1).
BRAF is a protein kinase that catalizes the phosphorylation of serine and threonine residues in consensus sequences of protein substrates using ATP. The products of this reaction are ADP and a phosphorylated protein. Under normal conditions, BRAF is kept inactive by auto-inhibition of the Ras-GTP-binding CR1 domain and the hinge domain. In contrast, oncogenic BRAF is constitutively active independently of mitogenic activation.
BRAF plays an important role in endothelial development. This feature was demonstrated by Wojnowski et al. (1997), who developed a mouse with a targeted disruption in the Braf gene. Heterozygous mice did not exhibited obvious defects. However, homozygous Braf-deficient mice showed an increased number of endothelial precursor cells, enlarged blood vessels and died of vascular defects during midgestation.
In 2007, Schubbert et al. (2007) reviewed the developmental disorders associated with mutations in the Ras/MAPK signaling pathway. In the CFC syndrome, there was neither an overlap in the mutation pattern, nor an association with cancer, quite opposite from the other developmental syndromes. Nevertheless, another study identified mutations in

different components of the MAPK cascade, including BRAF, that were implicated in acute lymphoblastic leukemia (ALL) and non-Hodgkin lymphoma (Aoki and Matsubara, 2013).

1.2 Ras/MAPK pathway deregulation in developmental disorders

The term "RASopathies" was coined in an attempt to cluster developmental disorders that result from germline mutations in genes encoding components of the canonical Ras/MAPK signaling pathway. Some affected genes include *PTPN11*, *NRAS*, *HRAS*, *BRAF*, *RAF1*, *SOS*, *MEK1*, *MEK2* (fig. 1.3), and share phenotypic features that includes craniofacial manifestations, cardiac, skin, muscular and ocular abnormalities, neurocognitive disabilities and an increased risk of developing cancer (Rauen et al., 2011). Some of these disorders, such as the cadio-facio-cutaneous syndrome (CFC), Noonan, LEOPARD (acronym for multiple Lentigines, Electrocardiographic conduction abnormalities, Ocular hypertelorism, Pulmonic stenosis, Abnormal genitalia, Retardation of growth, and sensorineural Deafness) and Costello syndromes are difficult to diagnose due to overlapping symptoms.

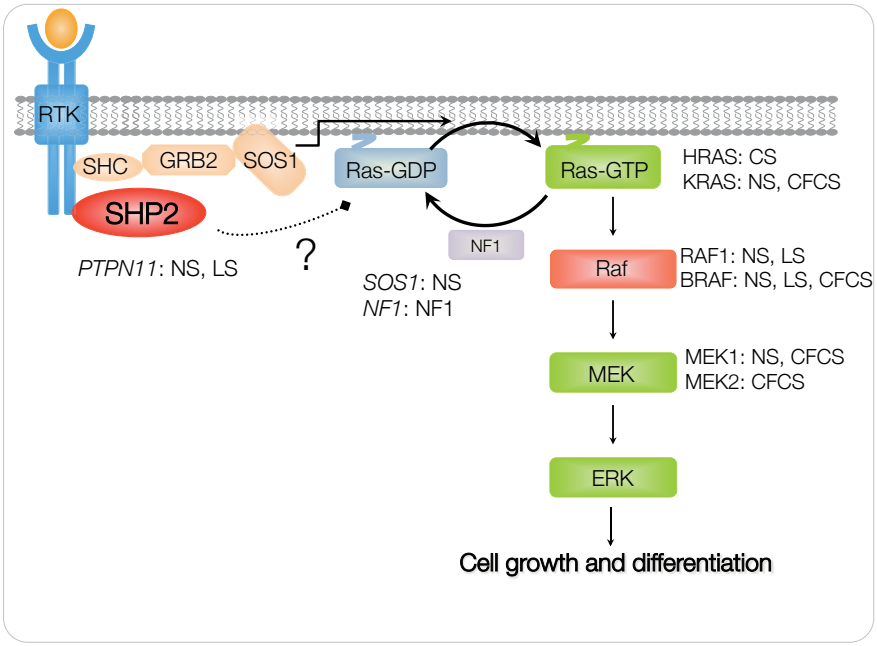

Figure 1.3: Regulation of Ras/MAPK pathway by SHP2 and genes affected in developmental disorders. RTK: Receptor tyrosine kinase. SOS1: Son Of Sevenless 1. NF1: Neurofibromin 1. NF1: Neurofibromatosis type 1. NS: Noonan syndrome; LS: LEOPARD syndrome; CS: Costello Syndrome; CFCS: Cardio-facio-cutaneous syndrome. Modified from Tartaglia et al. (2010).

In 2011, Kratz et al. revised 1900 cases of diverse RASopathies reported in the literature since 1937 and its association with cancer. They found that, indeed, there is an increased incidence of cancer, particularly in patients with Costello syndrome (11%), followed by Noonan (3.9%), CFC (3.5%) and LEOPARD (1.6%) syndromes. The cancer types ranged from diverse leukemia forms such as acute lymphocytic leukemia (ALL), acute

myeloid leukemia (AML), juvenile myelomonocytic leukemia (JMML) to neuroblastomas.

1.2.1 Noonan syndrome

In the late 50's the pediatrician Jacqueline Noonan described a new syndrome that had similarities in phenotype with the previously reported Turner syndrome but with associated congenital heart disease (Noonan and Nadas, 1958). The Noonan syndrome (OMIM163950) is a relatively common autosomal dominant disorder with an estimated incidence of 1 in 1000-2500 live births. The most characteristics of Noonan patients comprise dysmorphic facial features, proportionate short stature, pulmonic stenosis and hypertrophic cardiomyopathy, webbed neck, chest deformity, cryptorchidism, mental retardation and bleeding diatheses.
It took approximately 40 years to identify the genes responsible for this syndrome. Tartaglia et al. (2001) performed a mutation screening of two families with Noonan syndrome and identified a series of substitution mutations in the gene *PTPN11*. These missense mutations were found to be involved in switching the SHP2 protein into a constitutionally active conformation. Most of the Noonan-associated mutations are located in the exon 3, which encodes for the N-SH2 domain and in the PTP domain.
In addition to *PTPN11*, germline mutations in *KRAS*, *RAF1* and *SOS1* have been found to be associated with Noonan syndrome, though in a lower frequency.

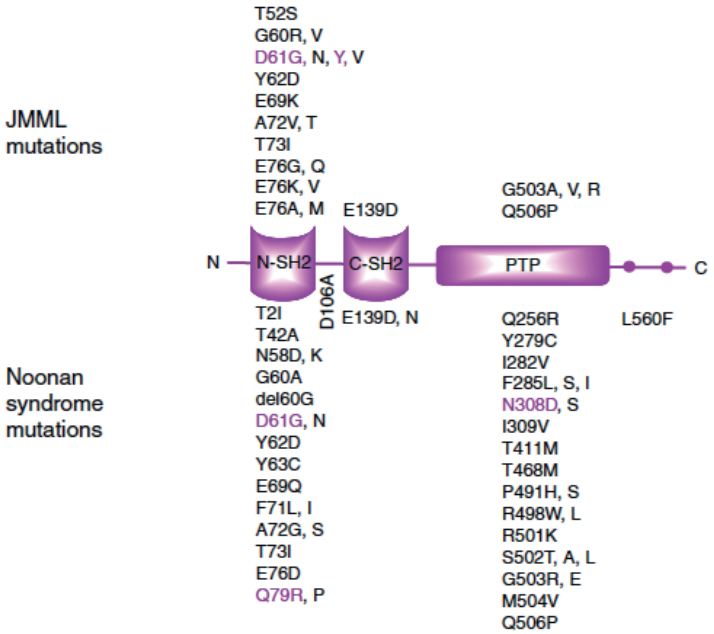

Figure 1.4: Mutations associated with Noonan syndrome and leukemia. From Grossmann et al. (2010).

Then, Araki et al. (2004) generated a knock-in mouse model for the Noonan syndrome by inserting the Noonan-related mutation D61G by cre recombination. Homozygous mice for the D61G mutation died, whereas less than 50 % of heterozygous mice were viable. Here, they demonstrated that the SHP2 phosphatase activity increased, while the highest level was reached in homozygotic cells. Consistent with the phenotype observed in individuals with Noonan syndrome, heterozygotic mice also showed short stature

and, after some months, mice developed splenomegaly and myeloid expansion. They concluded that D61G+/- mice developed a myeloproliferative syndrome.

1.2.2 LEOPARD Syndrome

Leopard syndrome (LS; OMIM 151100) is a rare multisystemic disorder, mainly characterized by facial, skin and cardiac anomalies. LEOPARD is an acronym described by Gorlin et al. (1969) that resumes the major features that characterize this disorder.
By 2008, there were approximately 200 LEOPARD patients worldwide, though it is considered that there are many underdiagnosed or misdiagnosed cases (Sarkozy et al., 2008).
Mutations associated with this disorder have been identified mostly in the gene *PTPN11* and *RAF1* (Tartaglia and Gelb, 2005; Pandit et al., 2007). Interestingly, the mutations associated with NS and LS are exclusive. Most NS mutations occur within the N-SH2 domain that results in gain-of-function with increased phosphatase activity (Keilhack et al., 2005). However, LS mutants in zebrafish are found to have dominant negative effects (Jopling et al., 2007).

1.2.3 Cardio-facio cutaneous syndrome

The CFC syndrome (OMIM115150) was first described in the late 1980's by Reynolds et al. and Neri et al. Typical manifestations include congenital heart defects, characteristic facial appearance, ectodermal abnormalities and mental retardation. CFC patients carry germline mutations in four different genes: *KRAS*, *MEK1*, *MEK2* and *BRAF* (for review, see Roberts and Der, 2007). Approximately 75% of the patients have BRAF mutations, found to be the most frequently mutated locus in CFC patients.
Anastasaki et al. (2009, 2012) expressed a panel of BRAF and MEK alleles in zebrafish embryos. Both kinase-activating and kinase-impared CFC mutants promoted similar developmental outcome during early development. There was a developmental time window in which a constant low-dose therapeutic MEK inhibition restore the normal development.
In 2011, Urosevic et al. presented a mouse model for the CFC syndrome with a germline mutation in the V600E hypomorphic allele which resembled partially phenotypical aspects observed in humans, including cardiomegaly, small dysmorphism and a reduced life span. However, these mice developed neuroendocrine tumors, which have not been observed in CFC patients.

1.3 MUTANOM Consortium

This thesis was accomplished as part (subproject 7) of the MUTANOM Project - Systems Biology of Genetic Diseases funded through the NGFN Plus Research Initiative (http://www.mutanom.org/). The overall objectives of the MUTANOM consortium were to characterize the functional consequences of somatic mutations in cancer and to develop models that predict the outcome of such genetic alterations on a molecular pathway, cellular and organism level. Initially the consortium concentrated on characterizing driver mutations selected from databases and publications (Table 1.1). Based on complementary expertise in the fields of proteomics, functional genomics (available from the partner institutions Max-Planck-Institute for Molecular Genetics, Max-Delbrück-Center for Molecular Medicine, German Cancer Research Center Heidelberg and Charité), a systematic assessment of the downstream consequences of driver mutations using mass spectrometry analysis, expression profiling and phenotypic analysis was performed (Fig. 1.5).

The task of subproject 7 (Cellular Signalling Networks) was to investigate the roles of candidate genes in controlling proliferation, cellular survival and various neoplastic properties. The standard approach for testing putative oncogenes was to express the candidate gene and its mutated derivative under the control of heterologous promoters in appropriate recipient cells and to assess their impact on cellular parameters, typically associated with the transformed state such as proliferation without anchorage. Conversely, putative tumor suppressing activity of candidate genes was assayed in tumorigenic cell lines by RNA interference or forced expression of the candidate gene in tumorigenic cell lines (see Ph.D. thesis by Sha Liu, in preparation). At the molecular level, the effects of candidate genes on receptor tyrosine kinase/Ras/ MAP-kinase signal transduction and related pathways were analyzed. To begin to understand candidate gene effects at the systems level, their impact on the genetic program of cells expressing the candidate cancer or anti-cancer gene by expression profiling was assessed as well.

Table 1.1: Cancer mutations selected for analysis in the MUTANOM consortium.
Somatic mutations in the candidate genes were selected according to their number of reported cases from the COSMIC database.

Gene	Gene name	Mutation	
		Nucleotide	Aminoacid
APC	Adenomatous polyposis coli	4348C→T	R1450∗
		4666insA	T1556fs*6
BRAF	v-raf murine sarcoma	1798GT→AA	V600K
	viral oncogene homolog B1	1799T →A	V600E
		770A→G	Q257R
		1399T→G &	S467A
		1455G→C &	L485F
		1495A→G &	K499E
CDH1	cadherin 1, type 1,	786_794CAC	T263fs*3
		CCAGGA→T	
	E-cadherin (epithelial)	1108G →C	D370H
CDKN2A	cyclin-dependent kinase inhibitor 2A	172C→T	R58*
	(melanoma, p16, inhibits CDK4)	238C→T	R80*

Gene	Gene name	Mutation	*(continued)*
		Nucleotide	Aminoacid
CTNNB1	catenin (cadherin-associated protein), beta 1, 88kDa	121A→G	T41A
		134C→T	S45F
		c.110C→T	S37F
EGFR	epidermal growth factor receptor	del2235_2249	del E746-A750
		2573T→G	L858R
FBXW7	F-box and WD repeat domain containing 7	1393C→T	R465C
		1394G→A	R465H
HRAS	v-Ha-ras Harvey rat sarcoma viral oncogene homolog	182A→G	Q61R
		35→G	G12V
		350A→G	K117R
IDH1	Isocitrate dehydrogenase 1 (NADP+), soluble	395G→A	R132H
JAK2	Janus kinase 2	1849G→T	V617F
		1624-1629delAATGAA	N542_E543del
		16111616delTCA CAA	F537_K539→L
		1615_1616AA→TT	K539L
KIT	Mast/stem cell growth factor receptor Kit	1676T→A	V559D
	(Proto-oncogene tyrosine-protein kinase Kit (c-kit) (CD117 antigen)	2447A→T	D816V
		1669_1672TGGA→G	W557_K558del
		1509_1510insGC CTAT	Y503_F504insAY
KRAS	v-Ki-ras2 Kirsten rat sarcoma viral oncogene homolog	35G→A	G12D
		35G→T	G12V
		101C→G	P34R
		458A→T	D153V
		467C→A	F156L
MLH1	mutL homolog 1, colon cancer, nonpolyposis type 2	1151T→A	V384D
		697T→C	C233R
MSH6	mutS homolog 6	insC3261	F1088fs*3
		3261delC	F1088fs*2
NF1	neurofibromin 1	1381C→T	R461*
		2033delC	P678fs*10
NRAS	neuroblastoma RAS viral (v-ras) oncogene homolog	37G→C	G13R
		35G→A	G12D
		182A→G	Q61R
		181C→A	Q61K
NRK	Nik related kinase	1270A→T	S424G
PIK3CA	phosphoinositide-3-kinase, catalytic, alpha polypeptide	1633G→A	E545K
		3140A→G	H1047R
		c.1258T→C	C420R
PTCH1	patched homolog 1	2975A→G	E992G
PTEN	phosphatase and tensin homolog	697C→T	R233*
		800delA	K267fs*9
		388C→G	R130G
		389G→A	G132
PTPN11	protein tyrosine phosphatase, non-receptor type 11	227A→G	E76G
		226G→A	E76K
		417G→T	E139D
		1403C→T	T468M
RET	ret proto-oncogene	2753T→C	M918T
		1894_1906→AGCT	E632_T636→SS
		1900T→C	C634R
MYLK4	Myosin Light Chain Kinase Family, Member 4	232G→T	A78S
SMAD4	SMAD family member 4	1051G→C	D351H

Gene	Gene name	Mutation	*(continued)*
		Nucleotide	Aminoacid
		733C→T	Q245*
SMO	smoothened homolog	c.1210G→A	V404M
		1604G→T	W535L
		1918A→G	T640A
SRC	v-src sarcoma (Schmidt-Ruppin A-2) viral oncogene homolog	1591C→T	Q531*
STK32B	serine/threonine kinase 32B	940G→T	E314*
TP53	tumor protein p53	743G→A	R248Q
		818G→A	R273H
		c.524G→A	R175H

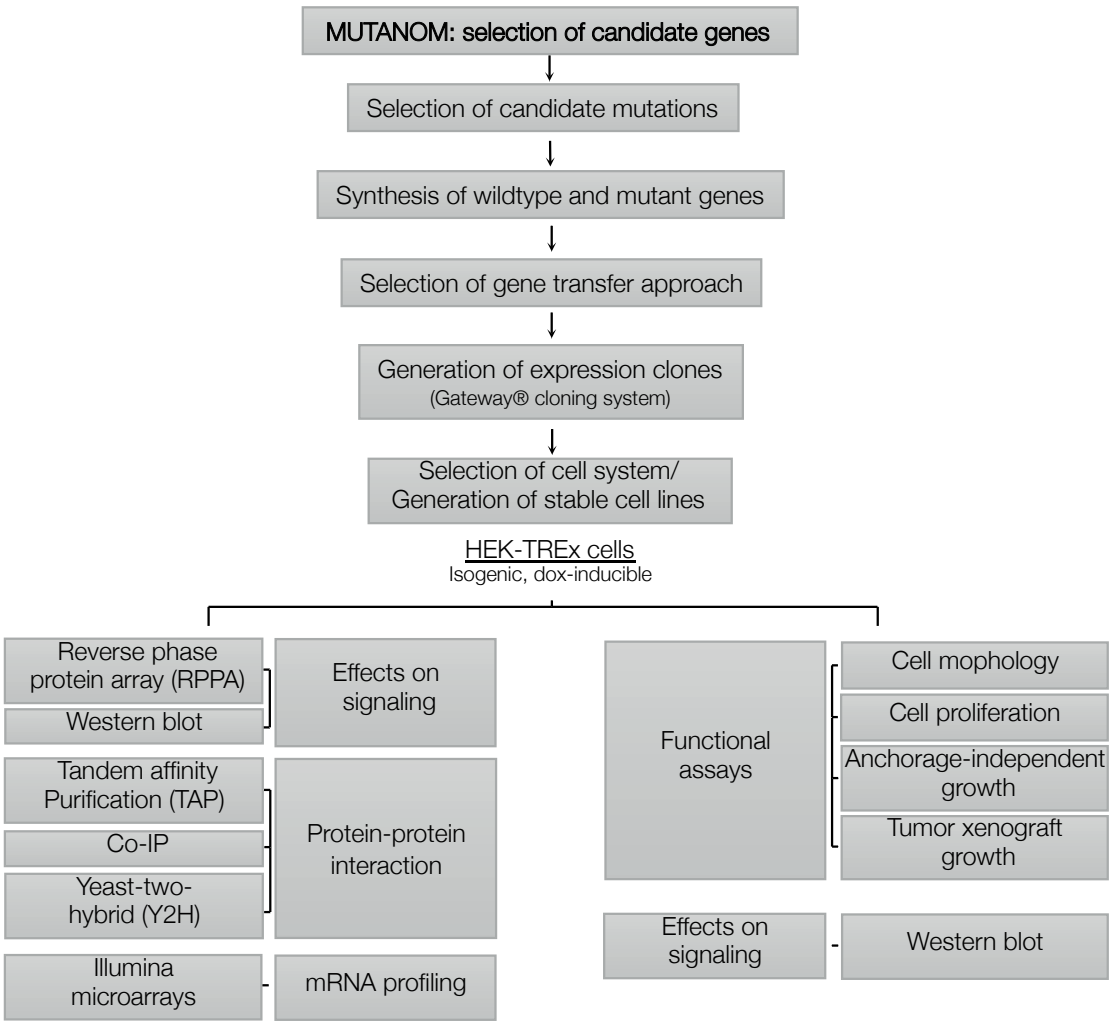

Figure 1.5: Experimental workflow of the MUTANOM consortium

1.4 Aims of this work

This thesis focuses on the characterization of mutations in *PTPN11*/SHP2 and *BRAF* genes. Both genes have been associated with the so-called "RASopathies", a group of developmental disorders caused by germline mutations of members of the RAS/MAPK pathway (Tartaglia and Gelb, 2005), and with somatic mutations that have been found in different forms of leukemia. (Grossmann et al., 2010).

Although somatic mutations in SHP2 associated with cancer have been phenotypically well characterized, it is still unclear whether RASopathies-associated mutations have the potential for oncogenic transformation.

Therefore, the aim of this work was to investigate the influence of leukemogenic and RASopathies-associated mutations in SHP2 and BRAF on the cellular phenotype, proliferation and anchorage-independent growth using non-transformed cell systems.

Furthermore, to elucidate the molecular mechanisms that stimulate modifications of the cellular phenotype, protein signaling and gene transcription analysis using high-throughput methods were explored. The experimental work-flow applied for this study is shown in fig. 1.6.

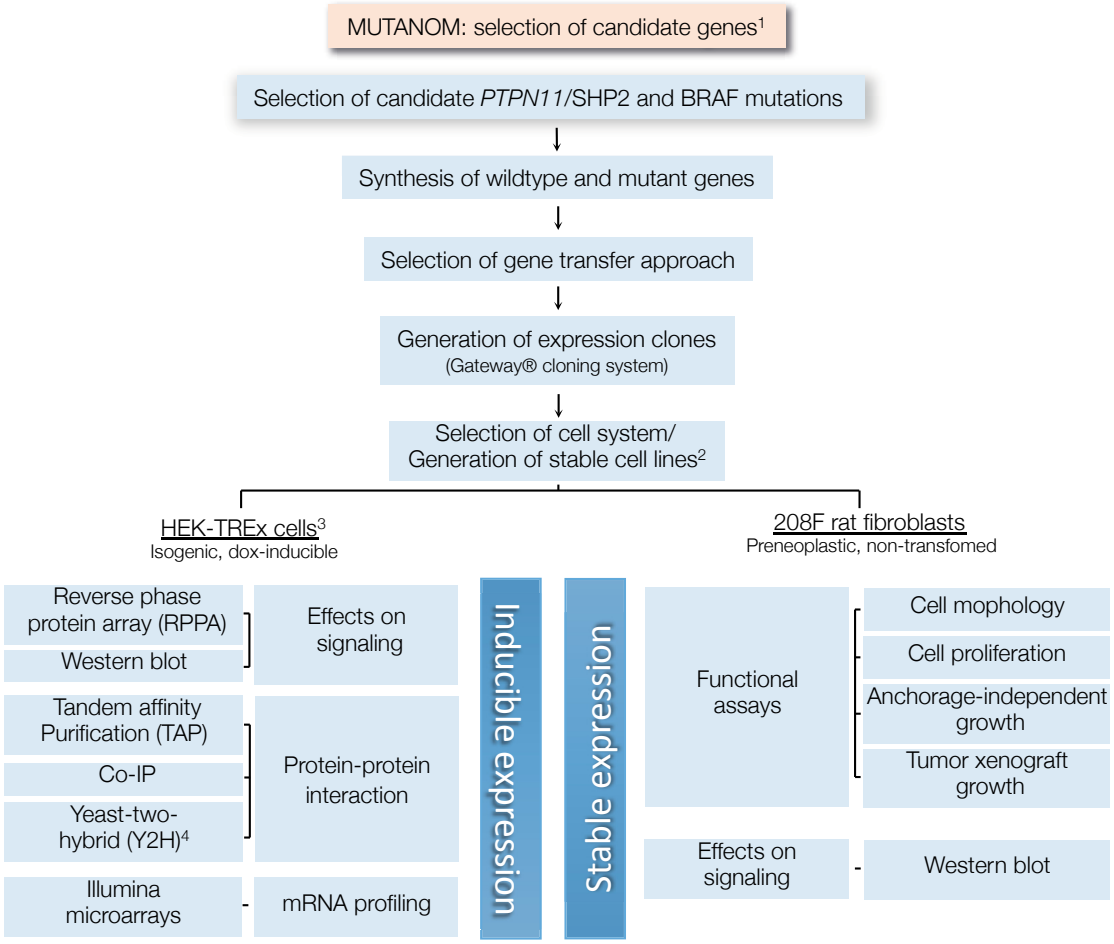

Figure 1.6: Experimental workflow of this project

[1] Following cell lines were generated for the MUTANOM consortium as part of the selection of candidate cancer mutations for characterization: stable TAP-tagged expressing HEK-TREx cell lines were generated for TAP assay and tested for protein expression of the Ras-MAPK signaling components by western blot (each with and without Stop codon): A). K-Ras wt, G12D (35G→A), G12V (35G→T), D153V (458A→T), P34R (101C→G) and F156L (467C→A); B). SMAD4 wt, Q245∗ (733C→T) and D351H (1051G→C).

[2] Human breast epithelial MCF10A populations were generated by lentiviral transduction to stable express H/K-Ras wt and G12V and BRAF wt, V600E and V600K. The resulting cell lines were tested for cell morphology and proliferation, anchorage-independent growth (except for BRAF V600K), and activation of the MAPK signaling pathway.

[3] To test whether the YFP-tagged TREx-HEK cell system was suitable for anchorage-independent growth assay, a soft agar assay was performed with the following cell lines (YFP-tagged expressing cells generated by Sha Liu): K-Ras wt and its corresponding mutations G12D, G12V, P34R, D153V and F156L. The TREx-HEK cell system resulted not appropriate for functional assays due to its ability to form colonies in soft agar assay without the expression of the corresponding oncogene mutation. An additional test under serum starvation conditions (0.2% FCS) showed that the HEK-TREx cells were unable to form colonies even though an oncogene such as H-Ras G12V was expressed.

[4] Yeast-two-hybrid assay was performed with SHP2 wt.

2 RESULTS

2.1 Generation of an efficient gene transfer approach to meet Mutanom requirements

2.1.1 Description of the selected mutations

To select the appropriate *PTPN11* and *BRAF* mutations, a wide literature search was performed using the PubMed database. The query was focused on reported mutations without a biological characterization. Additionally, a search was performed in the Catalogue of Somatic Mutations in Cancer (COSMIC) (Forbes et al., 2008) for frequency in leukemia and solid tumors (Table 2.1).

Table 2.1: Missense mutations in *PTPN11* and *BRAF* selected for functional studies.

Gene	Substitution		Syndrome	Cancer type	Reference
	Nucleotide	Aminoacid			
PTPN11	124A→G	T42A	NS	-	(Tartaglia et al., 2002)
	228G→C	E76D	NS	-	(Tartaglia et al., 2002)
	227A→G	E76G	NS	Colon adenocarcinoma, JMML	(Tartaglia et al., 2003)
	226G→A	E76K	NS	JMML, AML	(Tartaglia et al., 2003)
	417G→T	E139D	NS	JMML	(Tartaglia et al., 2002)
	844A→G	I282V	NS	-	(Tartaglia et al., 2002)
	1403C→T	T468M	LS	Rectal adenocarcinoma	(Digilio et al., 2002)
BRAF	770A→G	Q257R	CFC	-	(Niihori et al., 2006; Rodriguez-Viciana et al., 2006)
	1399T→G	S467A	CFC	-	(Rodriguez-Viciana et al., 2006)
	1455G→C	L485F	CFC	Malignant melanoma	(Niihori et al., 2006; Rodriguez-Viciana et al., 2006; Gallagher et al., 2008)
	1495A→G	K499E	CFC	-	(Niihori et al., 2006)
	1799T→A	V600E*	-	Malignant melanoma, thyroid carcinoma, colon cancer	(Davies et al., 2002)

*control; NS: Noonan syndrome; NS/JMML: Noonan syndrome with juvenile myelomonocytic leukaemia; LS: LEOPARD syndrome: lentigines, ECG conduction abnormalities, ocular hypertelorism, pulmonic stenosis, abnormal genitalia, retardation of growth, and sensorineural deafness syndrome; CFC: Cardio-facio-cutaneous syndrome; JMML: juvenile myelomonocytic leukaemia; AML: acute myeloid leukaemia.

The reference sequences, corresponding to *Homo sapiens*, were taken from the Concensus Coding Sequence Database (CCDS), accession numbers CCDS9163.1 for *PTPN11*/SHP2 and CCDS5863.1 for *BRAF*. Each mutated and wild-type gene variant was synthe-

sized containing a stop codon (TAA) and assembled into a vector backbone containing the flanking sequences attB for posterior gateway cloning (GeneArt, Germany). BRAF^{K499E}, SHP2^{wt} and its mutant derivates were assembled into the vector pMK-RQ (Kanamycin^r), BRAF^{L485F} in pMA (Ampicillin^r), BRAF^{S467A} and BRAF^{Q257R} in pMS (Spectinomycin^r). BRAF^{wt} and BRAF^{V600E} were also synthesized by GeneArt and assembled in the entry vector pDONR221 (kindly provided by Bodo Lange, MPI, Berlin). The mutations are located across all domains of both SHP2 and BRAF proteins as indicated in fig. 2.1.

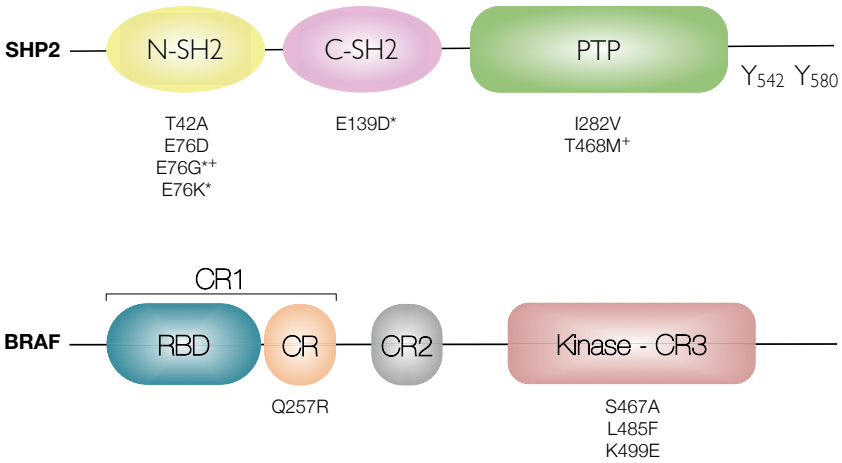

Figure 2.1: SHP2 and BRAF protein domains with the localization of leukaemogenic, Noonan/LEOPARD and CFC mutations. N-SH2: N-terminal src-homology domain; C-SH2: C-terminal src-homology domain; PTP: Phosphotyrosine domain. Mutations marked with an asterisk (*) correspond to those reported in juvenile myelomonocytic leukaemia (JMML) and with a cross (+) reported in adenocarcinoma. N-SH2: N-terminal src-homology domain; C-SH2: C-terminal src-homology domain; PTP: protein tyrosine phosphatase domain. CR: conserved region; CR1 corresponds to the Ras-binding domain (RBD) and a cystein-rich domain (CR); CR2: serine- and threonine-rich regulatory domain; CR3: kinase domain.

2.1.2 Selection of the gene transfer conditions

To develop a pipeline for the evaluation of mutations by functional assays, different mammalian cell lines were tested for overexpression by combining transfection reagents, transfection time and expression vectors.

The first issue to assess was the suitability of the expression vector. The isogenic and doxycycline-inducible TREx-HEK cell system, which was selected by the MUTANOM consortium for functional and high-throughput assays, resulted not appropriate for functional assays due to its ability to form colonies in soft agar assay without the expression of the corresponding oncogene mutation (Sha Liu, personal communication). An additional test under serum starvation conditions (0.2% FCS) showed that the HEK-TREx cells were unable to form colonies even though an oncogene such as H-Ras^{G12V} was expressed.

For this reason, the following target cell lines were used for selection of the gene transfer conditions: 208F (rat fibroblasts), MCF10A (human breast epithelial cell line) and

Cos7 (simian kidney fibroblast-like cells), this latter used as an easy-to-transfect control, were transiently transfected with the CMV-driven, YFP-tagged expression vector N-eYFP-amp carrying HRas^{wt}. The cells were treated with different transfection reagents (Lipofectamine2000, Polyethylenimine [PEI], Amaxa, Fugene and Effectene) overnight, and the transfection efficiency was monitored 48h later by fluorescence microscopy. As expected, Cos7 cells showed a moderate to high transfection efficiency with all tested reagents. Amaxa nucleofection and Lipofectamine2000 transfection were toxic for MCF10A, whereas PEI and Effectene did not affect the cell viability, though they were not effective for the target cell lines. Fugene was the less toxic reagent but still not efficient enough to detect YFP protein expression in 208F and MCF10A. In contrast, the transfection efficiency of the empty vector, as well as the YFP-amp-Ras vector in Cos7 cells was moderate (Fig 2.2A). Since the expressed proteins were N-terminal YFP-tagged, it might be possible that the YFP-tag or the polypeptide linker interfered with the protein folding, thus affecting the protein structure as reported previously (Prescott et al., 1999). To test the protein expression of YFP-HRas cell lysates were obtained from transiently transfected cells (96-120h after transfection) and subjected to SDS-PAGE and western blot. Both Cos7 and 208F cells showed a homogeneous expression of endogenous H-Ras protein. Although YFP-H-Ras was expressed with the predicted protein size in Cos7 cells under the CMV promoter, 208F cells failed to expressed YFP-HRas (Fig. 2.2B). These results are consistent with the lack of fluorescence in 208F cells compared to Cos7.

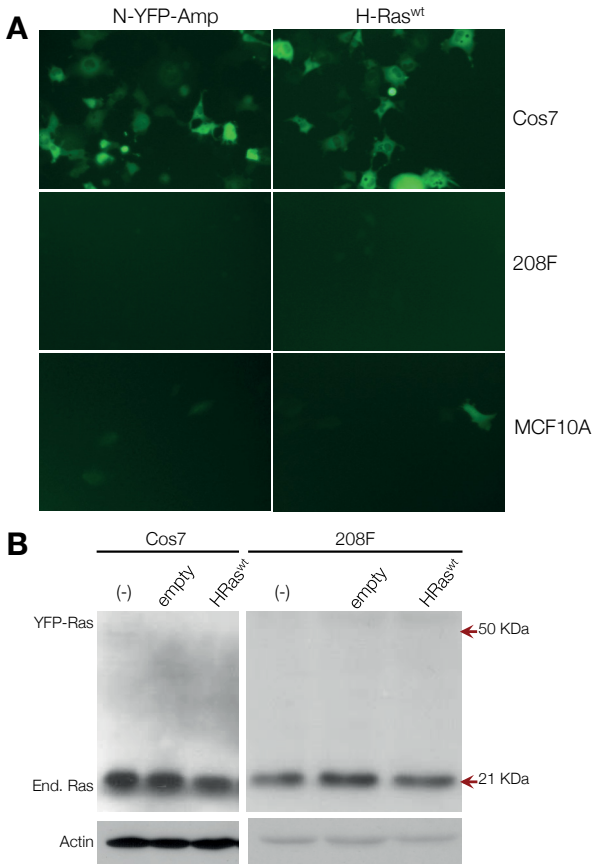

Figure 2.2: Transfection efficiency of target cell lines. Cos7, 208F and MCF10A were transfected with the expression vector N-YFP-Amp or N-YFP-H-Ras^{wt}. 48h after transfection, the expression of the YFP-HRas protein was monitored by fluorescence microscopy (A). 96h-120h after transfection, cells were subjected to SDS-lysis. Ras protein expression was evaluated by western blot for Cos7 and 208F cells (B). (-): parental cell line, Empty: N-YFP-Amp, H-Ras^{wt}: N-YFP-H-Ras^{wt}.

Since 208F and MCF10A were selected for functional assays, a lentiviral transduction protocol was used to enhance the gene transfer efficiency. This approach was chosen due to the high-efficiency gene transfer that is required for a well-detectable and constitutive expression of the gene of interest. For this purpose, SHP2^{wt} and BRAF^{wt} were cloned into the lentiviral vector pLenti6-CMV-YFP to obtain a N-terminal YFP-tagged protein and lentiviral particles were produced (for method description, see 4.2.9 and 4.2.10). 208F and MCF10A cells were seeded in 6-well plates until they reached 70% confluency and infected with the corresponding high-titer lentiviral particles. YFP-tagged SHP2 expression was monitored by fluorescence microscopy 48-72h after infection. 208F cells overexpressing SHP2 showed no significant morphological changes and low fluorescence, that disappeared two weeks after being puromycin selected (data not shown).
Taking together, both expression vectors, eYFP-CMV-amp and pLenti6-CMV-YFP used for constitutive expression in 208F showed an early low transfection/transduction efficiency, but they were not able to produce YFP-protein expression over time. This fact might be explained by a possible promoter silencing effect, as it has been previously observed in the generation of human stable tumor cell lines, where the CMV-driven promoter showed a significant low expression efficiency compared to the human elongation factor 1-alpha (EF1α) promoter (Teschendorf et al., 2002). Furthermore, another

study demonstrated that when rats were given intramuscular injections of CMV-driven adenovirus containing the human fibroblast growth factor 4 (hFGF4), a sustained decrease of hFGF4 transcription was observed as a result of the extensive methylation of CpG- and non CpG-sites of the CMV promoter (Brooks et al., 2004). Furthermore, Qin et al. (2010) compared the most common used promoters across different cell types and came to the conclusion that the CMV promoter performance varies considerably depending on the cell type in contrast to other promoter sequences such as the EF1α or the chicken β-actin promoter coupled with the CMV early enhancer (CAGG) promoters.

2.1.3 Comparison of different lentiviral vectors

Due to the inefficient protein expression under the control of the CMV promoter, the CMV sequence of the pLenti6-CMV-YFP was excised and replaced by the EF1α promoter (for details, see section 4.2.3). The correct insertion was verified by restriction digestion with AflII and PstI (fig. 2.3). This new vector was denominated pLenti6-EF1a-YFP. Additionally, the lentiviral vector pCDH-EF1a-IRES-GFP, a bicistronic vector, also EF1α-driven and with an internal ribosomal enhanced sequence (IRES), was simultaneously tested.

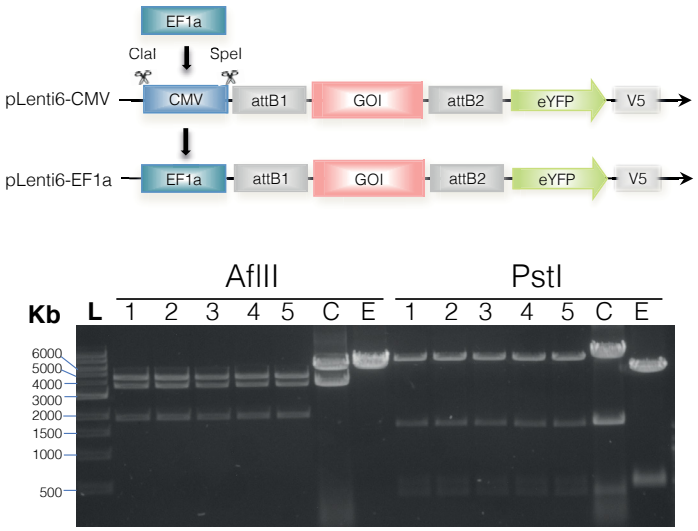

Figure 2.3: EF1α promoter cloning in pLenti6 expression vector. The CMV promoter was replaced by the EF1α promoter obtained by PCR. After cloning, five clones (1-5) of the new vector pLenti6-EF1a-V5-eYFP were picked, DNA isolated and restriction digested with AflII or PstI. AflII corresponding bands for are 4466 bp, 3656 bp and 1906 bp. PstI restriction bands are 7145 bp, 1580 bp, 505 bp, 400 bp and 398 bp. C: pLenti6-CMV-V5-eYFP. E:pEF1-V5-HisC.

To test the transduction efficiency of both vectors, 208F and Cos7 were seeded in 6-well plates for posterior infection with pLenti6-CMV, pLenti6-EF1α or pCDH-IRES-GFP lentiviral particles. 48-72h after infection, cell morphology and eYFP/GFP expression was monitored by fluorescence microscopy. 208F cells performed substantially better with pCDH-IRES-GFP, showing an homogeneous fluorescence pattern and no decrease in GFP expression along time (fig. 2.4). Although pCDH-IRES-GFP did not contain a resistance marker for selection, it met the requirements for a homogeneous and stable constitutive

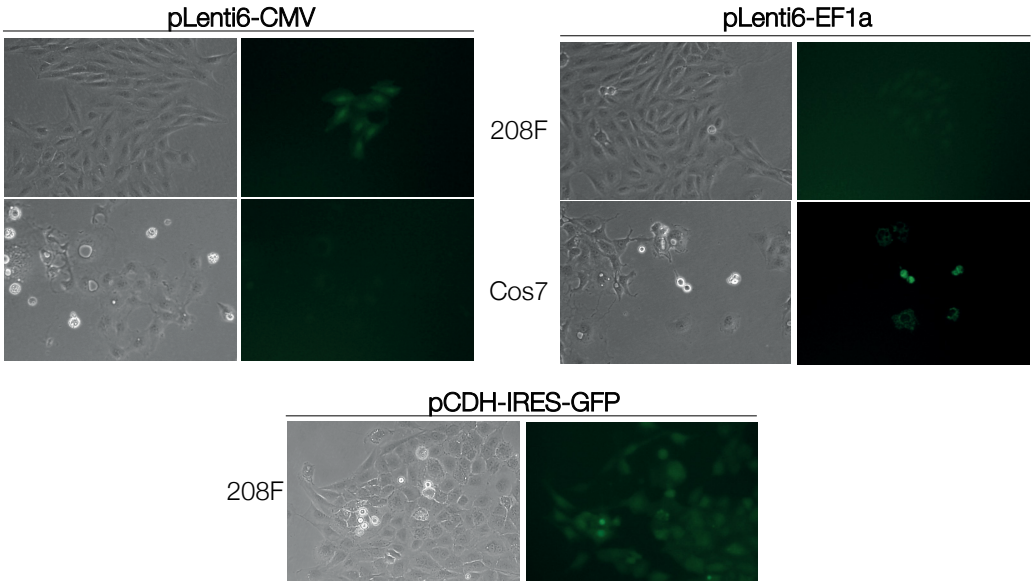

Figure 2.4: Comparison of lentiviral vectors in infection efficiency in 208F and Cos7.

expression of GFP, and hence the target protein, with the additional advantage that GFP was transcribed independently from the target gene due to the IRES sequence. Therefore pCDH-IRES-GFP was chosen for further assays.

2.1.4 Generation of the new lentiviral vector pCDH-EF1a-Puro

As a strategy for cloning simplification, all target genes from the MUTANOM were synthesized as cDNAs to be compatible with the gateway cloning system, which required that the gene of interest contained attB-flanking sequences to allow cloning by recombination. Consequently, the first step was the construction of a gateway-compatible destination vector (fig. 2.5. For details, see section 4.2.4).
To test the expression efficiency of pCDH-Gate-GFP, expression clones were obtained by recombination of the destination vector pCDH-Gate-GFP with the entry clones H-Ras^{wt} or H-Ras^{G12V} and lentiviral particles were generated. 208F and HEK293FT cells were seeded in 6-well plates until 70% confluency was reached. Then, cells were transduced with the empty vector, pCDH-Gate-HRas^{wt} or pCDH-Gate-HRas^{G12V}. fter 48h after transduction it was possible to visualize a homogeneous fluorescence, which indicated a successful IRES-GFP expression, with a high infection efficiency (data not shown).
To ensure the stable expression of the gene of interest by selection, the puromycin cassette under the control of SV40 was cloned into the vector pCDH-Gate-GFPin a further cloning step. This new expression vector was used for functional assays and was denominated pCDH-Gate-Puro.

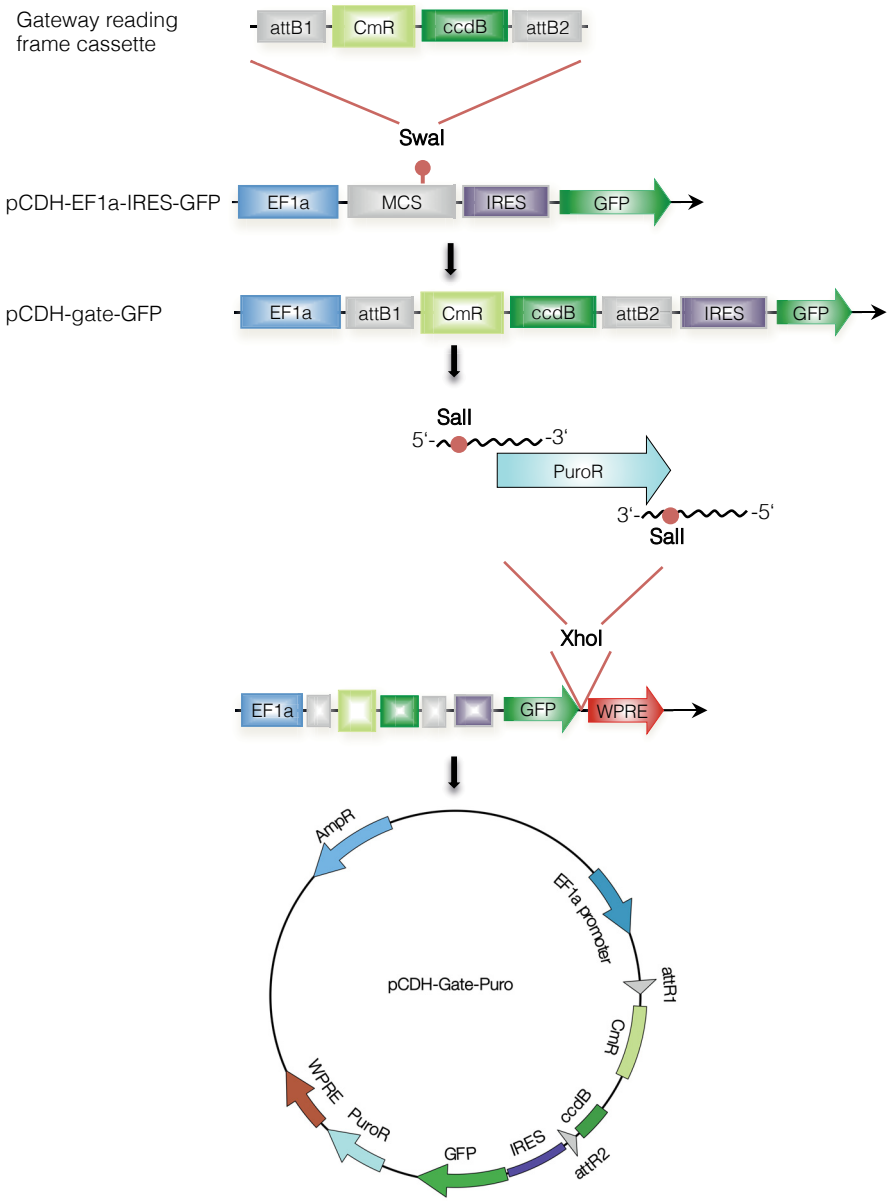

Figure 2.5: Generation of the expression vector pCDH-gate-Puro.

2.1.5 Optimization of protein expression using the destination vector pCDH-Gate-Puro

To check the suitability of the expression vector pCDH-Gate-Puro for ectopic expression, expression clones and lentiviral particles containing H-Ras^{wt} and its mutant derivate H-Ras^{G12V} were generated (pCDH-HRas^{wt}-puro and pCDH-HRas^{G12V}-puro, respectively). HEK293FT and 208F cells were seeded in 6-well plates and transduced with 10 μl of high-titer lentivirus-containing concentrate carrying pCDH-empty, H-Ras^{wt} or ^{G12V}. Cell morphology was monitored by light microscopy for up to 6 days after infection. HEK293FT cells expressing either the emtpy vector or H-Ras did not show an altered morphological phenotype (data not shown). 208F cells carrying the pCDH-empty vector were morphologically similar to the 208F parental cells. In contrast, HRas^{wt}-expressing

208F cells showed a modest cell elongation pattern four days after infection. This phenotype strengthened in the sixth day with a strong cell elongation and islet-like growth. Additionally, HRas^{G12V}-expressing 208F cells showed the classical feature of transformation, that is cell density-independent growth and light refraction, cellular characteristics became more evident on prolonged cultivation (fig. 2.6A). Additionally, cell lysates were prepared and the overexpression of Ras in both cell types was evaluated by immunoblot (fig. 2.6B).

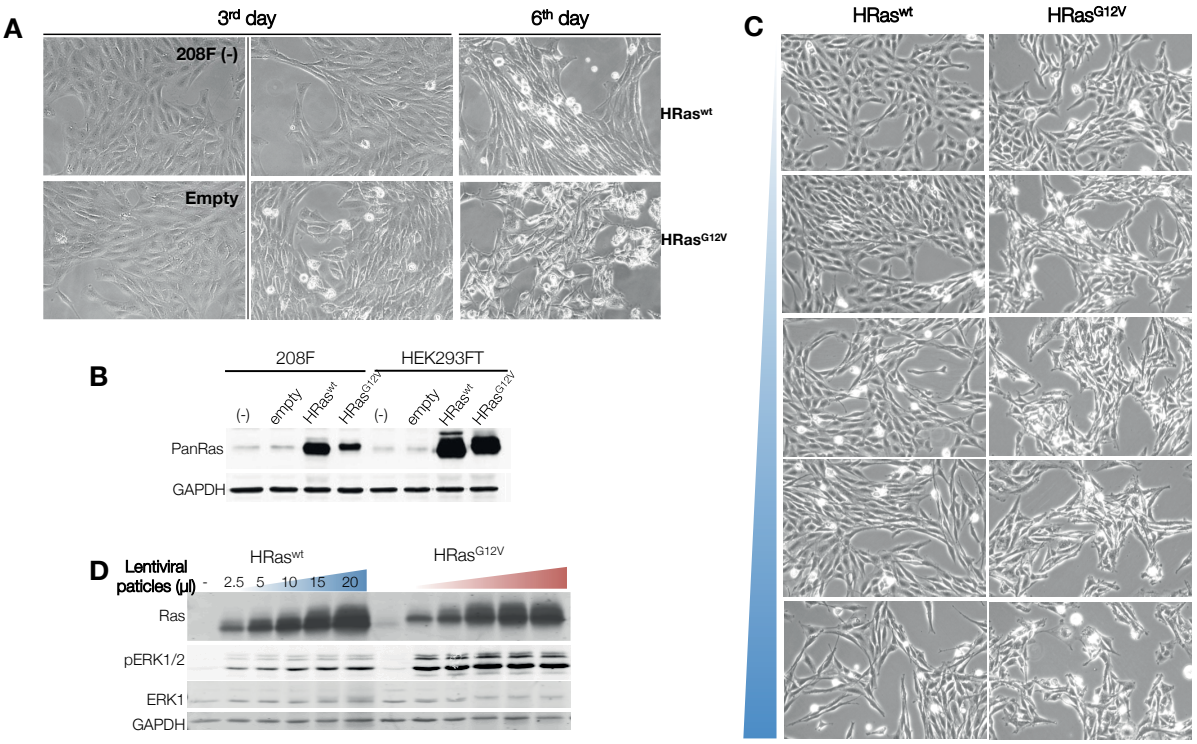

Figure 2.6: Optimization of H-Ras ectopic expression in 208F rat fibroblasts. 208F fibroblasts were transduced with pCDH^{empty}, H-Ras^{wt} or H-Ras^{G12V}. Cell morphology was evaluated 2, 3 and 6 days after infection (A). On the 6^{th} day, cell lysates were prepared and subjected to immunoblot (B). Different amounts of lentiviral particles were tested for influence on cell morphology (C) and protein expression (D). GAPDH was used as a loading control.

In order to test whether small amounts of lentiviral particles were enough to trigger a detectable protein expression to generate a differential morphology phenotype, 208F cells were transduced with increasing concentrations of pCDH-H-Ras. Ras protein expression was evaluated by immunoblot after 48h of infection. As expected, by increasing the concentration of lentiviral particles, Ras protein expression also increased as well as ERK phosphorylation (fig. 2.6D). These factors led to a constitutive activation of the MAPK signaling pathway, which in turn, was also reflected in the strong transformed phenotype (Fig. 2.6C).

Taking together, it was possible to establish the appropriate lentiviral expression vector pCDH-Gate-Puro to be used for the functional assays. Additionally, the rat fibroblasts 208F were also suitable for lentiviral infection and a well-studied cell system for functional assays, in contrast to other recipient cells used within the MUTANOM consortium.

2.2 Influence of SHP2 and BRAF mutations on cell phenotype

Additional to the 208F cells, human cell line models that exhibit a non-transformed morphology were also tested for lentiviral infection suitability, efficient ectopic expression and cell morphology. The breast epithelial MCF10A, the bladder fibroblast BJ-ELB and the kidney epithelial HA1EB cell lines were transduced with lentiviral particles carrying SHP2, BRAF or H-Ras wild-type or their corresponding mutant derivatives.
HEK-TREx cells, an inducible cell system used also in this work for proteomic approaches (see 4.3.10), were not adequate for transformation assays due to their ability to grow in an anchorage-independent manner in soft agar (Sha Liu, personal communication).

2.2.1 SHP2$^{wt/mutants}$ do not affect cell morphology of the epithelial HA1EB cells but BRAF$^{wt/mutants}$ influence cell growth pattern

The human kidney epithelial cell line HA1EB was originally derived from the parental HEK cells transfected with the telomerase catalytic subunit (hTERT), followed by a transfection with the simian virus 40 large-T (SV40-ER), and a control vector, and described as non-tumorigenic (Hahn et al., 1999; Zimonjic et al., 2001). HA1EB were transduced with the corresponding SHP2 or BRAF lentiviral particles and cell morphology was monitored for one week by microscopy. As a positive control for oncogenic transformation, both H-Ras^{wt}- and HRas^{G12V}-carrying cell lines were also generated. The parental HA1EB and the HA1EB$^{pCDH-empty}$ showed an adherent appearance without overgrowth. Cells carrying the oncogenic Ras variant exhibited a clear overgrowth and crisscross growth pattern when confluency was reached. In contrast, cells expressing SHP2^{wt} displayed a relaxed distribution and a flattened morphology but were not significantly different from the parental cell line, as well as all SHP2 mutants. In the case of BRAF, the cells grew tighter, with an apparent reduced cytoplasmatic area and with a higher cell density growth compared to SHP2 or the empty vector, but with no significant differences in morphology. Moreover, there was no particular divergence in morphology among BRAF mutants (fig. 2.7).
Since this cell line already used three selection markers, including puromycin, it was not possible to generate stable populations. This issue was essential to maintain the ectopic expression during functional assays. For these reasons, HA1EB cells were not further considered for additional tests.

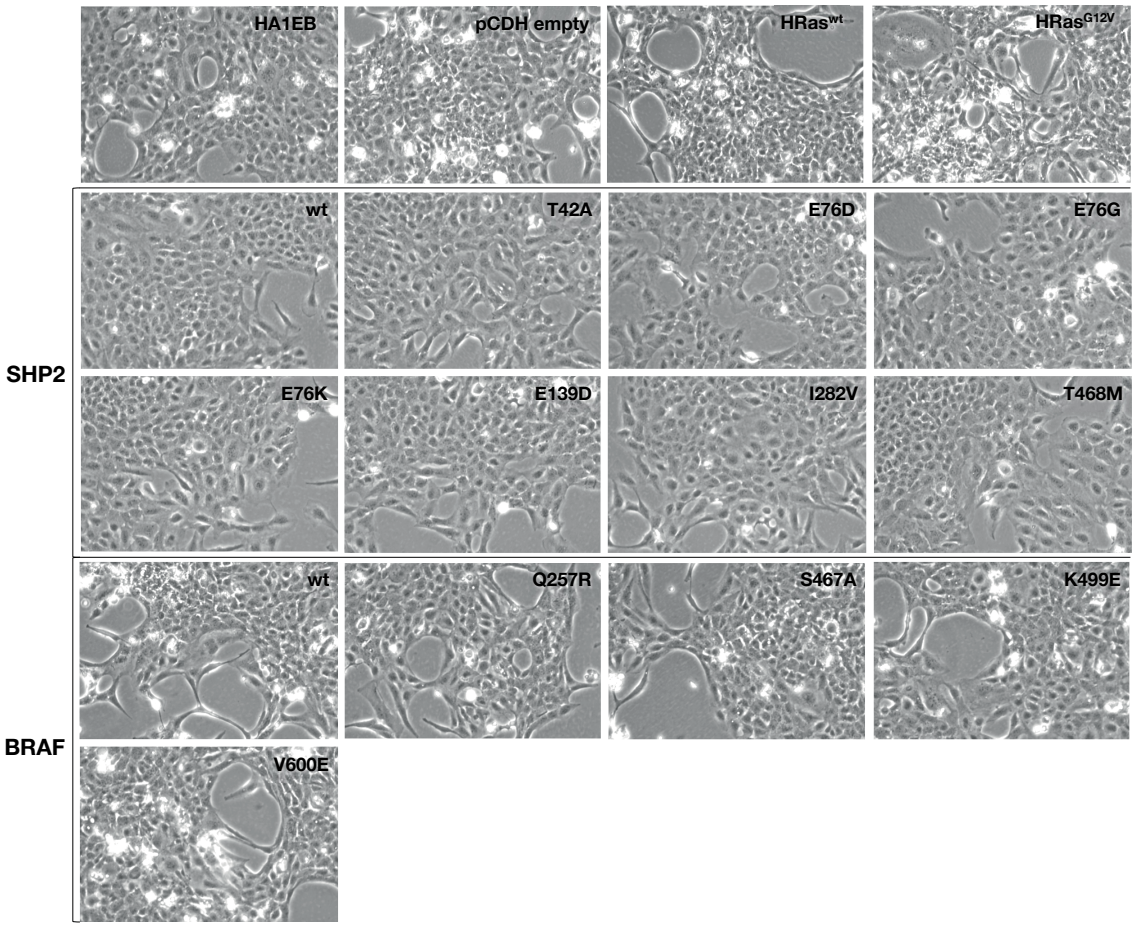

Figure 2.7: Morphological changes of HA1EB after transduction with SHP2 or BRAF. 1x10^5 HA1EB cells were seeded in 6-well plates and infected with 1x10^5 TU of the concentrated lentiviral particles carrying the corresponding mutation. Non-infected HA1EB and HA1EB transduced with the empty lentivirus pCDH-gate-Puro were used as a negative and HA1EB^{H-Ras} cells as positive control for oncogenic transformation. The pictures show cells after one week of infection.

2.2.2 SHP2, but not BRAF, decelerates cell growth of BJELB fibroblasts

The human BJELB fibroblast cell line was derived from primary human neonatal foreskin fibroblasts after sequential transduction with hTERT, SV40-ER and a control vector. This cell line has disrupted Rb- and p53-regulated checkpoints but remains non-tumorigenic and grows anchorage-dependent (Bodnar et al., 1998; Hahn et al., 1999).

BJ fibroblasts were transduced with the corresponding lentiviral particles, and were monitored for one week after infection. HRas^{wt}-expressing cells displayed a homogeneous morphology that did not greatly differ from the parental and pCDH-empty BJ fibroblast cells, while HRas^{G12V}-expressing cells exhibited a heterogeneous appearance compared to HRas^{wt}. In contrast, although the same amount of cells were seeded and all variants were infected simultaneously, SHP2$^{wt/mutants}$ decelerated cell growth and resulted in cell loss suggesting apoptosis (fig. 2.8 and 2.9). This was not the case of the BRAF$^{wt/mutants}$-expressing cells, which phenotype was comparable to the observed oncogenic phenotype in cells overexpressing H-Ras (fig. 2.8).

Due to the inherent tendency of the parental cell line to regress to a transformed state in a confluence-dependent mode, the preservation of a consistent phenotype is challenging, with the additional issue that its phenotype depend on the constant selection pressure (hygromycin, geniticin and puromycin), this cell line was not further considered for functional assays.

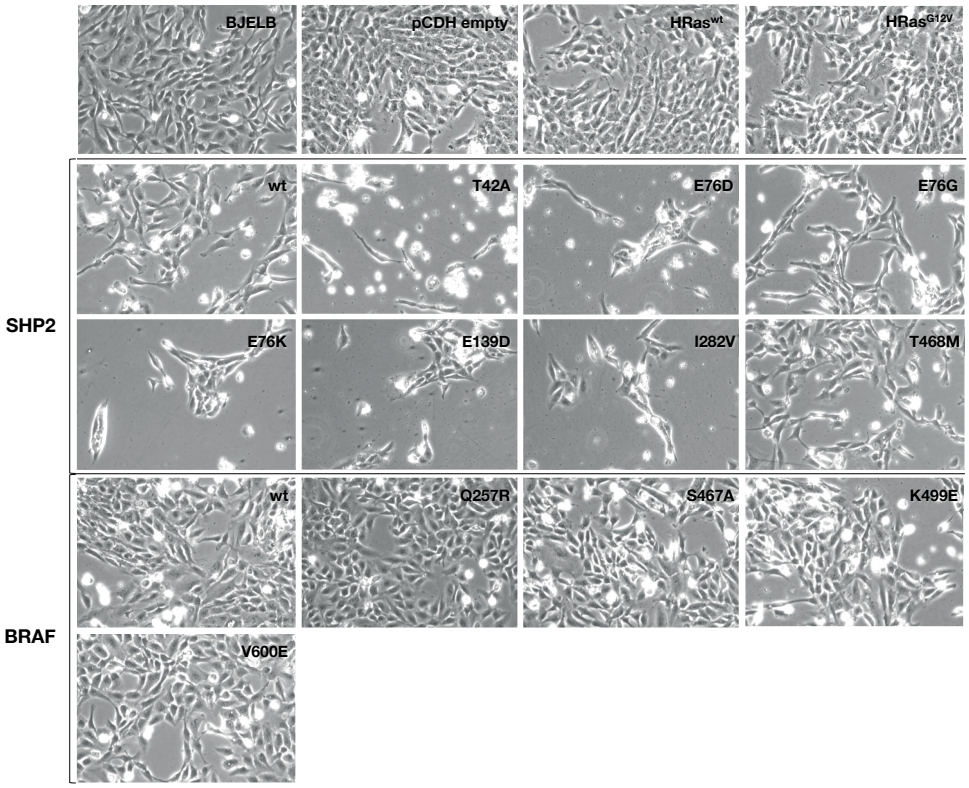

Figure 2.8: Cell morphology of BJELB after transduction with SHP2 or BRAF. 1x10^5 BJ fibroblasts were seeded in 6-well plates and infected with 1x10^5 TU of the concentrated lentiviral particles. Non-infected BJELB and BJ transduced with the empty lentivirus pCDH-gate-Puro were used as a negative and BJELB^{HRas} cells as positive control for oncogenic transformation. The pictures show cells after one week of infection.

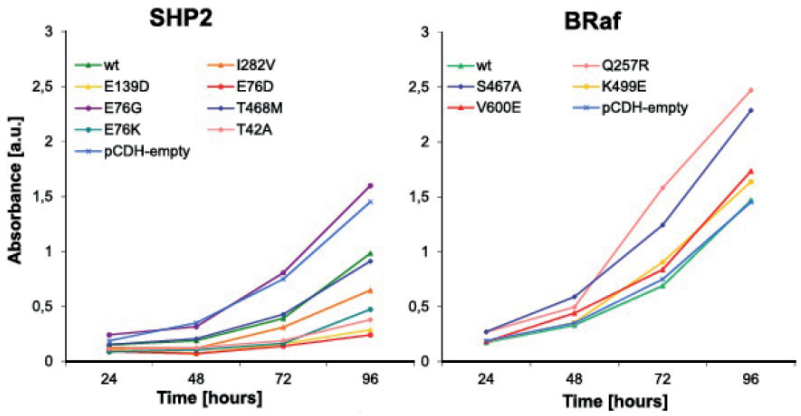

Figure 2.9: Overexpression of mutant SHP2/BRAF reduce cell proliferation in BJ-ELB cells. 2000 BJ-ELB fibroblasts/well were seeded in 96-well plates and cell growth was measured by XTT assay every day for 4 days. Representative results of two independent experiments.

2.2.3 The MCF10A epithelial cells exhibited a senescence-like state with SHP2$^{wt/mutants}$ and a transformed phenotype with BRAF^{mutants}

The human MCF10A is a well-characterized breast epithelial cell line obtained from spontaneous immortalized cells, with a non-transformed phenotype that lack the ability to form colonies in soft agar (Heppner and Wolman, 1999).
MCF10A cells, as HA1EB and BJELB, were proposed by the MUTANOM consortium for oncogene characterization. This cell line was infected with concentrated lentiviral particles and monitored for one week after transduction. MCF10A cells do not contain any selection marker, and this fact made this cell line useful for the generation of stable populations. MCF10A epithelial cells overexpressing either H-Ras^{wt} or H-Ras^{G12V} displayed a clear transformed phenotype, also described in previous studies by Li et al. (2012), with a high degree of crisscross formation, a reduced cytoplasmic area and a cell density-independent growth. This phenotype was stronger when cells were infected with lentiviral particles containing BRAF^{mutants} (fig. 2.10). Cells expressing CFC-associated BRAF mutant proteins were round-shaped, with a reduced cytoplasmic area, increased light refractory membrane and showed a tendency to surface detachment, while MCF10A cells expressing BRAF^{wt} did not differ substantially from the parental and pCDH-empty cell lines. Additionally, MCF10A cells expressing mutated BRAF proteins showed an increased ERK activation moderate higher than the cells overexpressing BRAF^{wt} (fig. 2.11). On the other hand, either SHP2^{wt} or SHP2^{mutants}-expressing cells revealed a similar phenotype regardless of phosphatase gain- or loss-of-function activity, with the common features of growth arrest, cytoplasmatic expansion and difficulties to reach confluency, when compared to the empty vector-carrying or the parental cell lines.
After the generation of stable populations by puromycin selection, BRAF-MCF10A epithelial cells conserved the transformed phenotype described here, while SHP2-MCF10A cells stopped cell division and entered in growth arrest. Therefore, SHP2-MCF10A was not further considered for functional assays.

2.2.4 SHP2 Mutations confer a transformed phenotype in rat fibroblasts

The 208F rat fibroblast cell line are a derivate from HPRT^{-} Rat-1 cells (Griegel et al., 1986). The parental 208F as well as the 208F$^{pCDH-empty}$ cells showed a flattened morphology and grew as an adherent monolayer on the culture flask (fig. 2.12 and 2.13). 208F expressing H-Ras^{wt} or H-Ras^{G12V} displayed a transformed phenotype, which made them an appropriate model system for oncogenic transformation. When 208F fibroblasts were transduced with SHP2^{wt} or SHP2^{mutants}, the cells showed an elongated shape, with a density-independent growth and crisscross morphology, typical of a transformed phenotype. Particularly, cells expressing the phosphatase gain-of-function, Noonan- and leukemia-associated mutations exhibited a stronger phenotype than the loss-of-function, LEOPARD-associated SHP2^{T468M} mutation (fig. 2.12). Cells overexpressing either BRAF^{wt} or the CFC-associated BRAF^{mutants} did not differ significantly from the

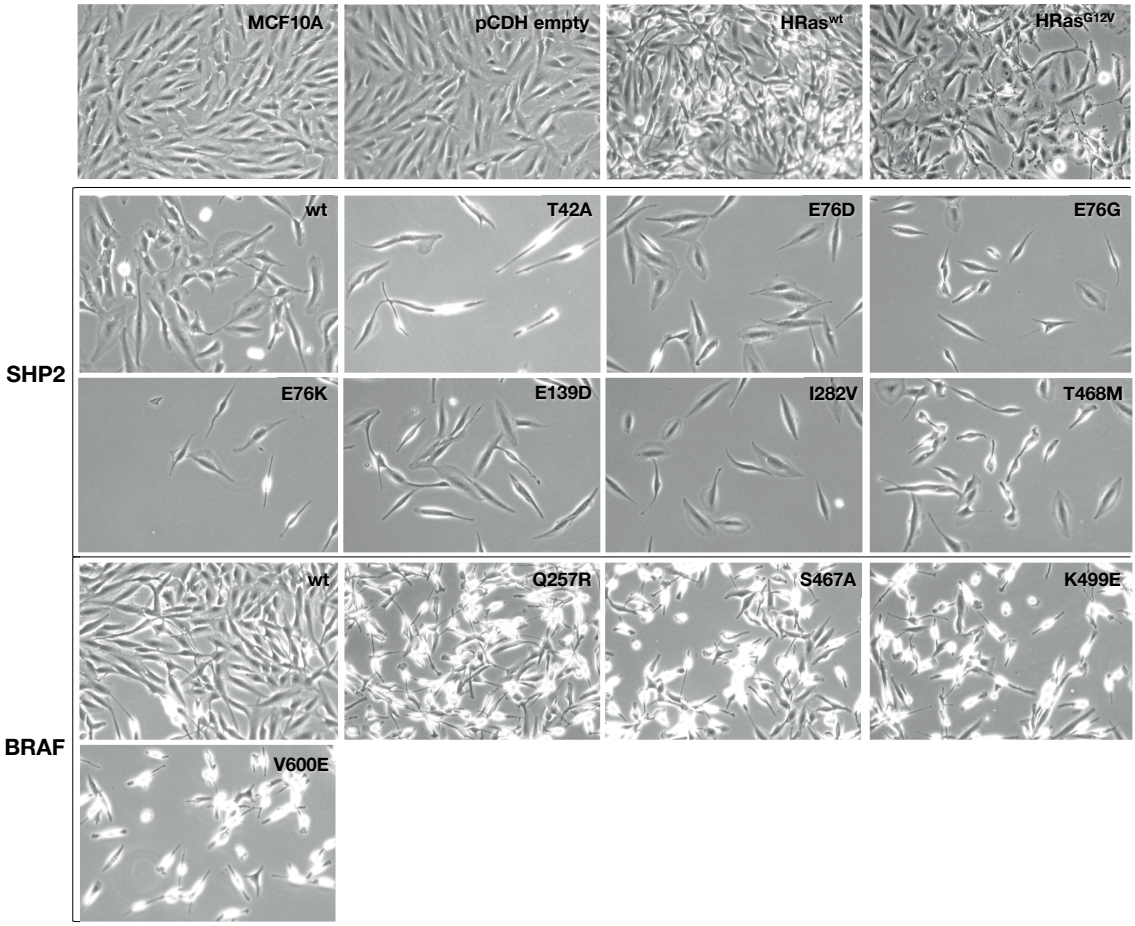

Figure 2.10: Morphological phenotype of MCF10A after transduction with SHP2 or BRAF. $1x10^5$ MCF10A cells were seeded in 6-well plates and infected with $1x10^5$ TU of the concentrated lentiviral particles. Non-infected MCF10A and MCF10A transduced with the empty lentivirus pCDH-gate-Puro were used as a negative and MCF10A^{HRas} cells as positive control for oncogenic transformation. The pictures show cells after one week of infection, without selection.

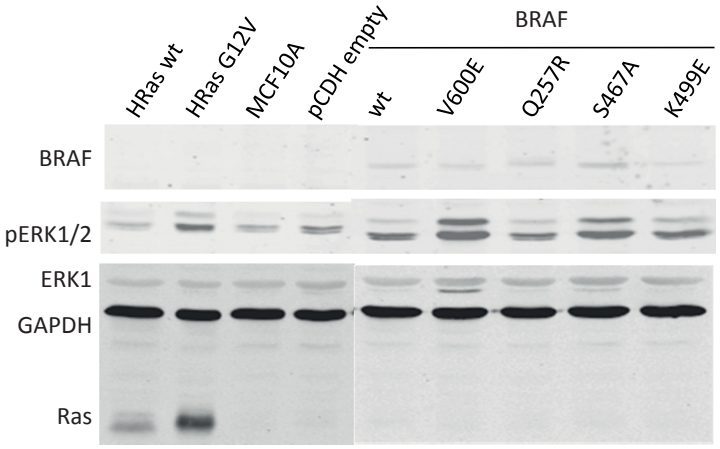

Figure 2.11: CFC-associated BRAF mutations lead to moderate ERK1/2 activation in mammary epithelial cells. MCF10A cells were transduced with lentiviral particles carrying the corresponding mutant BRAF. 72h after infection, lysates were prepared and subjected to immunoblot.

parental or the pCDH-empty-carrying cells. They conserved a cell flat appearance, but showed light refraction (fig. 2.13).
The observed phenotype in both SHP2 and BRAF expressing cell lines was conserved even after puromycin selection and multiple passaging.
To quantify to which extent the cell length was affected by the expression of mutant SHP2 and BRAF variants, the length of thirty cells from each strain was measured. As shown in fig. 2.14, $SHP2^{wt}$ expressing cells did not affect substantially the cell length, as well as the LEOPARD-associated mutation T468M. On the other hand, the Noonan-associated mutations significantly affected the elongation of the rat fibroblasts, being the longest E76D, followed by E139D, I282V, E76G and E76K. Furthermore, 208F fibroblasts expressing CFC-associated BRAF mutations exhibited a shorter appearance compared to $BRAF^{wt}$ cells (fig. 2.14 *right*).
Taking together, a divergent morphology phenotype was observed in the human cell lines BJELB and MCF10A between SHP2 and BRAF mutants. In contrast, there was no significant differences between SHP2 and BRAF expressing cells nor among wt and the mutations in HA1EB cells. In 208F rat fibroblasts, SHP2-expressing cells showed a strong oncogene-mediated transformed phenotype, equivalent to Ras oncogene, while BRAF-overexpressing 208F cells showed a similar phenotype to $BRAF^{wt}$ expressing cells and the parental cell line. This fact was surprising, considering that both SHP2 and BRAF mutations exhibit overlapping phenotypes on human disorders.

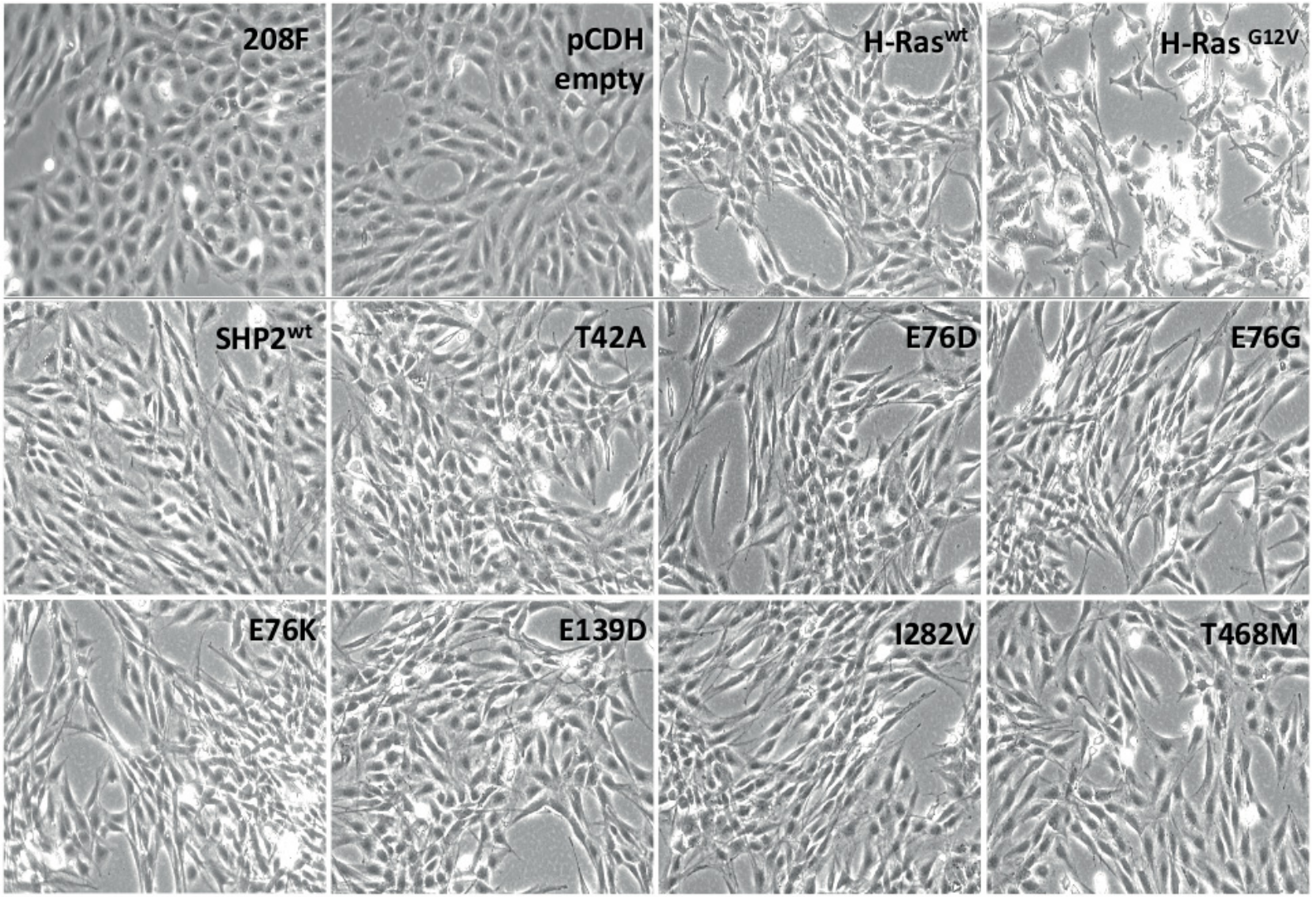

Figure 2.12: Cell density-independent growth of 208F after transduction with SHP2. 1x10^5 208F cells were seeded in 6-well plates and infected with 1x10^5 TU of the concentrated lentiviral particles carrying the corresponding mutation. After 48h of infection, cells were selected for 2 weeks with puromycin (10μg/ml) to generate stable cell lines. Non-infected 208F and 208F transduced with the empty lentivirus pCDH-EF1-puro were used as a negative and 208F^{HRas} cells as positive control.

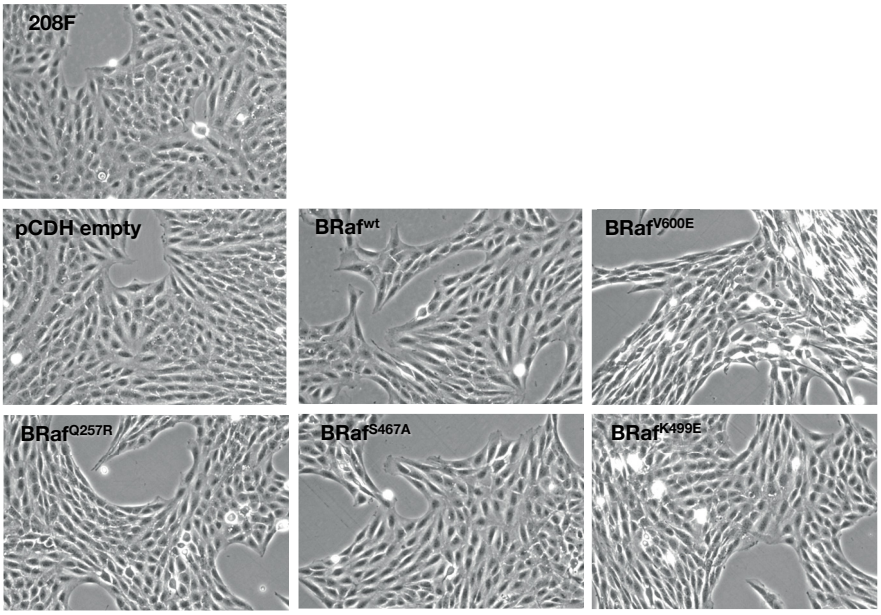

Figure 2.13: Morphological changes of 208F after transduction with BRAF. 208F cells were seeded in 6-well plates and infected with 1x10^5 TU of the concentrated lentiviral particles. After 48h of infection, cells were selected for 2 weeks with puromycin (10μg/ml) to generate stable populations. Non-infected 208F and 208F transduced with the empty lentivirus pCDH-EF1-puro were used as a negative transformation control.

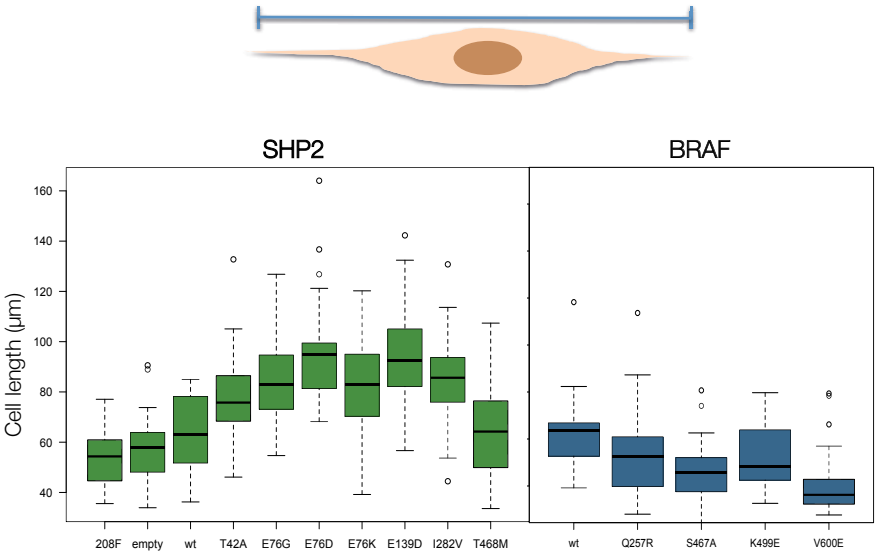

Figure 2.14: Cell length effect of SHP2 and BRAF mutations on 208F. The longitudinal length of each cell line (n=30) was measured as indicated (*top*).

2.2.5 CFC-associated BRAF and SHP2 mutations stimulate cell proliferation in rat fibroblasts

To test whether mutations in SHP2 and BRAF influenced cell proliferation, lentiviral-transduced 208F cells were subjected to a XTT assay. 2x10^3 cells/well were seeded in 96-well plates and the cell growth was measured every day for up to six days by a colorimetric approach that registers active cell metabolism. The 208F cells carrying the pCDH-empty vector showed a similar growth rate as the parental and SHP2^{wt} expressing cells. Cells overexpressing SHP2^{mutants} proliferated more slowly than 208F cells carrying

the pCDH-empty vector and the parental 208F cells, but once they reached confluence after day 4, they overcame density-dependent growth control and reached higher cell densities (fig. 2.15). In fact, cells overexpressing the SHP2 mutations E76G/K and D, and T468M triggered the strongest proliferation phenotypes among the SHP2 group, and was comparable to the growth pattern observed in HRas^{wt} and HRas^{G12V} expressing cells. In contrast, 208F cells carrying the BRAF mutations S467A, Q257R and the oncogenic V600E, but not K499E, promoted a steady growth rate over the parental and pCDH-empty cell line.

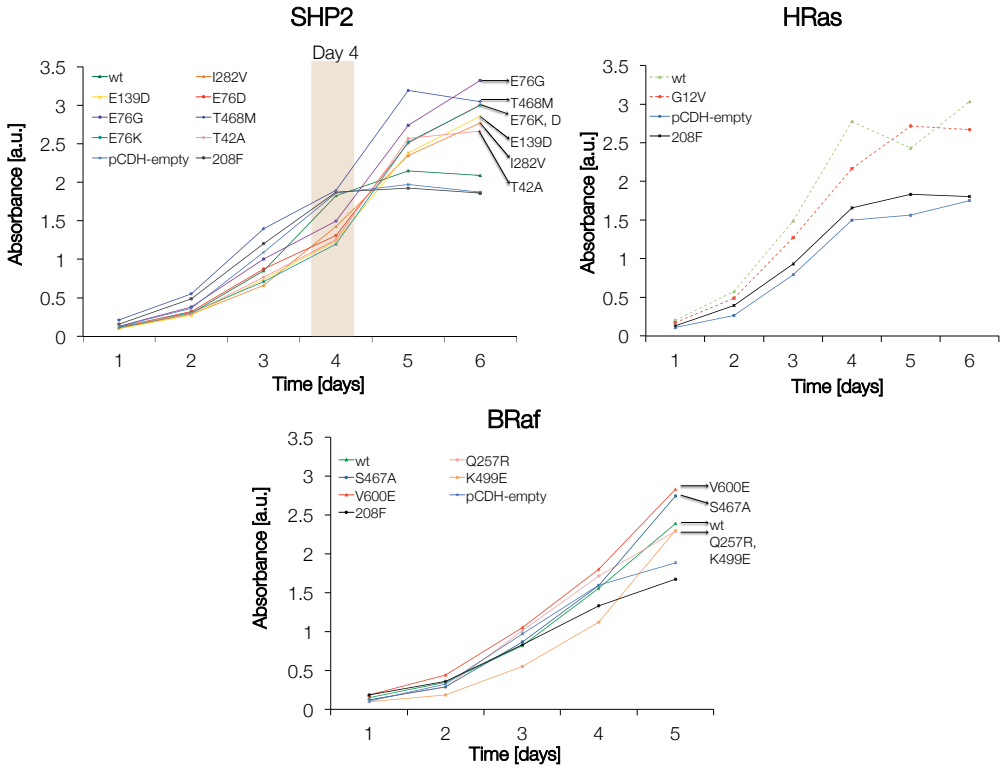

Figure 2.15: SHP2/BRAF mutants influences density-dependent cell proliferation. 2000 cells/well were seeded in 96-well plates and cell growth was measured by XTT assay every day for one week. Non-infected 208F and 208F transduced with the empty lentivirus pCDH-EF1-puro were used as a negative and 208F^{HRas} cells as positive control.

2.2.6 Mutations in SHP2 and BRAF promote anchorage - independent growth of 208F cells

In order to evaluate whether cells expressing the leukaemia-, Noonan-associated SHP2 and CFC-associated BRAF mutations were able to grow in a non-adherent context, soft agar assays were performed. The parental 208F and pCDH-empty cell lines were used as negative controls and HRas^{wt} and HRas^{G12V} expressing cells were used as positive controls of anchorage-independent growth. 10^2, 10^3 and 10^4 SHP2- and BRAF-208F cells were seeded in 25-cm^2 culture flasks containing soft agar and incubated for up to six weeks at 37°C and 5% CO_2. The absence or presence of colonies were checked once a week.

Colonies arose after two weeks of culture in those cells expressing HRas^{wt}, HRas^{G12V} and BRAF^{V600E}, but not in the parental 208F and those carrying the empty vector cells (fig. 2.16). Oncogenic HRas^{G12V} overexpressing 208F cells formed larger colonies than 208F-HRas^{wt}. BRAF^{wt} and BRAF^{V600E} expressing cells strongly differed in colony size, but not significantly in colony number. After six weeks, all colonies expressing SHP2 and BRAF mutants gave rise to anchorage-independent colonies, particularly SHP2^{E76G,K} and SHP2^{T42A}. Despite CFC-associated BRAF^{mutatnt}-carrying 208F cells did not show a higher number of colonies, the colony size was significantly larger than the observed in SHP2.

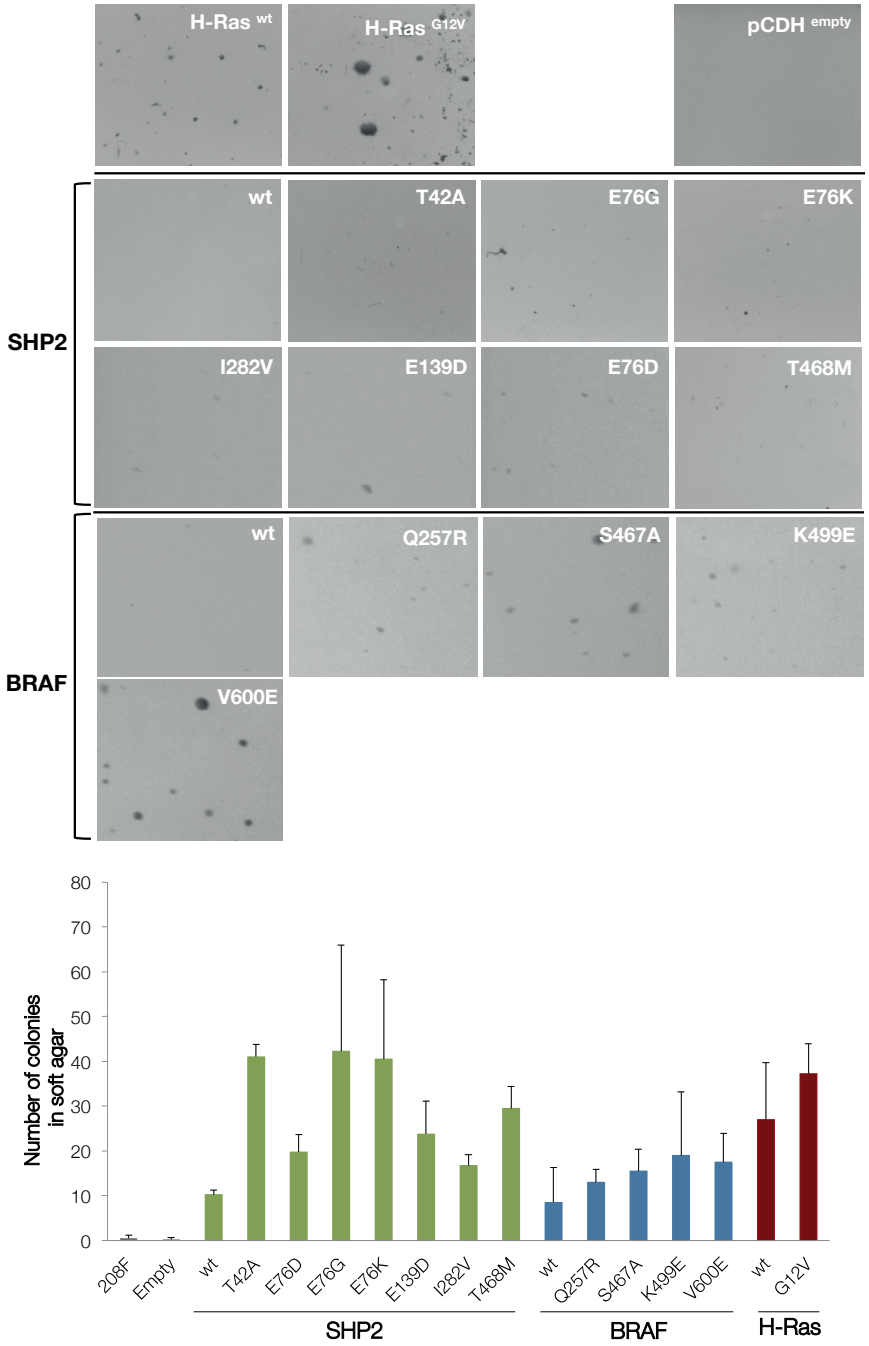

Figure 2.16: SHP2 and BRAF mutations promote anchorage-independent growth of 208F cells. $1x10^5$ 208F cells were seeded in 6-well plates and infected with $1x10^5$ TU/ml of the corresponding concentrated lentiviral particles. After 48h of infection, cells were trypsinized and 10^2, 10^3 and 10^4 cells were seeded in duplicates in 25-cm^2 culture flasks containing soft agar and incubated for up to 6 weeks. Results from the 10^3 dilution are here depicted. The mean of the number of colonies is shown as a bar diagram (bottom). Non-infected 208F and 208F transduced with pCDH-empty were used as a negative and $208F^{HRas}$ cells as positive control.

2.2.7 NS- and LS-associated SHP2 mutations promote tumor growth in nude mice

To evaluate whether mutations on SHP2 lead to tumor growth *in vivo*, 208F cells that stably expressed either the empty vector pCDH-Gate-Puro, $SHP2^{wt}$, or the mutant

variants E76G or T468M were injected subcutaneously in nude mice. The protein level of each cell line was previously evaluated by immunoblot, to guarantee the homogeneous protein expression (fig. 2.23). Tumor volume was monitored every 3-4 days for six weeks (Fig. 2.17A). There was no tumor growth in the empty vector 208F mice, whereas mice injected with SHP2^{wt} expressing cells gave rise to small xenografts after the 3rd week. Similarly, cells carrying the mutation E76G formed a tumor after the 2nd week, with a constant tumor volume that after five weeks achieved a similar size comparable to SHP2^{wt} expressing xenografts. Surprisingly, cells expressing the LEOPARD-associated, loss of function mutation T468M not only generated a steady tumor volume during the time course analysis, but also it seemed to be highly irrigated with strong development of angiogenesis compared to the tumors generated from WT- and E76G-expressing cell populations (fig. 2.17B). To corroborate this observation, the xenograft tissues were subjected to immunohistochemistry analysis with the angiogenesis marker platelet endothelial cell adhesion molecule-1 (PECAM-1), also known as CD31 (Wang et al., 2008). PECAM-1 is a transmembrane glycoprotein that is highly expressed in endothelium. Its localization at the endothelial cell junctions suggests an important role in transendothelial cellular migration (Zocchi et al., 1996), interendothelial cell migration and angiogenesis (Piali et al., 1995). As shown in fig. 2.17C, SHP2^{wt} and E76G-carrying tumors exhibited a homogeneous staining, with a slight blood vessel formation, while tumors generated from T468M-carrying 208F cells displayed a higher blood vessel density. Additionally, immunoblot analysis of the tumors showed an increased MEK/ERK activation that correlated with SHP2 overexpression (fig. 2.18).

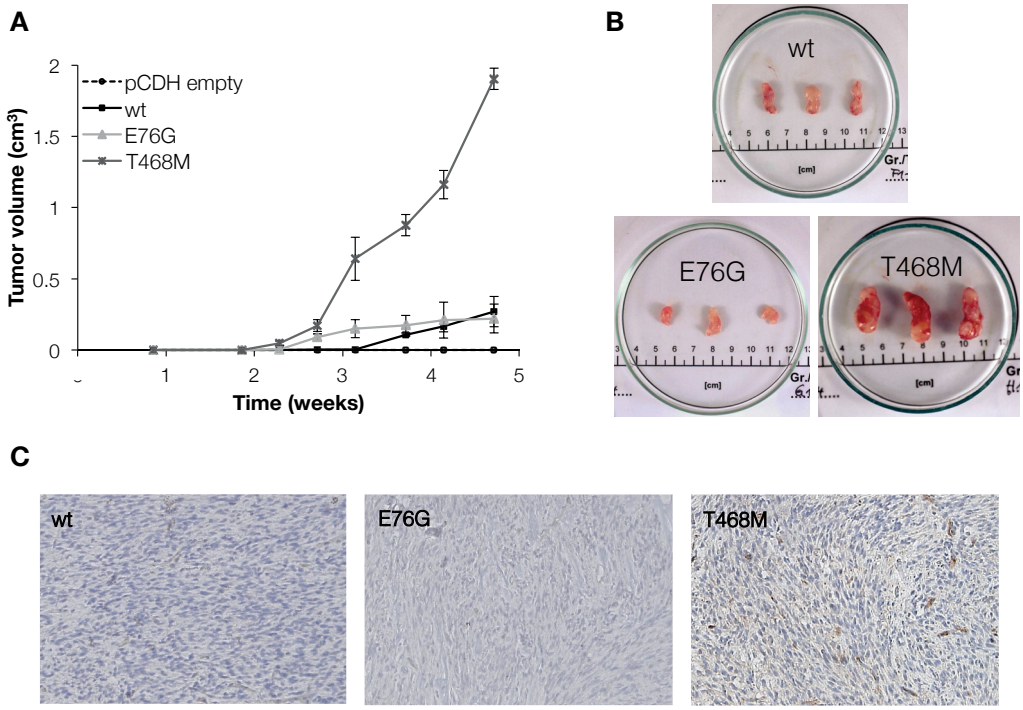

Figure 2.17: SHP2 mutations promote tumor growth in nude mice. (A) Time course analysis of tumor growth after subcutaneous injection of 1x10^6 cells that stably expressed either the control vector pCDH empty or the SHP2-lentiviral vectors wt, E76G or T468M. Three animals with a single flank injection were used in each group. After six weeks the tumors were excised (B) and subjected to immunohistochemistry analysis for the angiogenesis marker PECAM-1 (C).

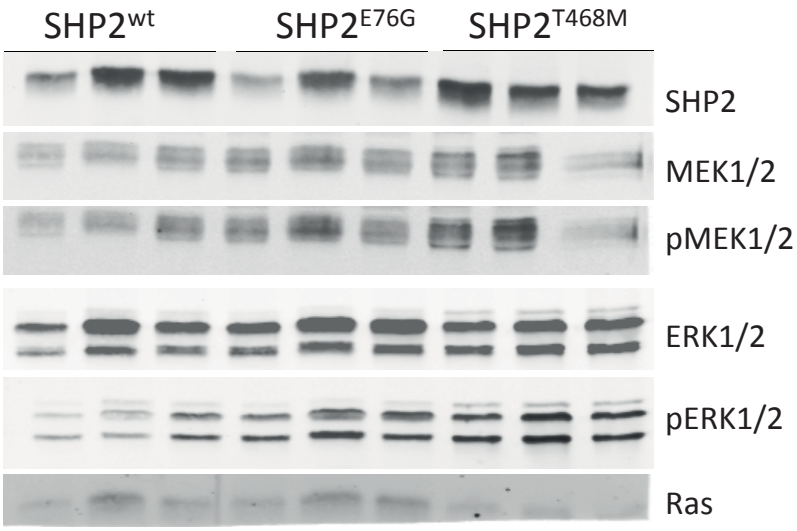

Figure 2.18: MEK/ERK activation in xenografts of rat fibroblasts carrying NS/LS-associated SHP2 mutants. Three animals were used in each group. Six weeks after subcutaneous injection of the corresponding 208F cells, the tumors were excised and subjected to lysis for protein analysis by immunoblot.

2.3 Effects on the MAPK signaling cascade

2.3.1 Signaling studies in isogenic HEK-TREx cells by Reverse Phase Protein Array (RPPA)

To investigate possible signaling perturbations as a result of mutations on SHP2 or BRAF, stable doxycycline-inducible isogenic Flp-in HEK293-TRex cells were generated (for details, see section 4.3.10). These cell lines allow an homogeneous expression of the protein of interest. The expression of the corresponding YFP-tagged protein was induced by doxycycline (dox) for 48h, and monitored by fluorescence microscopy (for SHP2 fig. 2.19 and BRAF fig. 2.20). All generated cell lines exhibited an homogeneous fluorescent pattern, an evidence of the YFP-SHP2/BRAF fusion protein expression. However, none of the SHP2 or BRAF mutations triggered any significant change on cell morphology after induction.

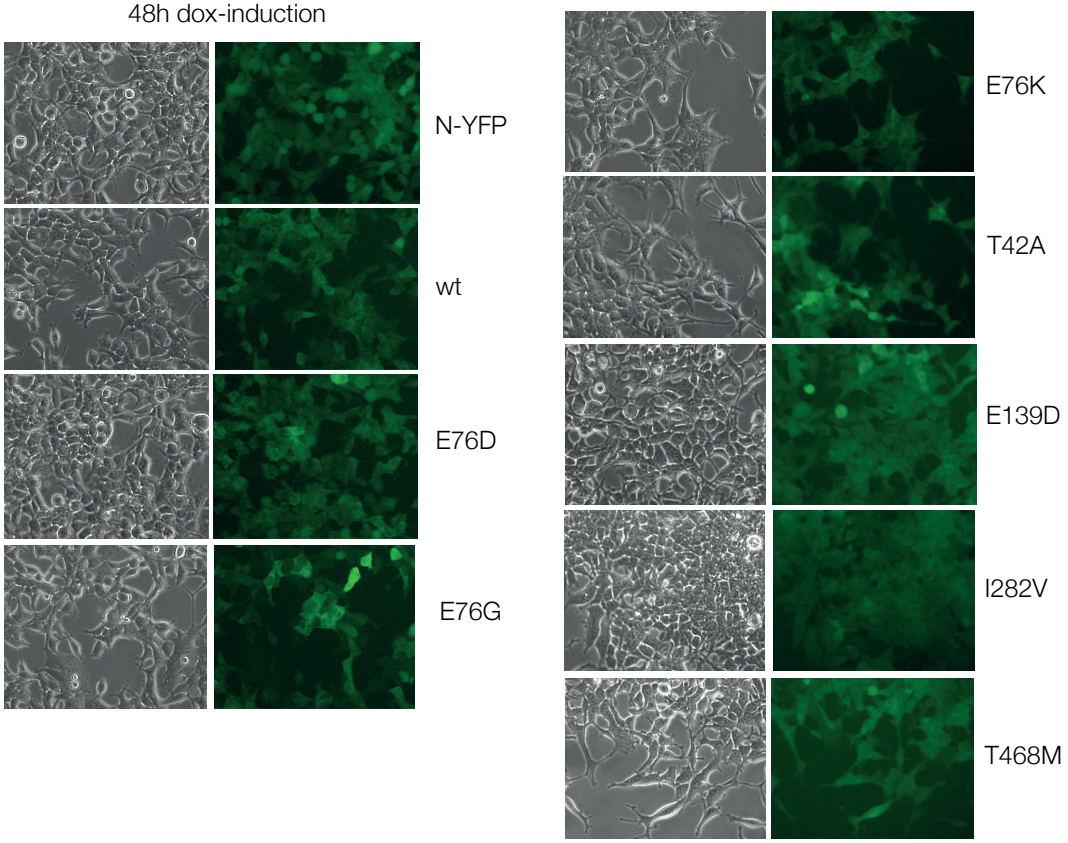

Figure 2.19: Induction of YFP-SHP2 overexpression in HEK-TREx cell lines. Isogenic HEK293-TRex cells carrying a dox-inducible YFP-tagged SHP2 were treated with doxycycline for 48h. YFP-SHP2 TRex cells were generated for posterior RPPA analysis and mRNA profiling.

Whole protein lysates were prepared in triplicate for 0h, 24h and 48h after induction and subjected to RPPA assay (in collaboration with Artur Muradyan, MPI Berlin and Julia Starmann, DKFZ Heildelberg), a quantitative approach that allows the analysis of a wide range of targets in a high-throughput manner (Spurrier et al., 2008). The

background signal generated by the second antibody was used as blank. Each signal value was normalized against the housekeeping protein GAPDH and median values were calculated. A second normalization was performed against N-YFP with or without dox for each time point.

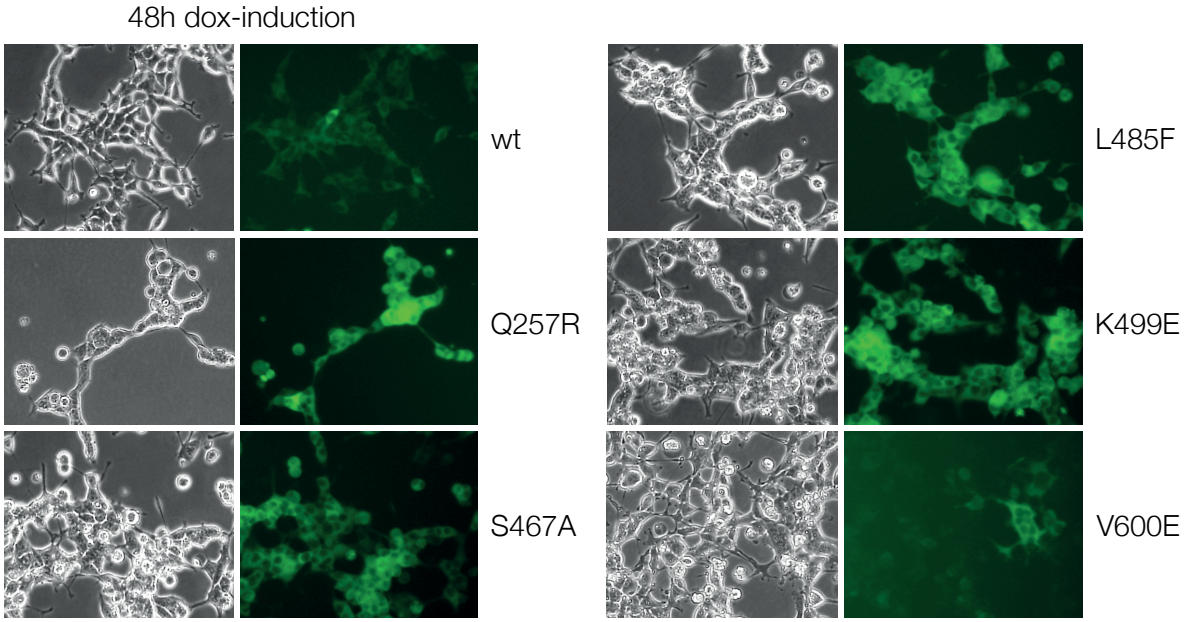

Figure 2.20: Induction of YFP-BRAF overexpression in HEK-TREx cell lines. Isogenic HEK293-TRex cells carrying a dox-inducible YFP-tagged BRAF were treated with doxycycline for 48h.

The protein expression of targets from the MAPK, mTOR, Jak/STAT and PI3K/Akt signaling pathways was evaluated (table 2.2). The role of SHP2 as an active adapter protein on the signal transduction of the mentioned pathways, particularly MAPK, has been extensively described. In *Drosophila*, the SHP2 ortologue Corkscrew (Csw) acts downstream not only of the receptor tyrosine kinase Torso (Perkins et al., 1992) but also of the *Drosophila* epidermal growth factor receptor (DER) and the fibroblast growth factor receptor Breathless (Btl) activating the MAPK pathway (Perkins et al., 1996; Hamlet and Perkins, 2001; Wilson et al., 2005). Additionally, the positive function of SHP2 upstream of the MAPK pathway has been demonstrated to be essential during the embryogenesis of *Xenopus* (Tang et al., 1995) and the vulva morphogenesis in *C. elegans* but with a negative function in the PI3K/Akt signaling cascade in this latter organism (Gutch et al., 1998; Hopper, 2006). Moreover, SHP2 is not only required for a sustained MAPK activation during mouse development but also it is implicated in the enhanced Erk activation in defective embryonic tissues in a mouse model for Noonan syndrome (Saxton et al., 1997; Araki et al., 2004).
Recently, SHP2 was also described as a key component of the Jak/STAT pathway in the pathogenesis of *H. pylori* (Hatakeyama, 2006a; Lee et al., 2010), during hematopoiesis and leukemia development (Zhang et al., 2004; Yu et al., 2003; Grossmann et al., 2010). In contrast, SHP2 acts as a negative regulation in the mTOR pathway in fibroblast cell growth and rat cardiomyocytes (Zito et al., 2007; Marin et al., 2008).

Table 2.2: Protein targets selected for RPPA analysis

Signaling pathway	Targets
MAPK	MEK1/2, pMEK1/2, ERK1/2, pERK1/2, Ras, Braf, SHP2
mTOR	mTOR, pmTOR, p70S6K, p-p70S6K
JAK/STAT	STAT3, pSTAT3
PI3K/Akt	Akt, pAkt, PI3K-p85α, PI3K-p110α/β, GSK3α/β , pGSK3α/β

The ectopic expression of YFP-SHP2 fusion protein was measured in all three time points (0, 24 and 48h). Surprisingly, no differential expression was observed in any of the induced SHP2-cell lines (fig. 2.21A, *left*). The same result was obtained for pERK1/2 (fig. 2.21A, *center*) and pAKT (fig. 2.21A, *right*) as well as for the additional targets (Appendix A.1-3). Since the dox-induced cell lines previously showed a clear fluorescence pattern after 48h of induction, a validation by immunoblot with the same protein lysates was performed. The corresponding intensity value for each band was quantified and normalized to GAPDH, followed by a second normalization against the N-YFP intensity value for each time point, as also performed with the RPPA data. In contrast to the obtained results by the RPPA assay, a significant YFP-SHP2 protein expression, was observed in all cell lines after 24h and 48h of dox treatment that was at least 20-fold higher compared to the control cell line expressing N-YFP (fig. 2.21B, *left*).
In the case of ERK1/2 activation, a strong protein expression was observed after 24h of induction, specially in cells expressing wt, E76D, E139D and I282V that dropped after 48h. Interestingly, Cells carrying the loss-of-function mutant T468M showed a sustained increase of phosphorylated ERK1/2 (fig. 2.21B, *center*). Again, these results did not correlate with those obtained by the RPPA assay. Conversely, pAKT protein expression on western blot did not reflect any significant regulation, which correlates with the RPPA data.
In contrast, the YFP-BRAF expressing cells showed phospho-ERK1/2 and phospho-MEK1/2 protein overexpression after 24h- and 48h-induction, particularly the cell lines expressing the CFC-associated mutations S467A, L485F and K499E (Fig. 2.22A *left* and *center* and Appendix A.5). The oncogene BRAF-expressing cells (V600E) exhibited a lower YFP-BRAF and pERK1/2 protein expression than $BRAF^{wt}$ and the CFC-associated SHP2 mutants. On the other hand, Ras protein amount did not show any significant regulation after BRAF induction (Fig. 2.22A, *right*). These three targets were validated by western blot and provided similar results for the CFC-associated mutants in both YFP-BRAF and pERK1/2, but not for Ras (Fig. 2.22B). All cell lines exhibited the same downward tendency in the Ras expression after 24h induction and persisted even after 48h of induction. The RPPA analysis of the other target proteins did not show a significant difference after induction (Appendix A.4-6).

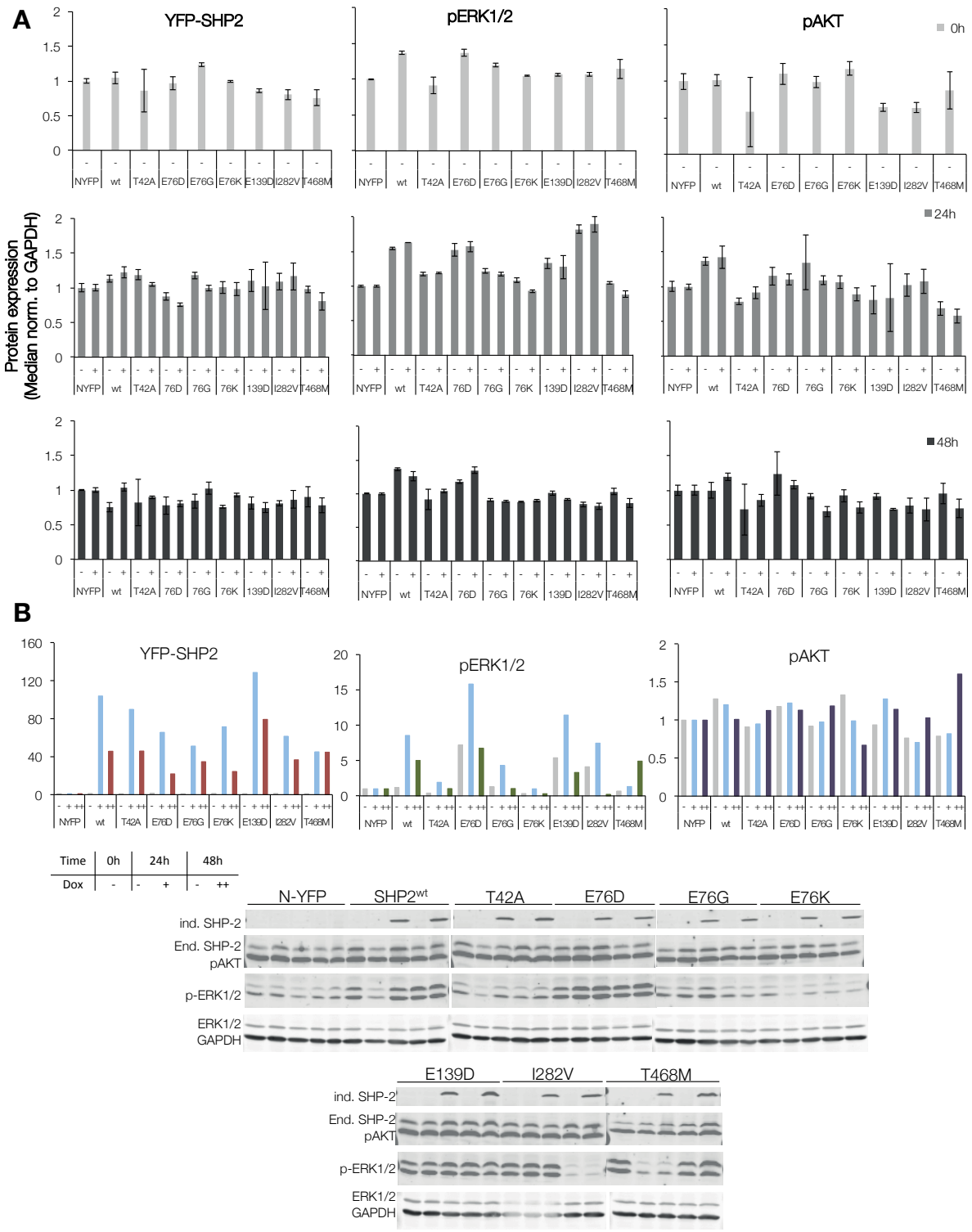

Figure 2.21: RPPA analysis of SHP2 mutations in isogenic HEK-TEx cell lines. Shown are the median values for 0, 24 and 48h of Dox induction after normalization to GAPDH and against N-YFP with or without dox for each time point and cell line (A). These data were validated using western blot (B). Data were first normalized to GAPDH and then to N-YFP. Each experiment was performed in triplicate.

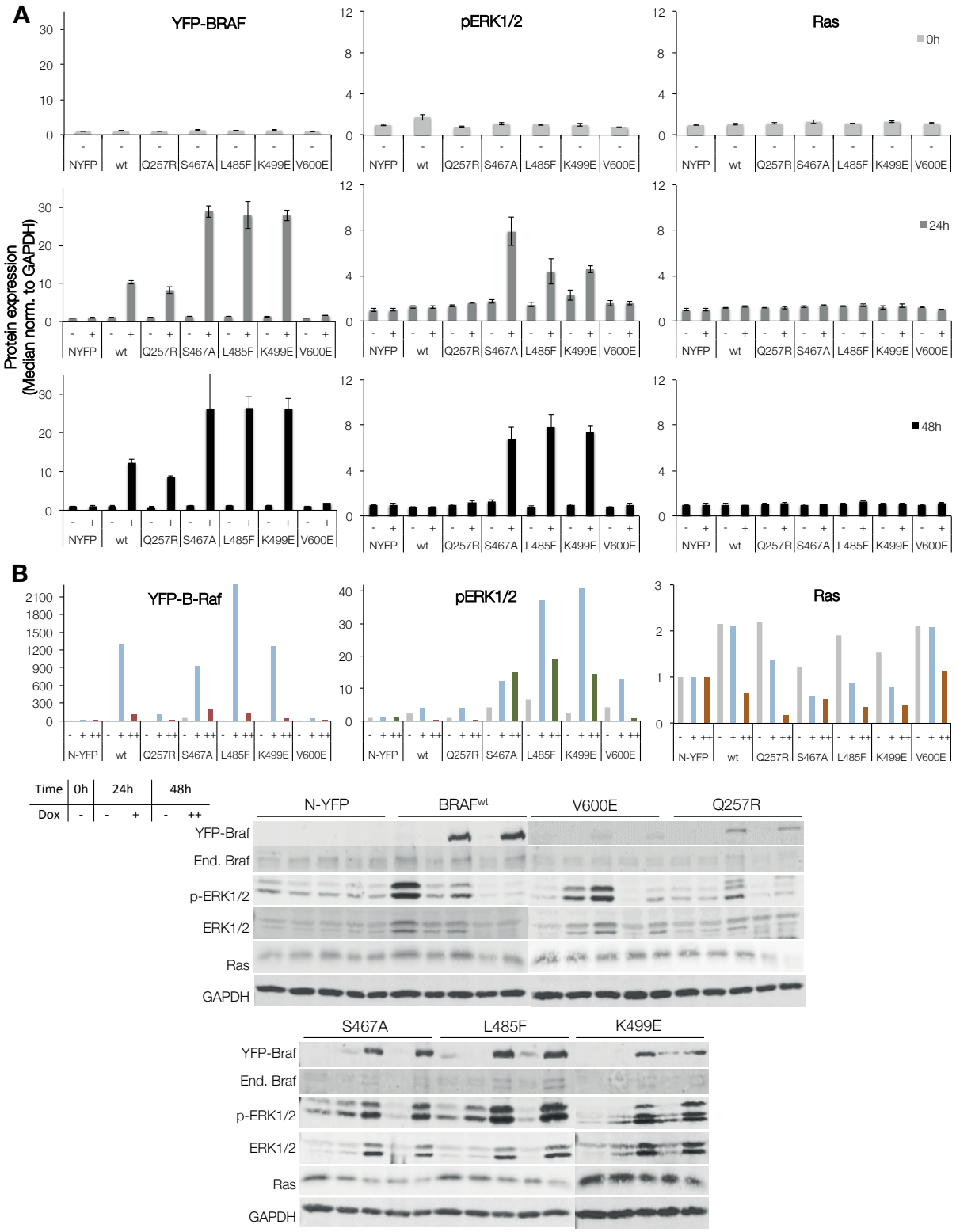

Figure 2.22: RPPA analysis of BRAF mutations in isogenic HEK-TEx cell lines. Shown are the median values for 0, 24 and 48h of Dox induction after normalization to GAPDH and against N-YFP with or without dox for each time point and cell line (A). These data were validated using western blot (B). Data were first normalized to GAPDH and then to N-YFP. Each experiment was performed in triplicate.

2.3.2 SHP2 and BRAF mutations effects on signaling in 208F cells

To further investigate whether ERK activation, as observed in the HEK-TREx cell lines, was also altered in the cell system with a transformed cellular phenotype or whether an additional molecular mechanism was involved in the phenotype output, whole lysates from each cell line were prepared and subjected to immunoblot.

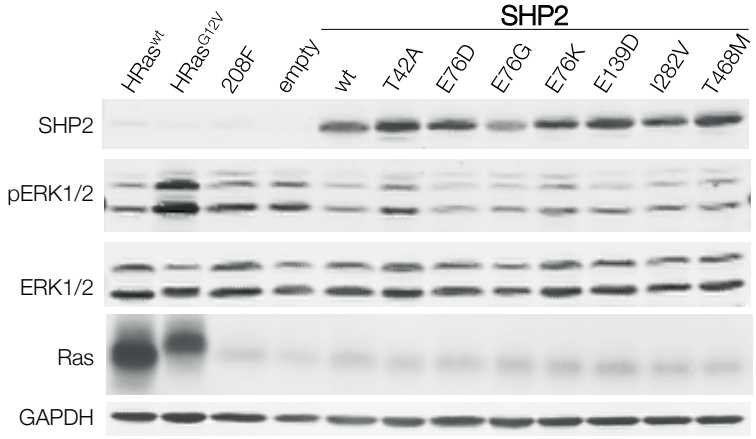

Figure 2.23: MAPK signaling after overexpression of SHP2 mutants.

Stable 208F rat fibroblast populations overexpressing either the wild-type or the mutant variant of SHP2 or BRAF were generated by lentiviral transdution and selected with puromycin. H-Ras^{wt} and H-Ras^{G12V} -expressing 208F populations were also tested and used as a control for strong pERK activation pattern. As expected, both H-Ras cell lines displayed a high pERK expression, specially cells overexpressing the oncogenic G12V mutant, compared to the parental and the 208F cells carrying the empty vector. On the other hand, SHP2^{wt} expressing 208F cells showed a slight lower pERK level than the parental- and empty-208F. Cells expressing the SHP2 mutants T42A, E76K and T468M were able to induce higher p-ERK1/2 levels compared to SHP2^{wt} expressing cells, which might be correlated with the increased number of colonies after anchorage-independent growth (fig. 2.16). Ras protein expression was homogeneous in all cell lines (Fig. 2.23). Furthermore, pAKT as well as pSTAT3 levels were considerably low to be detected (data not shown). Moreover, BRAF overxpression was detected in all BRAF-208F cell lines, with a substantial band shifting compared to cells overexpressing BRAF^{wt} (Fig. 2.24). Moreover, BRAF levels were almost identical in cells transduced with either WT-BRAF, V600E and S467A BRAF mutants, but clearly reduced in Q257R and K499E expressing cells. Both wt and oncogenic HRas expressing 208F cells showed activation of pAKT, comparable to the parental, the empty-carrying and BRAF^{wt} cell lines. pAKT activity was markedly decreased in 208F cells carrying the oncogenic V600E or CFC-associated mutations on BRAF. Furthermore, the CFC-associated mutant BRAF^{S467A} showed a strong ERK activation similar to V600E. BRAF^{K499E} pERK levels resulted lower than

the other BRAF mutants, but comparable to H-Ras^{wt}. This observations correlated with the increased cell growth proliferation rate compared to the parental and empty-vector expressing cells (fig. 2.15). On the other hand, BRAF^{Q257R} exhibited a reduced ERK phosphorylation compared to BRAF^{wt} expressing and the parental 208F cells. Additionally, increased Ras protein levels could only be detected for H-Ras^{wt} and H-Ras^{G12V}.

Altogether, these results showed that Noonan-, LEOPARD- and Leukemia-associated SHP2 mutations modulate positively ERK activation, albeit in a lower level, in rat fibroblasts, while CFC-associated BRAF mutations exhibited a stronger positive influence not only on the MAPK pathway, but also a negative effect on AKT phosphorylation.

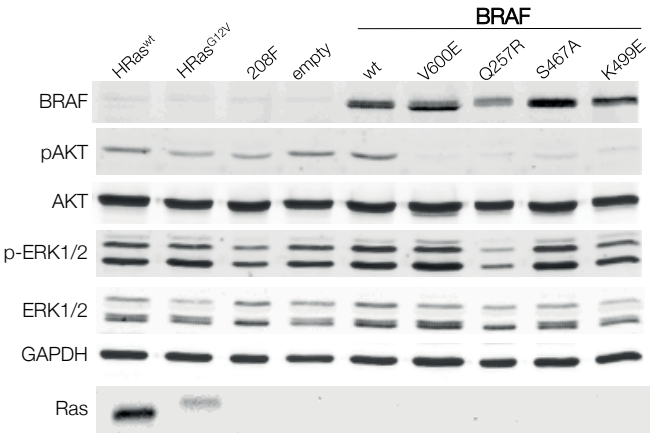

Figure 2.24: MAPK signaling after overexpression of BRAF mutants.

2.4 Effects of mutations in SHP2 on Protein-protein interactions

2.4.1 Yeast Two-Hybrid Assay

Next, to investigate whether protein-protein interactions were affected by mutations in SHP2, a yeast two-hybrid (Y2H) screening was performed for SHP2^{wt} (Sean-Patrick Riechers, MDC Berlin). First, a meta-database retrieve in the Search Tool for the Retrieval of Interacting Genes/Proteins (STRING, version 9.1, Franceschini et al. (2013)) and in the Unified Human Interactome (UniHI, version 7, Kalathur et al. (2014)) predicted 212 and 301 interaction partners, respectively. When results from both databases were compared, 146 common targets were found (fig. 2.25 *top left*; for the complete list of targets, see Appendix A.2). From these, 18% of the protein partners were clustered as Tyr-protein kinases (26 proteins), followed by the cytokine receptor family and immunoglobulin superfamily (Fig. 2.25 *right*).
The yeast two-hybrid screening for SHP^{wt} was performed in 4 repetitions against a prey library with approximately 17.000 components. From this assay, 70 interacting partners were found, but only one protein (TYK2) matched the components of the meta-database survey to characterize potential interaction partners (fig. 2.25 *bottom left*). To prioritize

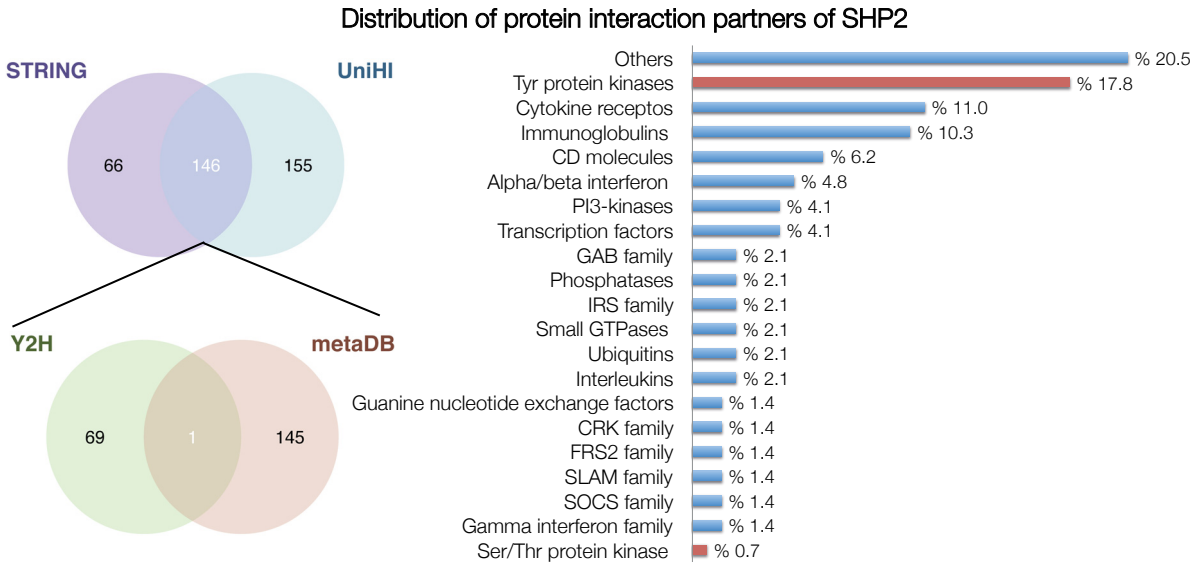

Figure 2.25: Comparison of Meta-database search of experimental/predicted protein partners. 146 binding proteins were found to overlap both STRING and UniHI databases (top left) and sorted in protein family groups (right). Then, the preys obtained from the yeast two-hybrid assay were contrasted with this group, finding a single prey matching the interaction partner list for SHP2.

interacting proteins, a Support Vector Machine (SVM) score for predicting protein-protein interactions was calculated. The SVM score considered true or false assumption between known interactions and random protein pairs in the seven dimensional scoring space: 1). the gene-atlas based co-expression scoring, 2). known orthologous protein-protein interaction scoring, 3). protein domain complementarity analysis, 4). and 5). biological process and cellular component GO term semantic similarity scoring, 6). and 7). shortest path analysis number and length scoring. Interaction protein pairs were classified into high confidence (HC), medium confidence (MC) or low confidence (LC), according to the SVM score. Protein interactions classified as high confidence are listed in the table 2.3 (for the complete interaction partners list, see table A.10).

Protein-protein interactions with the preys MSRB2, PI4KAP2, TYK2, ANKRD22, NLK, MYEOV, TCTE1, PTPRO, TOX2 and MEI1 reached a SVM score of more than 0.90. Nevertheless, these proteins not only belong to different protein families, but also they have not been predicted or described to be related to SHP2 to any extend. TYK2, a member of the Janus (JAK) kinases that precipitates with SHP2, was found to have no influence on SHP2 phosphorylation in human fibrosarcoma cells (Schaper et al., 1998). A search in different protein-protein interaction databases (UniHI, STRING) of the HC-identified proteins showed that they do not interact with each other. Moreover, five proteins (TYK2, NLK, MYEOV, PI4KAP2 and TOX2) share the common interaction partner Ubiquitin C (UBC), which have been reported as a common false positive in Y2H-assays. Additionally, the remaining proteins comprised a diverse group. MSRB2, a mitochondrial enzyme with methionine sulfoxide reductase properties (Ugarte et al., 2013), PTPRO is a transmembrane protein tyrosine phosphatase recently found to be methylated in several cancer types (Hsu et al., 2013; Huang et al., 2013; Yu et al., 2012), ANKRD22 encodes a membrane integrated protein with unknown biological function,

MEI1 is mainly expressed in testis and is involved in meiotic synapsis (Li and Schimenti, 2007) and TCTE1 is expressed in early stages of the spermatogenesis but its function is still unknown (Juneja et al., 1998).
Due to the large number of false positives, and the lack of detection of well-described SHP2 binding partners, the yeast two-hybrid results were not further considered. Instead, a tandem affinity purification (TAP) assay was performed.

Table 2.3: High confidence preys from the yeast two-hybrid assay with $SHP2^{wt}$ as bait.

GeneID		Prey (Protein ID)	Protein name	Svm score	Function (STRING)	Predicted functional partners (STRING)
Bait	Prey					
5781	22921	MSRB2	methionine sulfoxide reductase B2	1.19	Catalyzes the reduction of free and protein-bound methionine sulfoxide to methionine	MSRA, CALM1, TXN, CLCN1, PRDX5
5781	375133	PI4KAP2	phosphatidylinositol 4-kinase, catalytic, alpha pseudogene 2	1.15	Acts on phosphatidylinositol (PtdIns) in the first committed step in the production of the second messenger inositol- 1,4,5,-trisphosphate	PIK3R1, PIK3R2, PIK3C3, CDIPT, PIK3C2B, PLCD1, PIK3C2G, PLCD4, INPP5B, PTEN
5781	673	BRAF_1799TA	v-raf murine sarcoma viral oncogene homolog B1	1.02	Involved in the transduction of mitogenic signals from the cell membrane to the nucleus	HRAS, MAP2K2, KRAS, RAF1, NRAS, MAP2K1, YWHAB, CCND1, RAP1A, MAPK3
5781	7297	TYK2	tyrosine kinase 2	1.02	Probably involved in intracellular signal transduction by being involved in the initiation of type I IFN signaling.	IFNAR1, STAT1, SOCS3, STAT3, IFNG, STAT5A, STAT2, IL4, IL23A, IL12RB1
5781	118932	ANKRD22	ankyrin repeat domain 22	1	-	-
5781	51701	NLK	nemo-like kinase	0.98	Role in cell fate determination, required for differentiation of bone marrow stromal cells. Acts downstream of MAP3K7 and HIPK2 to negatively regulate the canonical Wnt/beta- catenin signaling pathway and the phosphorylation and destruction of the MYB transcription factor.	MYB, LEF1, STAT3, MYBL1, MAP3K7, TCF7L2, TCF7L1, GPI, TAB2, AMFR
5781	26579	MYEOV	myeloma overexpressed (in a subset of t(11;14) positive multiple myelomas)	0.97	-	CTTN, CCND1, TPCN2, SLC25A26, ANO1
5781	202500	TCTE1	t-complex-associated-testis-expressed 1	0.97	-	HSP90AB1, DYNLT1
5781	5800	PTPRO	protein tyrosine phosphatase, receptor type, O	0.96	-	PTS, PRODH2, SYNPO, ACTN4, NPHS2, WT1, TCF21
5781	84969	TOX2	TOX high mobility group box family member 2	0.94	Putative transcriptional activator involved in the hypothalamo-pituitary-gonadal system	ZNF461, ST5
5781	150365	MEI1	meiosis inhibitor 1	0.94	Required for normal meiotic chromosome synapsis. May be involved in the formation of meiotic double-strand breaks (DSBs) in spermatocytes	SPO11, DMC1
5781	11019	LIAS	lipoic acid synthetase	0.84	Catalyzes the radical-mediated insertion of two sulfur atoms to the lipoyl domains of lipoate-dependent enzymes.	LIPT1, LIPT2, TFB2M, C19orf26, TFAM, ALB, UCN3, AES, TFB1M, KLHDC2
5781	3064	HTT	huntingtin	0.84	May play a role in microtubule-mediated transport or vesicle function	HIP1, HAP1, ZDHHC17, OPTN, HIP1R, TCERG1, GAPDH, REST, SH3GL3, TRIP10
5781	343263	MYBPHL	myosin binding protein H-like	0.46		PSRC1, CELSR2
5781	23436	CELA3B	chymotrypsin-like elastase family, member 3B	0.37	Efficient protease with alanine specificity but only little elastolytic activity	SP8, BAT3, PHF1
5781	999	CDH1 _1108GC	cadherin 1, type 1, E-cadherin (epithelial)	0.37	Involved in mechanisms regulating cell-cell adhesions, mobility and proliferation of epithelial cells. Has a potent invasive suppressor role.	CTNNB1, CTNNA1, CTNND1, JUP, PSEN1, KLRG1, ZEB1, ZEB2, VCL, CBLL1
5781	29934	SNX12	sorting nexin 12	0.31	May be involved in several stages of intracellular trafficking	SNX12
5781	23769	FLRT1	fibronectin leucine rich transmembrane protein 1	0.24	May have a function in cell adhesion and/or receptor signaling	-
5781	10227	MFSD10	major facilitator superfamily domain containing 10	0.19	Confers cellular resistance to apoptosis induced by the non-steroidal anti-inflammatory drugs indomethacin and diclofenac.	-
5781	5519	PPP2R1B	protein phosphatase 2, regulatory subunit A, beta	0.16	The PR65 subunit of protein phosphatase 2A serves as a scaffolding molecule to coordinate the assembly of the catalytic subunit and a variable regulatory B subunit	PPP2CA, PPP2R5A, PPP2CB, PPP2R5C, PPP2R2A , PPP2R2D, PPP2R2B, PPP2R4, STRN3, STRN

SVM score: support vector machine scoring (see text for details). Database search parameters for predicted functional partners: high confidence (0.7). For the complete Y2H-prey list, see Appendix B.5.

2.4.2 Tandem Affinity Purification assay

In order to contrast the results obtained from the yeast two-hybrid assay, a tandem affinity purification (TAP) assay was performed. In addition to SHP2^{wt}, it was tested whether mutations on SHP2 had an effect on protein-protein interactions. For this assay, isogenic dox-inducible cell systems were generated from HEK-TREx cells, expressing a TAP-SHP2^{wt} fusion protein or the corresponding mutants. The TAP tag consists of a calmodulin binding peptide (CBP), the tobacco etch virus (TEV) protease cleavage site and Protein A, a construction that allows a sequential purification process. To evaluate TAP-SHP2 protein expression, HEK-TREx cell lines were dox-induced for 48h, lysed and probed by immunoblotting (fig. 2.26). In addition to SHP2, ERK phosphorylation was also tested. All HEK-TREx-cell lines overexpressed TAP-tagged SHP2 in an homogenous manner. Interestingly, cells expressing SHP2 mutants displayed an increased ERK phospholylation status in comparison with SHP2^{wt} and the negative control TAP-eGFP. Particularly cells expressing the mutant T42A showed the highest pERK levels closely followed by cells carrying mutations in the position Glu76. Together with T42A, the E76G mutant were chosen for the TAP assay.

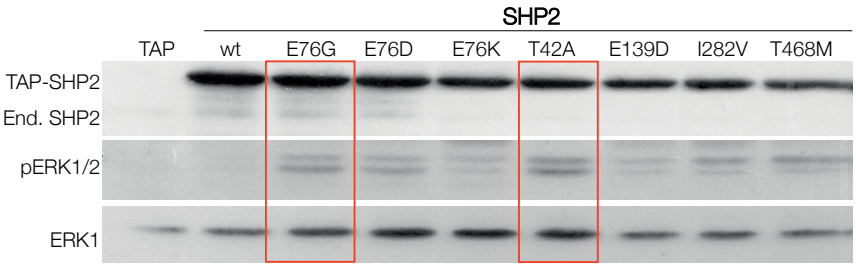

Figure 2.26: Overexpression of SHP-2-TRex cells after induction with doxycycline. Isogenic HEK293-TRex cells carrying a dox-inducible TAP-tagged SHP-2 were treated with doxycycline for 48h. TAP-SHP2 was detected by using the SHP2 and calmodulin binding antibody (CBP ab). Red rectangles show the protein expression of the mutants used for the Tandem Affinity Purification assay.

The TAP assay was performed twice with independent samples. HEK-TREx cells were induced for 48h with dox, whole protein lysates were prepared and eluted from calmodulin beads twice, followed by TCA/acetone precipitation. Then, protein pellets were resolved in SDS-PAGE for silver/coomassie gel staining prior to mass spectrometry analysis. In all three cell lines a high amount of TAP-SHP2 fusion protein was achieved (fig. 2.27A). Furthermore, not only SHP2 interacting protein partners were detected, but also the interaction strength. The interacting partners were selected according to the quantified unique spectra (qusm) with a threshold of more than 4 qusm value for each protein. To determine the fold-change of the binding strength/weakness, the ratio between mutant and wt (mutant/wt) was calculated and a threshold was set as a selection criteria for binding strength (>1.5) or binding weakness (<0.8) according to previous experiments (Gerard Joberty, Cellzome).

By comparing both TAP assays there was no overlap of decreased binding protein complexes for both mutants. However, an overlap of increased binding of six and one protein complexes were found in E76G and T42A lysates, respectively (fig. 2.27B; for the

complete list of proteins, see Appendix A.3). Among the proteins that built complexes with SHP2^{E76G} following proteins were found: one ubiquitin peptidase (USP11), two ribosomal proteins (RPS10 and RPS19), one ribonucleoprotein (HNRNPU), one helicase (DHX9), which additional to the ribosomal proteins, has been described as a common false positive in TAP experiments (Chen and Gingras, 2007) and the scaffolding protein GAB1 (3- to 7-fold). Interestingly, an increased GAB1 binding strength was also found in T42A (7- to 9-fold). GAB1 is a well-known interaction partner of SHP2. The increased binding of GAB1 to the mutated SHP2 proteins has not been yet reported.

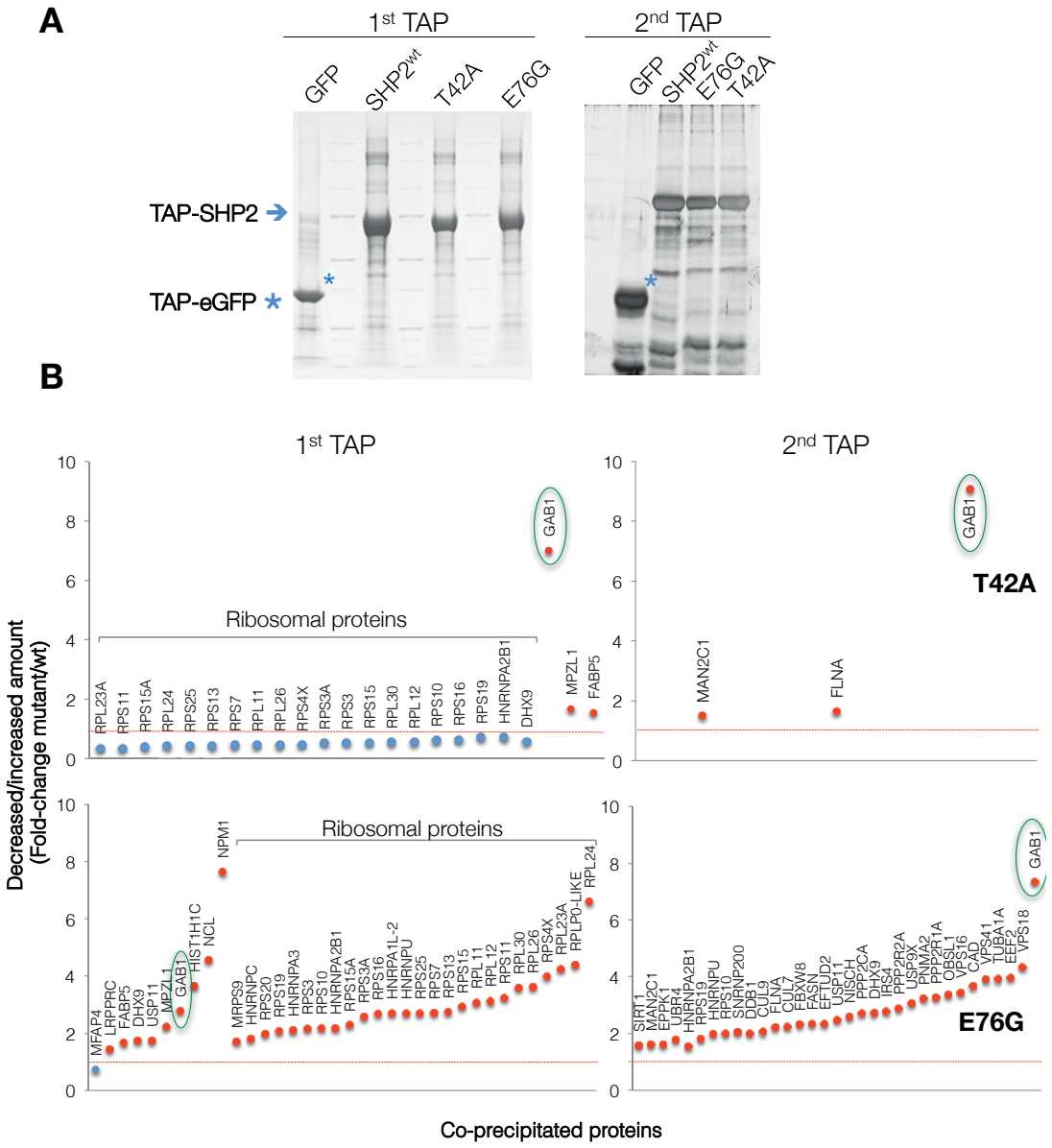

Figure 2.27: Tandem Affinity Purification (TAP) assay revealed an increased binding of SHP2 mutants to GAB1. HEK-TRex cells harboring dox-inducible TAP-tagged SHP2 expression vectors were generated. TAP-tagged SHP2^{wt}, SHP2^{T42A} and SHP2^{E76G} expression was induced for 48h and total lysates were subjected to immunoblotting and comassie/silver staining after TCA/acetone precipitation for posterior purification and mass spectrometry (A). An increased binding of SHP2^{E76G} (3- to 7-fold) and SHP2^{T42A} (7- to 9-fold) to Gab1 compared to SHP2^{wt} was observed (B).

2.4.2.1 Validation of the SHP2^{mutants}-GAB1 complex.

To confirm the altered GAB1-SHP2 binding complex detected in the SHP2 mutants by the TAP approach, a co-immunoprecipitation (co-IP) assay was performed.
First, a stable SHP2-overexpressing cell system was generated. HEK293 cells, the parental cell line of HEK-TREx (O'Gorman et al., 1991), were transduced with recombinant lentiviral particles and stable populations expressing the corresponding SHP2 proteins were generated and tested on western blot for SHP2, pERK1/2 and GAB1 protein levels (fig. 2.28). GAB1 expression was present in all cell lines, however, with an heterogeneous pattern: a stronger expression was observed in cells overexpressing SHP2^{wt}, and the mutant derivatives SHP2^{T42A}, SHP2$^{E76D/K}$, and SHP2^{E139D}, while cells expressing the mutants E76G and T468M displayed a very weak expression similar to the parental HEK293 and the control pCDH-empty cell lines. Increased ERK phosphorylation was observed particularly in cells expressing the mutants T42A and and E76K compared to wt.

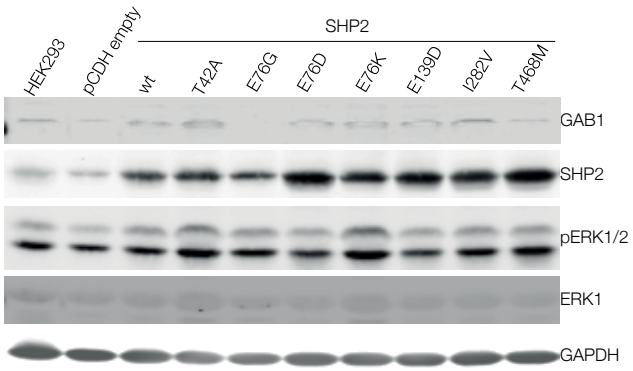

Figure 2.28: Stable SHP2-overexpressing HEK293 cells.

Subsequently, GAB1 was detected after co-immunoprecipitation with a SHP2 pull down from whole lysates of HEK293-SHP2 cell lines. In general, GAB1 co-precipitated with SHP2 in all cell lines, but not in the same manner. SHP2^{wt}, together with E76D/K SHP2 proteins were able to bind more GAB1 as the rest of the mutants, including T42A and E76G (fig. 2.29A). Although these results showed the formation of a SHP2-GAB1 protein complex, it did not answer the question of the eventual increased binding strength in the Noonan-associated T42A and the leukemia-associated E76G mutations. Hence, it was tested how GAB1 binding would respond under growth factor stimulation during a time course experiment. Cells were grown under normal conditions until they reached approximately 80 % confluency. Next, cells were starved for 16-18h and treated with 25 ng/ml of human epidermal growth factor (EGF) for 5, 10, 30 and 60 min. Homogeneous GAB1 protein levels were detected in the parental as well as in the pCDH-empty-carrying HEK293 cells. In SHP2^{wt} expressing cells, GAB1 reached a sustained SHP2 binding with a protein complex peak between 10-30 min after stimulation, similar to E76G, where the maximal protein amount was observed after 10 min. On the other hand, T42A SHP2 protein did not show a significant increased binding time after treatment (fig. 2.29B).

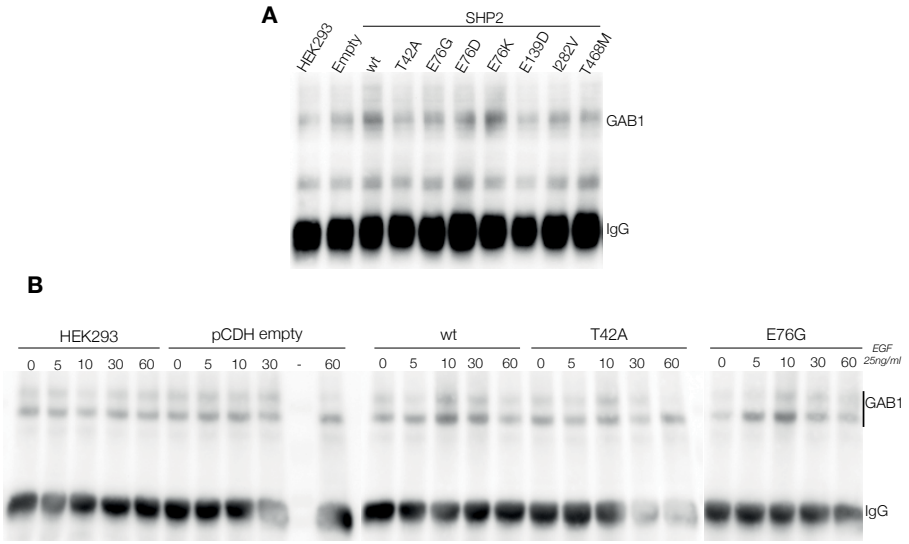

Figure 2.29: SHP2-GAB1 interaction complex in HEK293-SHP2 cells. HEK293-SHP2 lysates were subjected to co-IP after normal culture conditions with 10% FCS (without EGF stimulation) (A) or after 16-h starvation followed by 25 ng/ml EGF treatment (B).

To further investigate whether GAB1 protein binding strength was increased in SHP2 mutant proteins, 48h dox-induced YFP-HEK-TREx cells were also starved for 18h and stimulated with EGF for up to 60 min. Then, whole protein lysates were subjected to co-IP with a SHP2 antibody and GAB1 was detected by western blotting. Shortly after EGF stimulation, all SHP2-YFP expressing cell lines respond with an increased precipitated GAB1 level, but not the control eGFP-YFP. While $SHP2^{wt}$-YFP showed a sustained GAB1-SHP2 binding for 30 min that then decayed, $SHP2^{E76G}$-GAB1 displayed a constant binding for up to 1h. Additionally, $SHP2^{T42A}$ bound less GAB1 during the first 30 min, but the $SHP2^{T42A}$-GAB1 complex was bound for a longer time than E76G and $SHP2^{wt}$ (fig 2.30).

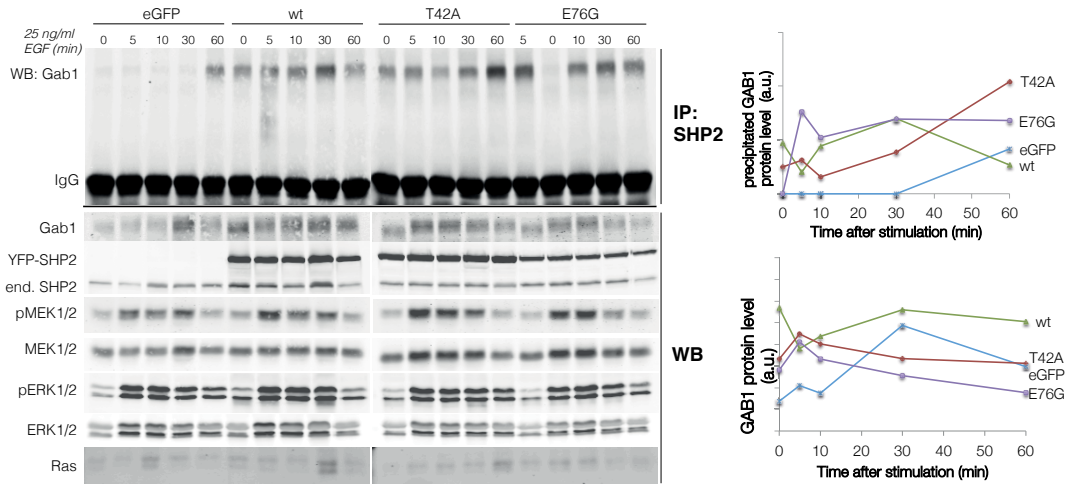

Figure 2.30: SHP2-GAB1 interaction complex in YFP-HEK-TREx cells after EGF treatment. Cell lysates were subjected to co-IP with a SHP2 antibody after 25 ng/ml EGF treatment for up to 1h, and probed on western blot. GAB1 levels after co-IP and western blot were quantified and normalized to IgG or MEK, respectively (*right diagrams*).

On the other hand, when lysates were subjected to immunoblot, GAB1 levels did not show a significant increase or decrease band intensity. However, cells overexpressing SHP2^{wt} showed a higher GAB1 protein amount than the mutant proteins (fig. 2.30 *bottom right*). Activation of the MEK1/2 was markedly stronger in T42A, while ERK phosphorylation was similar in both mutants.
Although these results indirectly suggested a stronger binding effect of SHP2-GAB1 complex with SHP2 mutant proteins and are difficult to quantify by co-IP, it clearly reflected the trend of a sustained binding that takes longer than the wild-type protein to dissociate.

2.5 Gene regulation in SHP2 and BRAF mutants at the transcription level

To determine the effects of the cancer- and RASopathies-associated mutations in SHP2 and BRAF on gene regulation, a global gene expression profiling was performed. For this aim, high-quality RNA was prepared from isogenic HEK-TRex cells expressing YFP-tagged proteins 48h after induction (see 4.2.7). Each sample was prepared in biological triplicates and hybridized on Illumina HumanHT-12 v3 Expression BeadChips. Then, raw data of all arrays, except for the BRAF-TREx^{K499E} array, which showed strong hybridization artifacts, was quantile normalized and log2-transformed. Then, all arrays were compared to the expression profile of the control YFP-HEK-TREx cell line (vs. YFP) followed by the comparison with the corresponding wild-type array (vs. wt). Significant regulated genes were selected after an adjusted p-val<0.05 and a log2 fold-change of 0.7< and >1.4 (table 2.4).

Table 2.4: Number of significant regulated genes in SHP2- and BRAF-HEK-TRex cells

Cell line		vs. YFP	vs. wt
BRAF	wt	21	-
	Q257R	30	266
	S467A	472	1758
	L485F	1075	1875
	V600E	544	1033
SHP2	wt	645	-
	T42A	3	124
	E76D	41	22
	E76G	87	221
	E76K	22	33
	E139D	6	196
	I282V	98	177
	T468M	4	550

Each value represents the number of Illumina-ID probes obtained after an adj. p-val<0.05 and a log2 fold change of <0.7 and >1.4.

Overall, the number of differentially regulated genes in the BRAF-expressing cell lines was distinctly higher than in the SHP2-TREx group.

2.5.1 Overlapping gene sets within BRAF- and SHP2-HEK-TREx

To determine whether mutations on SHP2 or BRAF have an influence on similar targets at the transcription level, all groups were analyzed for gene sets commonly regulated within both BRAF and SHP2 TREx cell lines. An overlap analysis showed that 230 genes were commonly regulated in CFC-associated BRAF expressing TREx cells (fig. 2.31 A, *top left*). When these CFC-associated BRAF profiles were compared to the profile of the oncogenic mutation BRAF^{V600E}, 156 genes were found commonly regulated (fig. 2.31 A, *top right*). On the other hand, a first glance analysis of the SHP2 group revealed no commonly regulated targets. However, a second analysis omitting the SHP2^{E76D} and SHP2^{E76K} arrays, which displayed only 22 and 33 regulated genes, respectively, showed 31 differentially regulated genes (fig. 2.31 B, *bottom left*). Interestingly, the genes *CDH1*, *CDH3*, involved in cell-cell adhesion and cell proliferation, were upregulated in

the compared SHP2 cluster (Appendix A.4, table A.13). However, when this set of 31 genes were compared to the oncogenic BRAF^{V600E} gene profile, only a target, that did not match any annotated gene (ILMN_1862013), was found to be regulated.
Comparing each single SHP2 profile against BRAF^{V600E}, additional targets were revealed. From all SHP2 mutants, T468M had the largest group of overlapping genes with the oncogenic BRAF (Appendix A.4, table A.15). Among this group, the gene *TSPAN7*, encoding for the tetraspanin 7, and *IRS4*, encoding the insulin receptor substrate 4, were found to be upregulated in both SHP2^{T468M} and BRAF^{V600E} (both 0.9 and 0.7/0.9 logFC in T468M/V600E over wt, respectively).

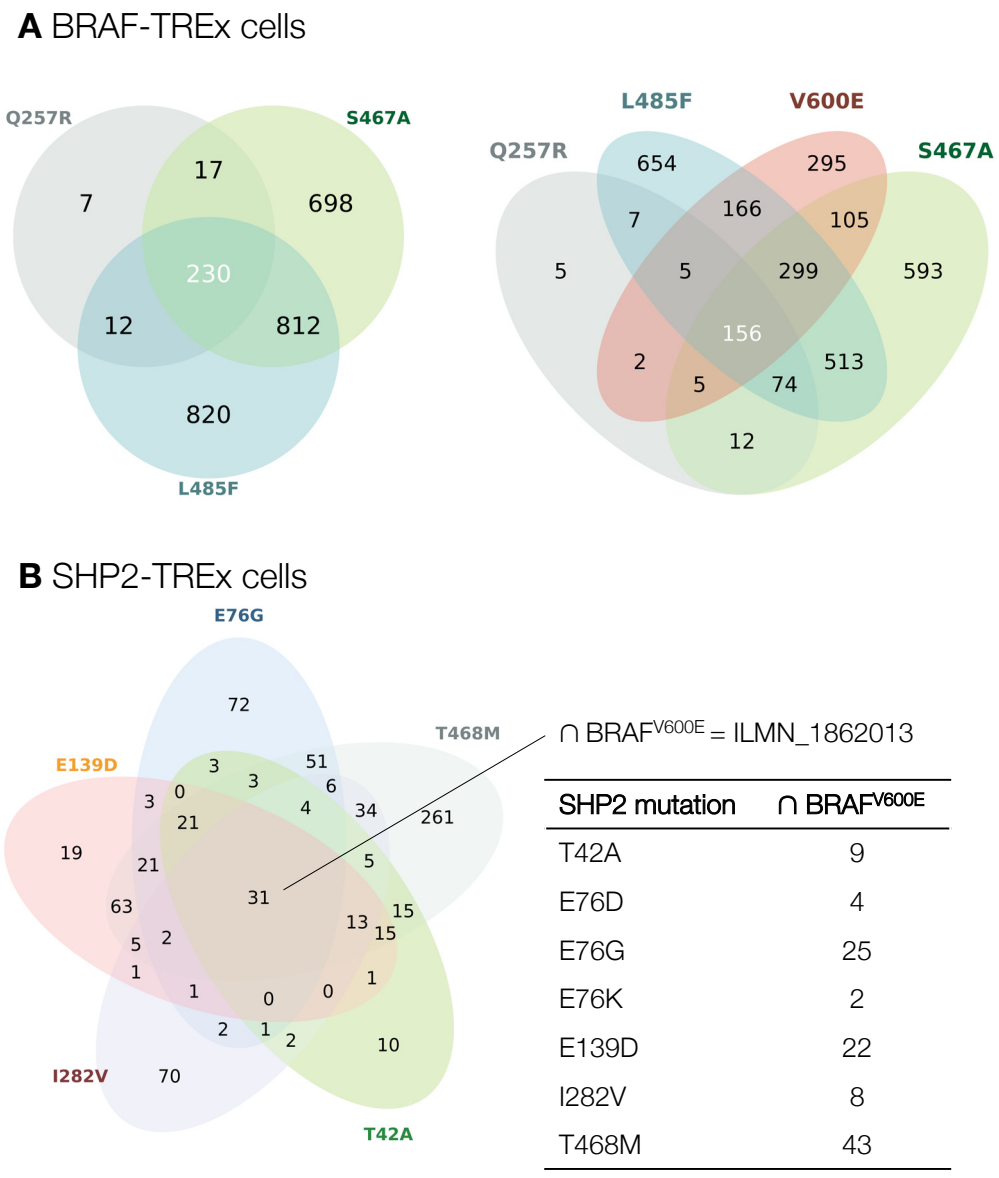

Figure 2.31: Common targets in SHP2- and BRAF-TREx expression profiles. Significantly regulated genes (Illumina probe IDs) were compared within each CFC-associated BRAF arrays (A) and cancer- and NS/LS-associated SHP2 arrays (B). Additionally, the ID probes that were commonly regulated in CFC-associated gene profiles were compared with the oncogenic BRAF mutation V600E. Differentially regulated genes in SHP2 mutant profiles were also compared to V600E, but only a single probe (ILMN_1862013) was found.

2.5.2 Overlapping gene sets within CFC-associated mutants and oncogenic BRAF

The differential regulated genes in both CFC-associated BRAF mutants and the oncogenic $BRAF^{V600E}$, were subjected to GO analysis for a better understanding of their biological significance (fig. 2.32 and appendix A.4, table A.15). From the 156 commonly significant probes of the BRAF mutants, 128 corresponded to annotated genes. The GO analysis was performed using the WEB-based Gene Set Analysis Toolkit (WebGestalt) with a Benjamini-Hochberg multiple test adjustment (adj. p-val <0.05) and a minimum of two genes for each category. Most of the hits were classified in the biological process (BP) GO terms response to stimulus (GO:0050896), organ development (GO:0048513) and cell differentiation (GO:0030154). Interestingly, the most proximal CFC-associated mutant to V600E was Q257R, followed by L485F and S467A in the cell differentiation cluster. The transcription factors *JUNB*, *STAT1*, *HEY1* and *CYR61*, were upregulated in all BRAF groups. In contrast, the tumor suppressor *TP53* was downregulated in both CFC-associated mutants and oncogenic V600E, as well as *MAP2K2* and *DVL1*.

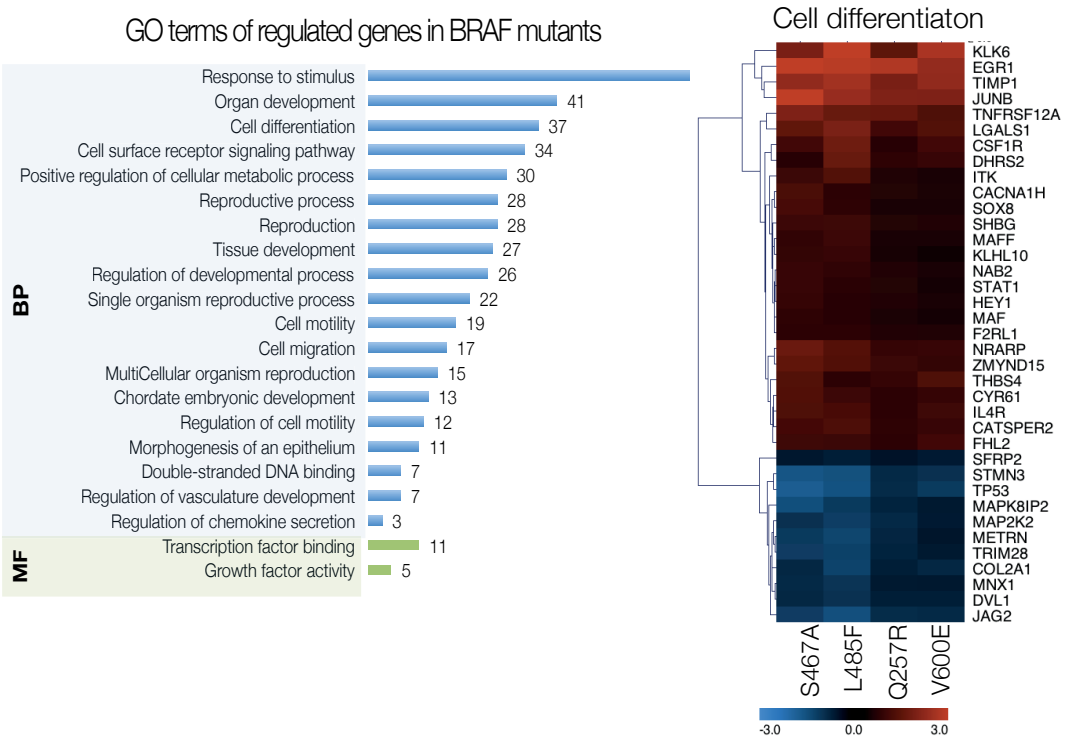

Figure 2.32: GO analysis and heatmap of commonly regulated genes in CFC-associated and V600E BRAF HEK-TREx cells. Shown are GO terms with an adj. P-val <0.05. The hits found under the GO term "cell differentiation" (GO:0030154) are represented in the heatmap.

To investigate which pathways are particularly affected by single mutations in the CFC- and cancer-associated BRAF cluster, the gene IDs were contrasted with 27 signaling pathways reported in the Kyoto Encyclopedia of Genes and Genomes (KEGG) database. From the 128 gene IDs, 18 genes matched at least one of the resulting seven signaling pathway, being the most representative the Ras-MAPK and the PI3K signaling cascades

(table 2.5).

In summary, these results provide interesting insights in the gene regulation of SHP2 and BRAF mutations associated with RASopathies and cancer. NS/LS-associated SHP2 mutations expressed in HEK-TREx cells did not show a significant influence on gene transcription. In contrast, CFC-associated BRAF mutations showed a cluster of genes that overlap with the BRAF oncogene V600E. Further validation analysis would clarify the role of the regulated genes in each case.

Table 2.5: Signaling pathways affected by CFC- and cancer-associated BRAF mutations

KEGG pathway	Pathway ID	Gene name	
Hematopoietic cell lineage	hsa04640	IL4R	interleukin 4 receptor
		CD44	CD44 molecule
		CSF1R	colony stimulating factor 1 receptor
HIF-1	hsa04066	MAP2K2	mitogen-activated protein kinase kinase 2
		NOS3	nitric oxide synthase 3 (endothelial cell)
		TIMP1	TIMP metallopeptidase inhibitor 1
PI3K-Akt	hsa04151	TP53	tumor protein p53
		COL2A1	collagen, type II, alpha 1
		MAP2K2	mitogen-activated protein kinase kinase 2
		THBS4	thrombospondin 4
		IL4R	interleukin 4 receptor
		CSF1R	colony stimulating factor 1 receptor
		NOS3	nitric oxide synthase 3 (endothelial cell)
Ras-MAPK	hsa04014, hsa04010	TP53	tumor protein p53
		MAP2K2	mitogen-activated protein kinase kinase 2
		MAPK8IP2	mitogen-activated protein kinase 8 interacting protein 2
		CACNA1H	calcium channel, voltage-dependent, T type, alpha 1H subunit
		CSF1R	colony stimulating factor 1 receptor
		FOS	FBJ murine osteosarcoma viral oncogene homolog
Toll-like receptor	hsa04620	MAP2K2	mitogen-activated protein kinase kinase 2
		STAT1	signal transducer and activator of transcription 1
		FOS	FBJ murine osteosarcoma viral oncogene homolog
VEGF	hsa04370	MAP2K2	mitogen-activated protein kinase kinase 2
		NOS3	nitric oxide synthase 3 (endothelial cell)
		SPHK1	sphingosine kinase 1
Wnt	hsa04310	TP53	tumor protein p53
		DVL1	dishevelled segment polarity protein 1
		SFRP2	secreted frizzled-related protein 2

Commonly regulated genes in CFC- and cancer-associated BRAF mutants were compared to all signal transduction pathways listed in the KEGG database. Signaling pathways with at least three genes are listed here.

3 DISCUSSION

The Ras/MAPK signaling pathway is a key network that is involved in cell proliferation, differentiation and survival. Alterations in its regulation are related to cancer and the recently described RASopathies, a variety of developmental disorders caused by germline mutations in genes that encode regulator proteins or components of this signaling cascade. Gene sequencing studies in the early 2000′s, almost 40 years after the first reports on clinical features describing the Noonan syndrome, showed that germline mutations in the genes *PTPN11*, *RAF1*, *NRAS*, *KRAS*, *SHOC2*, *SOS1*, *BRAF* and *CBL* were associated with this disorder (Sarkozy et al., 2009). Furthermore, patients with neurofibromatosis, Noonan, Costello, Legius and CFC syndrome show predisposition to some types of cancer (Rauen, 2013).
Although somatic mutations associated with cancer have been phenotypically well characterized, it is still unclear whether RASopathies-associated mutations have the potential for oncogenic transformation. Therefore, the aim of this work was to investigate the influence of leukemogenic and RASopathies-associated mutations in SHP2 and BRAF on the cellular phenotype.

3.1 Phenotype comparison of SHP2 in human cell lines

To assess the outcome of single mutations, finding a suitable cell model was crucial step. To date, the availability of an appropriate human cell system that resembles the normal, non-transformed state of human cells is limited, considering that many of the immortalized cells were obtained by expression of the SV40 large T antigen to prolong life span. As side effect, SV40-transformed phenotype includes altered cell proliferation, density- and anchorage-independent growth (Ahuja et al., 2005). Moreover, primary cell lines are difficult to obtain and keep under culture conditions for a prolonged time due to the inherent feature of diploid cells to reach growth arrest and become senescent (Hayflick and Moorhead, 1961).
Here, different cell lines of human and rat origin were tested for transduction efficiency and versatility in transformation phenotype and functional assays. Each cell line was transduced with lentiviral particles carrying mutant SHP2, BRAF and H-Ras variants. Initially, the human kidney epithelial HA1EB cell line expressing mutant and wild-type SHP2 displayed a flattened morphology, similar to the parental cell line and HA1EB$^{pCDH-empty}$ (fig. 2.7). In contrast, HRas-HA1EB and BRAF^{V600E}-expressing HA1EB cells, used as a positive oncogenic transformation phenotype, showed a clear cell

density-independent growth. Mutant and wt BRAF-HA1EB expressing cells exhibited an apparent reduced cytoplasmic area compared to the parental cell line, with a moderate crisscross arrangements where cell confluency was higher.
HA1EB was originally obtained after a two-step transfection with the SV40-ER followed by the hTERT gene, and described as near-diploid (44% diploid, 42% tetraploid, and 14% intermediate) without anchorage-independent growth in soft agar (Hahn et al. (1999); Zimonjic et al. (2001); Andrea Solf, Dissertation). This almost-euploid state might be responsible for the robust cellular phenotype and act as a protection against overexpression of the oncogene SHP2 or BRAF. Unfortunately, little is known about this cell line to date, and additional studies are difficult, as its maintainance require the permanent use of three selection markers.
The fibroblast cell line BJELB was also simultaneously tested. BJ cells were obtained after the sequential introduction of the hTERT gene, the SV40-ER and an emtpy vector (Zimonjic et al., 2001). In contrast to HA1EB, BJ cells overexpressing wt and mutant SHP2 variants drastically changed the cell appeareance to near apoptotic (fig. 2.8) and reduced cell proliferation (fig. 2.9 *left*). BJ-ELB fibroblasts lack both pRB and p53 (Hahn et al., 1999). As reported by Shinohara et al. (2006), these cells have the ability to continue the cell cycle after knocking down ERK1/2 by siRNA with an evident reduction of cytoplasmatic pERK up to 90%.
This observations, together with the cellular phenotype obtained after overexpresion of gain-of-function SHP2 variants, show that SHP2 act a robust regulator of cell morphology and proliferation as a consequence of the active saturation of the MAPK signaling cascade in BJ fibroblats.
Similar phenotypical features have been previously observed in cells infected by adeno-associated virus (AAV). The activation of the apoptosis mechanism via THOC1/Caspase-6 was described as a consequence of a defective p53 and pRb pathway and the subsequently deregulation of E2F1 (Garner et al., 2007; Pickering and Kowalik, 2006). Furthermore, a recent study suggested that SHP2, together with PTEN and PTP1B, might be directly activated by the absence of Rb/E2F1 repression, leading to cell death (Morales et al., 2014). This mechanism might explain the striking apoptotic-like phenotype observed in cells overexpressing gain-of-function proteins (T42A, E76D/G/K, E139D and I282V) and the moderate cell death in those with wt or phosphatase loss-of-function SHP2 (T468M). Interestingly, CFC-associated mutant BRAF expression in BJ fibroblasts sufficed to also decelerate cell proliferation, but in a less dramatic manner (fig. 2.9 *right*).
Additionally, the mammary epithelial cell line MCF10A overexpressing cancer- and Noonan-associated SHP2 mutants displayed a a similar phenotype as BJ cells, which involved growth arrest and morphological changes (fig. 2.10 *top*), while MCF10A cells expressing CFC-associated BRAF mutants showed a clear transformed morphology (fig. 2.10 *bottom*). MCF10A was originally obtained from spontaneous immortalized cells from adherent cells of a patient with fibrocystic disease (Soule et al., 1990; Heppner and Wolman, 1999). Due to its non-tumorigenic character, this cell line have been used to investigate oncogenic alterations. Oncogenic Ras-mediated transformation of MCF10A

was associated with increased focal adhesions, stress fibers and modified adherens junctions as a consequence of the increased tyrosine phosphorylation of β-catenin Kinch et al. (1995).
Different studies that aimed to investigate gene-specific copy number variation in MCF10A cells identified alteration in the chromosome 9, 13q21 and chromosome 20, a deletion of the *CDKN2A/B* locus, encoding for the tumor suppressor $p16^{INK4A/B}$ and *MYC* amplification (Worsham et al., 2006; Jonsson et al., 2007; Kadota et al., 2010). Both alterations confered sensitization to oncogenic-mediated transformation, as previously shown (Dawson et al., 1996) and was replicated here by the overexpression of wt and oncogenic $HRas^{G12V}$ (fig. 2.10 *top right*). Moreover, MCF10A cells overexpressing CFC-associated mutant BRAF proteins not only displayed an evident transformed phenotype, but also a moderate increased activation of the MAPK pathway (fig. 2.11). This observations, together with the growth arrest phenotype of SHP2-MCF10A, might indicate that SHP2 and BRAF regulate signaling by different pathways. BRAF mutations, regardless of its MAPK activation potential, evidently impinge a strong oncogenic phenotype in cell system models. Moreover, SHP2 mutations might not act as a driver-mutation but as a precursor alteration that could lead to the growth arrest phenotype observed in MCF10A epithelial cells and BJ-ELB fibroblasts.

3.2 Analysis of the effects of NS/LS- and leukemia-associated SHP2 mutations in rat fibroblasts

As previously discussed, it is a challenging task to find an appropriate model for the characterization of the oncogene-mediated transformation in vitro. As shown in this study, the available human cell lines with a non-transformed and non-tumorigenic phenotype, such as HA1EB, have a restricted selection marker choice as for their generation, multiple transfection plasmids were used to gene transfer genetic elements to allow the lifespan prolongation. Additionally, other cell models, such as BJ-ELB, tend to display transformed-related features under low selection conditions (absence of selection during cell culture) and high cell density. This conditions make the use of this latter cell line problematic, when oncogenic-mediated effects overlap with an spontaneous transformation of the parental cell line.
Therefore, the 208F rat fibroblasts, a non-tumorigenic non-transformed derivative of $HPRT^-$ Rat-1 cells that do not require selection markers (Griegel et al., 1986), represented an interesting choice. 208F fibroblasts are characterized by a flattened, cobblestone-like morphology and a monolayer growth on the culture flask. The expression of oncogenic proteins and evaluation by functional assays in rat fibroblasts was, in comparison with the human cell lines, more appropriate for the evaluation of mutant SHP2 and BRAF effects. The refractory character of human cells against oncogenic H-Ras transformation in vitro has been well documented (Akagi et al., 2003; Holliday, 1996). Human diploid fibroblasts require the overexpression of hTERT and the inactivation of both p53 and Rb elements to allow an elongation of life span and the expression of oncogenic proteins. In

contrast, rodent fibroblasts such as 208F, have been successfully used in oncogene studies due to its non-transformed phenotype and oncogene-mediated susceptibility (Griegel et al., 1986; Tchernitsa et al., 1999; Miller et al., 2004; Rangarajan et al., 2004).
Transient and stable wt and oncogene H-Ras overexpression in 208F led to a transformed phenotype even when the cells were transduced with small amounts of lentiviral particles (fig. 2.6, *right* and fig. 2.12, *top right*). Additionally, the transformation phenotype was proportional to the used amount of lentiviral particles.
Rat fibroblasts overexpressing mutant SHP2 displayed a density-independent growth and crisscross morphology. Interestingly, in cells carrying a gain-of-function *PTPN11* mutation not only the transformation phenotype was stronger but also cells appeared elongated than those with the loss-of-function T468M mutation (fig. 2.14). SHP2 is a regulator of the MAPK signaling cascade, and thus an important adaptor protein in the regulation of development and cell proliferation. This influence on the MAPK pathway was recently corroborated, when 208F overexpressing the NS/LS-associated mutants T42A and T468M, and the NS/leukemia-associated E76G/K mutants were treated with the MEK inhibitor U0126 and two PI3K inhibitors (LY294002 or PX-866). While the LY294002 treatment led to cell detachment of all mutant cells, MEK inhibition resulted in a regression of the oncogene-mediated transformation phenotype, characterized by a shortened cell length and a cobblestone-like phenotype similar to the parental cell line (Stefan Meltendorf, Master thesis). The influence of NS/LS-mutants on the Ras/MAPK pathway has been previously reported. For example, mouse fibroblasts NIH3T3 overexpressing E76K failed to show a transformed phenotype in a focus-formation assay (Miyamoto et al., 2008). In contrast, 208F fibroblasts overexpressing either NS/LS- or leukemia-associated mutant SHP2 displayed a density-independent growth, an increased cell proliferation and anchorage-independent growth in soft agar (figs. 2.12, 2.15 and 2.16).
LS-associated mutants has been described as catalytically impared thus loss-of-function phosphatases (Kontaridis et al., 2006). T468M-208F fibroblasts, however, displayed a transformed phenotype similar to $SHP2^{wt}$ and formed colonies in soft agar assay. Furthermore, when these cells were subcutaneously injected in nude mice, T468M gave rise to tumors even larger than those obtained from 208F cells overexpressing $SHP2^{E76G}$ (fig. 2.17A). In accordance to the present results, a recent biochemical report showed that although there is a reduced phosphatase activity, the alteration of intramolecular bindings drives SHP2 to a prolonged interaction with other adaptor proteins, guaranting the moderate but constant ERK activation (Yu et al., 2014). This effect might explain the increased MEK1/2 activation and the moderate phosphorylated ERK1/2 levels compared to wt and E76G (fig. 2.18) and perhaps this event might support the high blood vessel density observed in the xenografts from T468M rat fibroblasts (fig. 2.17 B and C).

3.2.1 Effects of SHP2 mutations on signal trasduction

One of the challenges working with high-throughput data is the concordance between the genetic background of the in vitro cell model and the biological significance of the

proposed hypothesis. Under optimal conditions, the experimental design might allow the use of the same cell system model to measure oncogene-mediated transformation, proteomics and transcriptomics.

Since this project was conceived as part of the MUTANOM consortium, human cell line models were chosen for signaling studies and transcriptomics to be in a similar species genetic background. However, as previously discussed, human cell systems are difficult to test for oncogene-mediated transformation due to the complexity of the cellular defense mechanisms (Hahn, 2002). In this case, a human cell system (isogenic HEK-TREx cells) was used for proteomics and transcriptomics, and a rat cell system (208F) was used for functional assays. One of the used tools to investigate signaling deregulation in BRAF and SHP2 mutants was the reverse phase protein array (RPPA) approach, which represents a powerful tool to explore qualitative- and quantitatively cellular signaling in a large number of samples. During this work, the high threshold detection and the specificity of the antibodies were the principal obstacles. This fact was evident when samples tested for ERK phosphorylation remained constant in three time points after induction of SHP2 expression in HEK-TREx cells, while the validation on western blot of the same samples with the same antibodies showed activation of the MAPK pathway after SHP2 induction (fig. 2.21). Additionally, as the protein presence is measured in a dot-blot platform, it is not possible to distinguish between the genuine protein signal and the background noise of unspecific bands. Here, the HEK-TREx cell line expressing a YFP-tagged protein was chosen for the analysis, due to a high background noise produced by the TAP-tag detected in isogenic HEK-TREx cells expressing a TAP-tagged protein. Nevertheless, this approach is a valuable tool in the exploration of large data, but validation by immunoblot or other method is required.

The non-receptor protein tyrosine phosphatase SHP2 is a positive regulator in many signaling cascades, including of the MAPK pathway and modulates a variety of biological processes such as embryonic development, cell proliferation, differentiation and survival (for review see Grossmann et al., 2010). As previously described, germline mutations in components of the canonical MAPK signaling cascade, including SHP2, are associated with developmental disorders that share phenotypic features. Currently, an increased incidence of cancer in patients affected by RASopathies has been documented.

To understand the influence of leukemia- and NS/LS-associated SHP2 on the MAPK signaling pathway in the transformed phenotype of preneoplastic rat fibroblasts, ERK activation was evaluated by immunoblot (fig. 2.23). Ectopic expression of SHP2 resulted in a subtle ERK1/2 phosphorylation, more pronounced in cells overexpressing the SHP2 mutants T42A, E76K and T468M. Additionally, isogenic HEK-TREx cells displayed a moderate activation of the MAPK pathway compared to the full activation in H-Ras^{G12V}-expressing cells after 24 and 48h protein induction (fig. 2.21). These mutations lead to conformational changes of the SHP2 protein, inducing to either constitutive activation or loss-of-function of the phosphatase activity. Mice transplanted with SHP2^{E76K}-transduced bone marrow developed leukocytosis, a symptom that involves increased leukocyte cell count associated with leukemia and other malignancies. Additionally,

Ba/F3 cells expressing the E76K SHP2 mutation displayed an enhanced cell motility and activation of the RhoA family small GTPases (Wang et al., 2009). These findings provide a complementary understanding of the signaling regulation by SHP2.

3.3 CFC-associated BRAF mutations confer a transformed phenotype in preneoplastic rat fibroblasts

In the case of CFC-BRAF mutations, 208F fibroblasts morphology did not differ strongly from the parental cell line. In fact, they conserved the cobblestone-like and density-dependent growth and were slightly shorter than $BRAF^{wt}$ expressing 208F cells (fig. 2.13 and 2.15). However, compared to SHP2-208F cells, mutant BRAF expression endowed rat fibroblasts with a steady growth above $BRAF^{wt}$ and cells transduced with the empty vector. Furthermore, all tested BRAF mutations induced anchorage-independent growth, forming larger colonies than those observed in mutant SHP2-expressing cells (fig. 2.16). All these features might indicate that the analyzed mutations gave rise to a transformed phenotype.
Nevertheless, previous studies aimed to functionally characterize the germline BRAF mutations T241P, W531C, L597V, E275K, T599R and K601Q associated with NS, CFC and LS. Sarkozy et al. (2009) concluded that, compared to the oncogenic V600E, the selected mutations did not confer any transfomation potential. Although the difference in the foci number between V600E and the studied germline mutations was significant, this conclusion results controversial, considering that the untransfected or empty vector-transfected cells, the NIH3T3 mouse fibroblast cell line, had the ability to form foci in the focus assay.

3.3.1 MAPK and AKT signaling impairment in CFC-associated BRAF-expressing cells

Among the studied group, cells expressing the mutant Q257R SHP2 displayed a moderate tranformed phenotype. The mutation Q257R is one of the most frequent alteration found in CFC patients and is located in the phorbol-ester/DAG-binding zinc finger motif (residues 234-280) of the cysteine-rich domain 1 (CR1) of the BRAF protein, responsible for BRAF membrane docking after interation with Ras (Morrison and Cutler, 1997). To date, there are no reports of cancer-associated mutations at this residue. However, further studies are needed to understand the relevance of the mechanism behind the phenotype observed in preneoplastic rat fibroblasts, as a mutation in this residue (Q257H) was recently reported in lung adenocarcinoma (Imielinski et al., 2012).
The mutants K499E and S467A are located in the protein kinase-CR3 domain, which responsible for the kinase activity of the BRAF protein. The mutation at S467 plays a central role in the activation of the protein. Located at the phosphate binding loop (P-loop) together with S465, S467 is described as a catalytically impared form that is able to stimulate downstream targets. A recent biochemically characterization showed that S467A had a higher catalytic activity than $BRAF^{wt}$ and were inhibited but not activated

by diffent BRAF inhibitors, meaning that the ATP activity at Ser467 is required for compound activation of BRAF (Wan et al., 2004; Holderfield et al., 2013). This might explain the oncogene-mediated transformed phenotype observed in all tested cell lines (all parental cell lines are BRAF^{wt}) and the low but constant MAPK activation compared to oncogenic V600E (fig. 2.24). There are five cases of mutations in this residue associated with cutaneous melanoma, lung adenocarcinoma (S467L) and colon carcinoma (S467P) (Seo et al., 2012; Akslen et al., 2008). Indeed, a mutation-sensitive hotspot is located in the region 459-469, which comprises mainly missense substitutions in 55 cases of different cancer types (COSMIC database). On the other hand, the mutation K499E has not been reported in cancer, nor the Lys499 residue. However, the phenotype exhibited in the functional assays implies a key role of this residue or the region for the activation of downstream factors.

A previous report found that the outcome of the impaired kinase activity, which was similar to V600E, was the activation of the downstream factors ERK and MEK (Rodriguez-Viciana et al., 2006). These findings correlate with the signaling studies performed in this work in a wide variety of cell lines: MCF10A, rat fibroblasts and HEK-TREx cells. Additionally, the transformed phenotype displayed by the CFC-associated mutant BRAF-expressing cells is directly associated with the increased catalytic activity of the mutant proteins and its subsequent MAPK pathway activation.

Moreover, cancer- and CFC-associated mutations, but not BRAF/H-Ras^{wt} or H-Ras^{G12V}, led to a reduced AKT phosphorylation in preneoplastic rat fibroblasts (fig. 2.24). The protein kinase B or PKB/AKT plays a key role in cell survival, cell proliferation and cell migration and its activation is associated with melanoma progression (Dhawan et al., 2002; Stahl et al., 2004; Song et al., 2005). However, ERK hyperactivation have been associated with impaired tuberus sclerosis complex (TSC1/2), which in a heterodimer form negatively regulate the mamalian target of rapamycin complex 1 (mTORC1). Subsequently, hyperactive ERK lead to suppression of pAKT through a negative feedback loop to the IGF-1 (Zhang et al., 2006). Furthermore, in the MLL-AF9-induced leukemia murine model, which resembles the human acute myeloid leukemia (AML), AKT was demonstrated to be repressed and FOXO, which is frequently found activated in AML patients, was active. By AKT activation or deletion of FOXO, a decrease of cell growth and promotion of apoptosis was observed (Sykes et al., 2011). Interestingly, it is claimed that CFC patients may have a predisposition to acute lymphoblastic leukemia (ALL), but this assertion is still controversial, due to the number of reported cases (van Den Berg and Hennekam, 1999; Makita et al., 2007; Rauen et al., 2011). Further studies are needed to investigate whether CFC-associated mutations are linked to a negative regulation of the mTORC and GSK3 signaling pathways.

3.4 Modified protein interactions in NS- and cancer- associated SHP2 mutations

To test whether cancer- and NS-associated SHP2 mutations generate modifications on protein-protein interactions, cells overexpressing the SHP2 mutants T42A and E76G, which significantly induced ERK phosphorylation in TAP-tagged SHP2 HEK-TREx cells (fig. 2.26), were selected For the tandem affinity purification (TAP) assay. Additionally, a yeast-two-hybrid (Y2H) assay of $SHP2^{wt}$ was performed (section 2.4.1). In the case of the Y2H assay, only one target (TYK2) coincided with the reported SHP2 interactors to date. However, previous attempts to finding SHP2 interaction partners using the same method reported overlapping interactions with GRB2 and FRS2, (Delahaye et al., 2000; Yamada et al., 2001), PDGFRB (Lechleider et al., 1993; Keilhack et al., 2001), GAB1, (Nishida et al., 1999) and GAB2 (Crouin et al., 2001; Cholay et al., 2010). Although the Y2H screening represents a valuable tool for the early identification of unknown interaction partners, the high sensitivity to bait a relevant number of false positive hits reduces substantially the confidence of the results. Furthermore, the selection of the prey library plays a crucial role in the identification of binding partners.

On the other hand, the TAP assay showed that both mutants had an increased binding strength to GRB2-associated binding protein 1 (GAB1) and later validated in co-IP experiments after EGF stimulation (figs. 2.27, 2.29 and 2.30). GAB1 is a 110-KDa docking protein that mediates the response from extracellular stimuli through the receptor-tyrosine kinase (RTK) signaling. The SHP2-GAB1 binding was previously described in yeast-two-hybrid screenings and in 293 cells after insulin/EGF stimulation (Rocchi et al., 1998; Agazie and Hayman, 2003). A recent report investigated the network signaling of GRB2 on HEK293T cells and found that GAB1-GRB2 binding only took place after PDGF but not EGF stimulation (Bisson et al., 2011).

Additionally, the T42A and E76G mutations are located in the β-chain C and the α-chain B of the N-terminal SH2-domain, respectively. Prediction studies could identify that a single mutation in the SH2-domain is sufficient to change the protein configuration and thus the strength to interaction partners (Huyer and Ramachandran, 1998). In a recent biochemical approach the binding specificity of different protein tyrosine phosphatases was explored. Ren et al. (2011) found that the PTP- and SH2- domains of SHP1 and SHP2 have similar specificity to substrates that contained at least two acidic residues. These findings were consistent with the in vivo dephospholylation sites in EGFR, FAK, HER2, PDGFRβ, RhoGAP and SPRY1. Moreover, a predicted dephosphorylation motif (EADG ELpY^{285}VFNTP and PTPGNTpY^{317}QIPRT) was proposed for GAB1.

Despite previous evidence in other NS-associated mutations suggesting that increased ERK activation was only observed after GAB1 coexpression and stimulation-dependent (Fragale et al., 2004), the present work demonstrated that, in the rat fibroblast context, an increased ERK activation was observed without previous stimulation with growth factors (fig. 2.23). This differences might have an explanation on a cell context-dependent action of SHP2, which has been also observed in Noonan mouse models, where an increased

Erk activation was observed in embryonic tissues, later affected by developmental abnormalities, but not in MEFs derived from these embryos (Araki et al., 2004).

3.5 Microarray analysis

3.5.1 Effects of cancer- and NS/LS-associated SHP2 mutations on gene transcription

The overall effect of mutations on SHP2 was rather moderate on the transcriptome. Even an overlap analysis of probe IDs among five SHP2 mutants (T42A, E76G, E139D, I282V and T468M) did not provide significant results (table 2.4 and fig. 2.31). However, a group of upregulated genes were interesting. The genes *CDH1* and *CDH3*, which encode members of the cadherin superfamily and play a key role in cell-cell adhesion and proliferation, were upregulated in the compared SHP2 arrays (Appendix D, table D.1). Expression of both genes have been associated with tumor-suppressing and tumor-promoting activities (van Roy, 2014). *CDH1* is involved in tumor-promotion by supporting EGFR signaling in glioblastoma, inflammatory breast carcinoma and ovarian cancer (Rodriguez et al., 2012). On the other hand, *CDH3*, encoding the protein P-Cadherin, supports CDH1 when co-expressed (Paredes et al., 2008). The used cell system for the transcription profile was the isogenic dox-inducible HEK-TREx cell line. The results obtained here are contrasting with those observed from the protein-protein interaction and protein signaling analysis, where SHP2 mutations not only altered the activation of the MAPK signaling cascade, but also the binding strength to one of its prominent binding partners. This might indicate, that SHP2 has a stronger regulatory potential at the protein level than on gene transcription in HEK-TREx cells. However, it would be necessary to test the impact of these mutations in other cell systems and with a longer induction of protein expression.

3.5.2 Effects of CFC-associated BRAF mutations on gene transcription

BRAF mutations had a significant impact on the gene transcription in the inducible HEK-TREx cell system. Surprisingly, the compared CFC-associated BRAF mutants had a gene cluster that overlapped with the oncogenic $BRAF^{V600E}$. Among the regulated genes, the transcription factors *JUNB*, *HEY1*, *CYR61* and *STAT1* were upregulated in all BRAF mutant array profiles. Increased STAT1 activation has been recently correlated with tumor progression in different types of cancer, including breast cancer (Hix et al., 2013). CYR61 upregulated also plays a role in cell proliferation, differentiation, angiogenesis, apoptosis, and extracellular matrix. By contrast, TP53 gene downregulation was found in all BRAF HEK-TREx profiles, including the oncogenic V600E. P53 plays a crucial role in cell growth regulation and apoptosis and its downregulation might be implicated in cell proliferation in breast cancer cells (Zheng et al., 2004)
Somatic mutations in BRAF occur with high frequency in human cancer and they are con-

centrated mostly in the kinase domain (COSMIC database). In contrast, BRAF germline mutations associated with the CFC syndrome are widely distributed (Rodriguez-Viciana et al., 2006). Although CFC syndrome has not been considered a cancer-predisposing syndrome, new reports of CFC patients with predisposition to acute lymphoblastic leukemia (ALL) indicate that this statement is not fully true (van Den Berg and Hennekam, 1999; Makita et al., 2007; Rauen et al., 2011).
Despite of the fact that there is a single report of the here studied CFC-associated mutant in cancer, the similarity of the transcription profiles with V600E indicates the essential role of BRAF on signaling and transformation phenotype.
It is still unclear, which are the mechanisms that differ downstream each BRAF mutation. In conclusion, further studies are necessary to elucidate the paradoxical mechanisms of SHP2 and BRAF on MAPK signaling pathways.

3.6 Outlook

In this work, the application of high-throughput approaches and functional assays was explored in different cell systems to characterize mutations implicated in RASopathies and cancer. Non-tumorigenic human and rat cell systems were used for the ectopic overexpression of SHP2 and BRAF mutations associated with diverse developmental disorders and cancer. Both SHP2 and BRAF mutations conferred a transformed phenotype to rat 208F fibroblasts, including increased cell proliferation, density-independent and anchorage-independent growth. Further studies are needed to understand the reprogramming events that take place during anchorage-independent growth in both SHP2- and BRAF-expressing rat fibroblasts. To explore this, evaluation of signaling regulation at transcription and protein level of the colonies from soft agar assay is necessary.
Additionally, it could be demonstrated that NS/LS-associated SHP2 as well as CFC-associated BRAF mutations constitutively activate the Ras/MAPK signaling pathway in a moderate manner compared to the oncogenic $BRAF^{V600E}$ mutation in rat fibroblasts and HEK-TREx cells. This findings might be useful for choosing an effective treatment of patients suffering from developmental disorders, having the components of the MAPK cascade, such as MEK1/2, as a target for therapy.
Using additional human cell systems for the morphological characterization after expression of SHP2/BRAF mutations was shown that, although both genes confer a clinical overlapping phenotype when mutated, the implications at the signaling level and their influence of the cellular phenotype are quite divergent as shown in the human cell lines BJ-ELB and MCF10A. Cells overexpressing SHP2 mutations were growth arrested, while BRAF mutations induced cell proliferation and a transformation phenotype. It would be necessary to consider the use of siRNA or pharmacological SHP2 inhibition to evaluate the regression of the oncogene-driven transformation phenotype in 208F cells, and the rescue of growth arrest phenotype in BJ-ELB and MCF10A cells. In addition to this, a knockdown of key components downstream of the SHP2 signaling such as RasGAP, Sprouty and Src, would deliver information about the regulatory mechanisms

of the MAPK signaling upstream of Ras. This effect might be explored as a therapeutic strategy to increase apoptosis in those cancer types were SHP2 activity is upregulated and thus increase apoptosis events of cancer cells. Furthermore, the differences in the mechanisms of action between BRAF and SHP2 might implicate the participation of additional signaling pathways that need to be further investigated.

It was also shown that SHP2 mutations have a relevant influence on the SHP2-GAB1 protein interaction. Two NS-associated SHP2 mutations showed an increased binding strength to the scaffold protein GAB1. In future studies, it would be interesting to extend the approach to evaluate the effect of other growth factors such as the platelet derived growth factor (PDGF) and the fibroblast growth factor (FGF). Additionally, it would be highly relevant to evaluate not only phospho-Tyr protein pattern but also investigate the outcome on the MAPK signaling activation and explore how this increased GAB1 binding leads to crosstalk signaling.

The impact on gene transcription was also analyzed. Interestingly, a gene cluster was found to be similarly regulated in both CFC-associated BRAF and the oncogenic V600E mutation. This is the first report on transcriptome analysis of CFC-associated mutations. Additional validation assays are needed to confirm the results presented here.

4 MATERIALS AND METHODS

4.1 Materials

4.1.1 Chemicals

Chemical	Source
1 Kb DNA ladder	NEB
2-Mercaptoethanol	Promega
6x DNA loading dye	Thermo Scientific
acrylamide	Roth
Agarose	Serva
Ampicillin (50 mg/ml)	Sigma-Aldrich
APS	Merk
Bacto Agar	BD Biosciences
Bacto yeast extract	BD Biosciences
Bacto-Tryptone	BD Biosciences
Boric acid	Merck
Bovine serum albumin (BSA)	Sigma-Aldrich
Bromphenol blue (BPB)	Sigma-Aldrich
Complete mini EDTA-free	Roche
DEPC-treated water	Sigma-Aldrich
Dithiothreitol (DDT)	Sigma-Aldrich
DOC	Sigma-Aldrich
Dynabeads Protein A	Novex, Life Technologies
EDTA	Merk
Ethanol	J.T.Baker
Ethidium bromide	Sigma-Aldrich
Formaldehyde	J.T.Baker
Glycerol	Merk
Glycine	Merck
Isopropanol	J.T.Baker
LI-COR blocking buffer	LI-COR
M-PER Mammalian Protein Extraction Reagent	Pierce
Methanol	Merck
N-Methyl-Pyrolidione	Sigma-Aldrich

Chemical	**Source** *(continued)*
PageRuler prestained protein ladder	Fermentas
Paraformaldehyde (PFA)	Merck
PhosSTOP	Roche
Potassium chloride (KCl)	Merk
potassium dihydrogen orthophosphate (KH_2PO_4)	Merk
S.O.C. medium	Life Technologies
Sodium acetate ($C_2H_3NaO_2$)	Merck
Sodium chloride (NaCl)	Merck
Sodium dodecyl sulfate (SDS)	Serva
Sodium hydroxide (NaOH)	Merck
Sodium phosphate dibasic (Na_2HPO_4)	Merck
Tetramethylethilenediamine (TEMED)	Sigma-Aldrich
Tris-Base	Merk
Tris-HCl	Merk
Triton X-100	Sigma-Aldrich
Trypan blue	Merk
Tween20	Serva

4.1.2 Cell culture reagents

Reagent	**Source**
4,6-Diamidino-2-phenylindole dihydrochloride (DAPI)	Sigma-Aldrich
5x PEG-it™Virus Precipitation Solution	System Biosciences
Agar noble	BD Biosciences
Amaxa nucleofector kit	Lonza
Blasticidin (10 mg/ml)	Invitrogen
Dimethyl sulfoxide (DMSO)	Sigma-Aldrich
DMEM	Invitrogen
DMEM, 10X	Sigma
Effectene	Qiagen
Fetal calf serum (FCS)	Biochrom AG
Fugene6	Promega
G-418 sulfate solution	Invitrogen
Glucose, 45%	Sigma-Aldrich
Hygromycin B (50 mg/ml)	Gibco
Kanamycin (50 mg/ml)	Sigma-Aldrich
Lipofectamine2000	Invitrogen
Medium-199	Lonza
MEGM bullet kit	Lonza
MEGM mammary epithelia cell growth medium kit	Lonza
MEM-alpha (M4526)	Sigma-Aldrich

Cell culture solutions	**Source** *(continued)*
Oligofectamine	Invitrogen
OptiMEM	Invitrogen
Penicilin/Streptomycin (10 mg/ml)	Biochrom AG
Poly-L-Lysine	Sigma-Aldrich
Polyethylenimine (PEI)	Polysciences
PolyHEMA	Sigma-Aldrich
Protamine-sulfate	Sigma-Aldrich
Puromycin dihydrochloride	Sigma-Aldrich
Recombinant human EGF	Peprotech
Sodium bicarbonate, 7.5% ($NaHCO_3$)	Biomol
Trypsin/EDTA	Biochrom AG
Ultraglutamine (200mM)	Lonza
Vitro-Clud	R. Langenbrick
Zeocin (100 mg/ml)	Invitrogen

4.1.3 Restriction enzymes

Restriction enzymes	**source**
AfIl	NEB
ClaI	NEB
PstI	NEB
SalI	NEB
SpeI	NEB
SwaI	NEB
XhoI	NEB

4.1.4 Consumables

Consumables	**Source**
0.2 m, 0.45 μm syringe filters	Sarstedt
0.5 μl PCR tubes	Applied Biosystems
1.5 ml, 2 ml reaction tubes	Eppendorf
10 cm, 15 cm cell culture dishes	BD Falcon
10 μl, 100 μl, 1000 μl pipet tips	Eppendorf
10 μl, 100 μl, 300 μl, 1250 μl filter tips	Sarstedt
2 ml, 5 ml, 10 ml, 25 ml plastic pipets	BD Falcon
25 cm^2, 75 cm^2, 175 cm^2 cell culture flasks	BD Falcon
2 ml, 5 ml Cryovials	Nalgene
5 ml polypropylene round tubes	Sarstedt
5 ml, 15 ml, 50 ml reaction tubes	BD Falcon
6-, 12-, 24-, 96-well plates	BD Falcon
96-well PCR plates	Biozym

Cell scraper, 25 cm	Sarstedt
Illumina HumanHT-12 v3 Expression BeadChip	Illumina
Lab glassware	Duran
Protran Nitrocelullose transfer membrane	Whatman
Glass coverslips	Carl Roth

4.1.5 Commercial kits

Name	**Source**
BCA protein assay kit	Pierce
CalPhos™Mammalian Transfection Kit	Clontech Laboratories
Cell Proliferation Kit II (XTT)	Roche
Dako kit for immunohistochemistry	Dako
EndoFree Plasmid Midi/Maxi Kit	Qiagen
Fast-Link™DNA Ligation Kit	Epicentre
Gateway®BP- and LR-Clonase®II Enzyme mix	Life Technologies
Protease-Inhibitoren	Roche
QIAprep Spin Miniprep Kit	Qiagen
QIAquick Gel Extraction Kit	Qiagen
QuickChange™Sitedirected Mutagenesis Kit	Agilent Technologies
Rneasy mini-kit (50)	Qiagen
Western Blot Recycling Kit	Alpha Diagnostic

4.1.6 Antibodies

Antibody	**Dilution conditions**	**Source**
Primary antibodies		
goat PECAM-1 (CD31, clone M20)	1:500 in Real Antibody Diluent (Dako)	Santa Cruz, sc-1506
mouse BRAF (F7)	1:500 in PBST:Licor (1:1)	Santa Cruz, sc-5284
mouse ERK1/2	1:1,000 in PBST:Licor (1:1)	BD Biosciences, 612358
mouse Gab1 (H-7)	1:1,000 in PBST:Licor (1:1)	Santa Cruz, sc-133191
mouse GAPDH (6C5)	1:10,000 in PBST:Licor (1:1)	Ambion, AM4300
mouse MEK1/2	1:1,000 in PBST:Licor (1:1)	CST, 4694
mouse Pan Ras	1:1,000 in PBST:Licor (1:1)	BD Biosciences, 610002
rabbit AKT	1:1,000 in PBST:Licor (1:1)	CST, 2146
rabbit β-tubulin	1:1,000 in PBST:Licor (1:1)	CST , 4267
rabbit BRAF	1:1,000 in PBST:Licor (1:1)	CST, 9434
rabbit CyclinD1	1:1,000 in PBST:Licor (1:1)	CST, 2922
rabbit ERK1/2	1:1,000 in PBST:Licor (1:1)	CST, 9102
rabbit Gab1	1:1,000 in PBST:Licor (1:1)	CST, 3232
rabbit GSK3α	1:1,000 in PBST:Licor (1:1)	CST, 4337
rabbit GSK3β	1:1,000 in PBST:Licor (1:1)	CST, 9315
rabbit MEK1/2	1:1,000 in PBST:Licor (1:1)	CST, 9122
rabbit p70S6K	1:1,000 in PBST:Licor (1:1)	CST, 9202

Antibody	Dilution conditions	Source *(continued)*
rabbit phospho-AKT	1:1,000 in PBST:Licor (1:1)	CST, 9271
rabbit phospho-ERK1/2	1:1,000 in PBST:Licor (1:1)	CST, 9101
rabbit phospho-GSK3$\alpha\beta$	1:1,000 in PBST:Licor (1:1)	CST, 9327
rabbit phospho-GSKα	1:1,000 in PBST:Licor (1:1)	CST, 9316
rabbit phospho-GSKβ	1:1,000 in PBST:Licor (1:1)	CST, 9315
rabbit phospho-MEK1/2	1:1,000 in PBST:Licor (1:1)	CST, 9121
rabbit phospho-p70S6K	1:1,000 in PBST:Licor (1:1)	CST, 9206
rabbit phospho-STAT3	1:1,000 in PBST:Licor (1:1)	CST, 9136
rabbit PI3 Kinase p85α	1:1,000 in PBST:Licor (1:1)	CST, 4292
rabbit SHP2	1:1,000 in PBST:Licor (1:1)	CST, 2297
rabbit STAT3	1:1,000 in PBST:Licor (1:1)	CST, 4904
Secondary antibodies		
IRDye680CW goat anti-mouse	1:15,000 in PBST:Licor (1:1)	LI-COR Biosciences
IRDye800CW goat anti-rabbit	1:15,000 in PBST:Licor (1:1)	LI-COR Biosciences
Rabbit anti-goat HRP IgG Conjugate	1:350 in Real Antibody Diluent (Dako)	Invitrogen, 81-1620

4.1.7 Buffers and media

Buffer/Media	Formula/Preparation
10% APS	1 g APS in 10 ml aq. dest.
Cryopreservation medium	10% DMSO, 90% D10
Culture medium for BJELB	400 ml DMEM, 100 ml Medium-199, 15% IFS, 1% ultraglutamine, 1% penicillin/streptomycin, 100 g/ml hygromycin, 400 μg/ml G418, 0.15 μg/ml puromycin.
Culture medium for HA1EB	500 ml MEM-alpha, 15% IFS, 1% ultraglutamine, 1% penicillin/streptomycin, 100 g/ml hygromycin, 400 g/ml G418, 0.15g/ml puromycin.
2x D10 for soft agar assay	100 ml 10x DMEM, 10% FCS, 1% penicillin/streptomycin, 2 mM ultraglutamin, 0.37% $NaHCO_3$. Adjust to 500 ml with sterile aq. dest.
2x agar solution for soft agar assay	0.3% agar noble in aq. dest. Autoclave at 121°C for 30 min
Culture medium for MCF10A	500 ml MEGM medium, 1x MEGM bullet kit, 1% penicillin/streptomycin
Culture medium for T-Rex-293	500 ml D10 high glucose, 15 μg/ml blasticidin, 100 μg/ml zeocin
D10 cell culture medium	500 ml DMEM, 10% FCS, 2 mM Ultraglutamine, 100U/ml penicillin/streptomycin.
D10 high glucose	500 ml D10, 3.5g/L glucose.
human EGF	Dilute in 0.1% BSA/PBS for a 1 mg/ml stock concentration.
LB-agar	15 g Bacto Agar in 1 l 1x LB
LB-medium	10 g Bacto Tryptone, 5 g Bacto yeast extract, 10 g NaCl. Add 1 l aq dest. pH 7.5
Low salt LB-medium	10 g Bacto Tryptone, 5 g Bacto yeast extract, 5 g NaCl. Add 1 l aq dest. pH 7.5

Buffer/Media	Formula/Preparation *(continued)*
Lysis buffer	1 ml 10x PhosSTOP solution, 400 l 25x complete EDTA-free solution, 9 ml M-PER mammalian protein extraction reagent.
PBS, 10x	80 g NaCl, 2 g KCl, 14.4 g Na_2HPO_4, 2.4 g KH_2PO_4. Add 1 l aq. dest., pH 7.4
PBST	0.1% Tween20 in 1x PBS
Poly-HEMA solution	5 mg/ml PolyHEMA to 96% Ethanol. Mix by RT until disolved.
Resolving gel 12.5% (SDS-PAGE)	6.3 ml 1.5 M Tris pH 8.6, 10 ml 30 % acrylamide, 240 l 10% SDS, 130 l 10% APS, 25 l TEMED, 8.3 ml aq dest.
Resolving gel 8% (SDS-PAGE)	6.3 ml 1.5 M Tris pH 8.6, 6.6 ml 30 % acrylamide, 240 l 10% SDS, 130 l 10% APS, 25 l TEMED, 11.7 ml aq dest.
Running buffer, 5x (SDS-PAGE)	15.1 g Tris-Base, 72 g Glycine, 5 g SDS. Add 1 l aq dest pH 8.3
SDS sample buffer, 2x	Tris-HCl pH 6.8 0.25 M, SDS 8 %, Glycerin 40 %, β-Mercaptoethanol 20 %, Bromphenol blue
Stacking gel 4% (SDS-PAGE)	2.5 ml 0.5 M Tris pH 6.8, 1.33 ml 30 % acrylamide, 100 l 10 % SDS, 50 l 10 mM APS,10 l TEMED, 6.1 ml aq dest.
TAE buffer, 10x	242 g Tris Base , 18.6 g EDTA. Add 1 l aq dest, pH 8.0
Transfer buffer, 2.5x (SDS-PAGE)	14.5 g Tris Base, 7.3 g Glycine, 4.7 ml 20% SDS, 500 ml Methanol. adj. to 1 l aqua dest

4.1.8 Vector backbones

Vector backbone	Description	Marker	Source
pBabe-Puro		Puro	
pCDH-EF1a-IRES-GFP		Amp	System Biosciences
pCDH-gate-GFP	ccdB cassette inserted for gateway cloning		
pCDH-gate-GFP-Puro			
pcDNA5-FRT-TO-N-TAP-eGFP-Hygro	destination vector	Amp	
pcDNA5-FRT-TO-N-YFP-eGFP-Hygro	destination vector	Amp	
pDONR221	Gateway entry vector	Amp, Cm	Life Technologies
pEF1/V5-HisC		Amp	Life Technologies
pLenti6-CMV-YFP	Gateway expression vector	Amp, Cm	kindly provided by B.Maier, Berlin
pLenti6-EF1-YFP	Generated from pLenti6-CMV-YFP		
pMD2G		Amp	kindly provided by B.Maier, Berlin
pOG44	Expresses Flp recombinase		
psPAX2		Amp	kindly provided by B.Maier, Berlin
pDONR/Zeo	entry vector	Zeo	Life Technologies

4.1.9 Competent bacteria strains

Strain	Transformation use	Source
E.coli ccdB survival	Gateway empty vectors	Life Technologies
E.coli DH10B	entry vectors	Life Technologies
E.coli DH5a	entry vectors	Life Technologies
E.coli Stlb3	Lentiviral vectors	Life Technologies

4.1.10 Cell lines

All cell lines were incubated at 37°C and with 5% CO_2 atmosphere.

Cell line	Description	Culture conditions	source
208F	Non-tumorigenic rat immortal fibroblasts	D10	(Griegel et al., 1986)
BJELB	Human hTERT-immortalized BJ foreskin fibroblasts	DMEM:Medium 199	kindly provided by Prof. W.C. Hahn
HA1EB	Human kidney epithelial cells	MEM-alpha	kindly provided by Prof. R.A. Weinberg
HEK293FT	Human embryonic kidney cells, transformed with the SV40 large T-antigen	D10 high glucose	Kindly provided by AG Kramer, Charité Berlin
Flp-In T-REx™-293	Human embryonic kidney cells; contains a stably integrated FRT site	D10 high glucose, 15g/ml blasticidin, 100g/ml zeocin	Invitrogen, Life Technologies
MCF10A	Human breast epithelial cells	MEGM	ATCC CRT-10317
Cos 7	African green monkey kidney fibroblasts, SV40 transformed	D10	ATCC CRT-1651

4.1.11 Software

Tool	URL/Source
Addgene	http://www.addgene.org/
BioGRID	http://thebiogrid.org/
cBioPortal	http://www.cbioportal.org/
Concensus CDS project	http://www.ncbi.nlm.nih.gov/CCDS/
COSMIC	http://cancer.sanger.ac.uk/
DAVID	http://david.abcc.ncifcrf.gov/
GeneCards	http://www.genecards.org/
KEGG	http://www.genome.jp/kegg/
NEBcutter v. 2.0	http://tools.neb.com/NEBcutter2
OMIM	http://www.ncbi.nlm.nih.gov/omim/
STRING	http://string-db.org/
UniHI	http://www.unihi.org/
Venny	http://bioinfogp.cnb.csic.es/tools/venny/
WebGestalt	http://bioinfo.vanderbilt.edu/webgestalt/
Software	
ApE plasmid editor v. 2.0.45	OpenSource
Gimp image manipulation programm v. 2.8.6	OpenSource
ImageJ v. 1.48	OpenSource
Microplate Manager v. 5.2.1	Bio-Rad
Microsoft Office 2011	Microsoft
Photoshop v. 5.0	Adobe
XPlasMap plasmid editor v. 0.96	OpenSource

4.1.12 Lab equipment

Equipment	Source
Agarose gel chamber	Bio-Rad
Balance	Sartorius
Centrifuge Allegra 6R	Beckman Coulter
Centrifuge Allegra X15R	Beckman Coulter
Centrifuge Avanti J-25	Beckman Coulter
Electrophoresis gel chamber	Bio-Rad
ELISA- plate reader	Bio-Rad
Fluorescence microscope	Keyence
Incubator Hera cell 240	Hera
Microcentrifuge 5415 C	Eppendorf
Mini-Protean Tetra Cell electrophoresis system	Bio-Rad
Neubauer Improved cell counting chamber	Carl Roth
Nanophotometer	Implen
Nucleofector™2b Device	Lonza
Odyssey CLx infrared imaging system	LI-COR Biosciences

Phase contrast microscope	Leica DMIL
Thermocycler	Genius, Progene
Thermomixer	Eppendorf

4.1.13 Company register

Company	**Location**
Agilent Technologies	Bblingen, Germany
Alpha Diagnostic	San Antonio, TX, USA
Applied Biosystems	
BD Biosciences	Heidelberg, Germany
BD Falcon	Bedfore, MA, USA
Beckman Coulter	Krefeld, Germany
Bio-Rad GmbH	Mnchen, Germany
Biochrom GmbH	Berlin, Germany
Biomol	Hamburg, Germany
Biozym GmbH	Hamburg, Germany
Carl Roth	Karlsruhe, Germany
Cell Signaling Technology (CST)	Leiden, Nethelands
Cellstar, Greiner Bio-One	Frickenhausen, Germany
Clontech Laboratories	Mountain View, CA, USA
Duran Group	Wertheim, Germany
Epicentre	Madison, USA
Eppendorf	Wesseling-Berzdorf, Germany
Eurons MWG Operon	Ebersberg, Germany
Fermentas	Darmstadt, Germany
GeneArt AG	Regensburg, Germany
Illumina, Inc	San Diego, CA, USA
Implen GmbH	Mnchen, Germany
J.T.Baker	Deventer, Netherlands
Keyence	Neu-Isenburg, Germany
Leica DMIL	Wetzlar, Germany
LI-COR Biosciences	Bad Homburg, Germany
Life Technologies	Karlsruhe, Germany
Lonza Group Ltd.	Basel, Switzerland
Merck	Darmstadt, Germany
Nalgene	Rochester, NY, USA
New England Biolabs (NEB)	Ipswich, MA, USA
Peprotech	Rocky Hill, NJ, USA
Pierce Thermo Scientific	Rockford, IL, USA
Polysciences Inc.	Eppelheim, Germany
Promega	Mannheim, Germany
Qiagen	Hilden, Germany
R. Langenbrick	Emmendingen, Germany
Roche	Mannheim, Germany
Santa Cruz Biotechnology	Heidelberg, Germany
Sarstedt AG	Nmbrecht, Germany
Sartorius AG	Gttingen, Germany

Company	Location	*(continued)*
Serva	Heidelberg, Germany	
Sigma-Aldrich	Mnchen, Germany	
System Biosciences	Mountain View, CA, USA	
Thermo Scientific	Darmstadt, Germany	
Whatman	Freiburg, Germany	

4.2 Molecular biology methods

4.2.1 Synthesis of wild-type and mutated genes

Mutated and wild-type *PTPN11* (CCDS accession number CCDS_9163.1) and *BRAF* (CCDS accession number CCDS_5863.1) genes were synthesized by GeneArt. Each construct contained a stop codon (TAA) and was assembled in a vector backbone flanked with attB sequences for posterior generation of entry clones. The constructs $BRAF^{K499E}$, $PTPN11^{wt}$ and its mutant variants were assembled in the vector pMK–RQ (Kanamycin^r), BRAFL485F in pMA (Ampicillin^r), $BRAF^{S467A}$ and $BRAF^{Q257R}$ in pMS (Spectinomycin^r) and $BRAF^{wt}$ and $BRAF^{V600E}$ in the entry vector pDONR221.

4.2.2 Gateway® Cloning

The Gateway cloning is based on site-specific recombination, which facilitates the shuttle of DNA coding sequences into multiple vectors. As previously mentioned, mutated and wild-type coding sequences were synthesized with attB flanking sequences to generate entry and destination clones (see subsection 4.2.1).

Generation of entry clones

Except for $BRAF^{wt}$ and $BRAF^{V600E}$, synthesized in pDONR221, all synthesized attB-flanked coding sequences were cloned in the pDONR/Zeo entry vector. Each BP recombination reaction was prepared with 1 µl of 150 ng/µ pDONR/Zeo vector, 1 µl of 150 ng/µl of the corresponding insert, 6 µl of TE buffer pH 8.0 and 2 µl of BP clonase. After 1 h incubation at RT, DH5α competent bacteria were transformed with 2 µl of the BP reaction and grew in low salt LB medium at 37°C ON as described in subsection 4.2.3.

Generation of expression clones

To generate expression clones, a recombination LR reaction was prepared as follows: 1 µl of the corresponding entry vector (150 ng/µl), 1 µl destination vector, 6 µl of TE buffer pH 8.0 and 2 µl of LR clonase. After 1 h incubation time at RT, DH5α or Stbl3 (for lentiviral vectors) competent bacteria were transformed with 2 µl of the LR reaction and grew in LB medium as described in subsection 4.2.3.

4.2.3 Generation of the EF1α promoter-driven pLenti6 expression vector

The EF1α promoter insert was obtained by PCR using the pEF1/V5-HisC promoter as template. The CMV sequence of the pLenti6-CMV-YFP was excised and replaced by the EF1α promoter. The cloning primers were designed as follows: the forward primer 5'-CGTCACATCGATGAGGAATCTT TGCAGCTAATGGACC-3' contained a 5' ClaI restriction site and the reverse primer 5'-CTAACGACTAGTCAAGCTAATTCCTCACGA CACCTG-3' contained a 3' SpeI restriction site. The PCR reaction was performed in 30 cycles with the following conditions: denaturation 30 sec at 95℃, annealing 30 sec at 64℃ and elongation 1,5 min at 72℃. After confirming the promoter insert by sequencing, both the PCR product (EF1α promoter) and the vector (pLenti6-CMV-YFP) were subjected to restriction digestion with ClaI and SpeI, to generate cohesive ends for the ligation. The correct insertion was verified by restriction digestion with AflII and PstI (fig. 2.3). This new vector was denominated pLenti6-EF1a-YFP.

4.2.4 Generation of the new lentiviral expression vector pCDH-EF1a-Puro

The Gateway reading frame cassette B (Invitrogen), containing two attR-flanking sequences, a chloramphenicol resistance gene (Cm^r) and the ccdB gene was cloned into the vector pCDH-EF1a-IRES-GFP and digested with SwaI at the multiple cloning site (MCS) to generate blunt ends and dephosphorylated with calf intestinal phosphatase (CIP) for 1h at 37℃to prevent self-ligation (fig. 2.5). The vector and gateway cassette insert were ligated in a ratio of 1:2 ON at room temperature. After ligation, ccdB survival T1 competent bacteria were transformed with 2 μl of the ligation reaction and incubated at 30℃ ON to reduce the number of random recombinations. The destination vector was sequenced and verified. This new expression vector, pCDH-gate-GFP, was verified by restriction digestion and sequencing. Next, the puromycin cassette, under the control of SV40, was cloned into the vector pCDH-Gate-GFP. This selection cassette was obtained by PCR from the vector pBabe-Puro, available at our plasmid collection. Both PCR forward primer 5'-CGTTACGTCGACTACGTAGGAATTCGCCAG-3' and reverse primer 5'-CTAATGGTCGACTCGTGCGCTCCTTTCGGTC-3' were designed with a SalI restriction site, to allow the integration between GFP and the woodchuck postranscriptional response element (WPRE). The PCR reaction was performed in 40 cycles with the following parameters: binding 30 sec at 95℃, annealing 30 sec at 62℃ and extension 2 min at 72℃. The synthesized fragment was 1000 bp, and was directly digested with SalI. It was necessary to introduce a XhoI unique restriction site by site-directed mutagenesis next to GFP. Complementary primers at 25 bp, except for a single G→C nucleotide exchange, were designed to generate the overhang 5'-TCGA, also compatible with SalI. The site-directed mutagenesis reaction was conducted in 14 cycles under the following conditions: binding 30 sec at 95℃ annealing 30 sec at 66℃ extension 10 min at 68℃. Once finished, the reaction tube was cooled down to 37℃ and 1 μl of DpnI

enzyme was added to digest the parental supercoiled dsDNA for 1h at 37℃. Next, the vector was digested with XhoI and ligated 45 min in a vector:insert ratio of 1:2 at room temperature. One Shot® ccdB-Survival competent bacteria were transformed with 2 μl of the ligation reaction, spreaded on ampicillin LB-agar plates and incubated ON at 30℃. At least five clones were picked and grew ON at 30℃ in ampicillin LB- broth media. To confirm the insertion of the puromycin cassette, the resulting expression vector was digested with NcoI. This new expression vector was used for functional assays and was denominated pCDH-Gate-Puro.

4.2.5 Transformation of plasmid DNA in competent cells

For transformation, at least 200 ng plasmid DNA or 2 µl of recombination reaction were gently mixed with 50 µl of thawed competent bacteria and incubated on ice for 30 min. After a 40 sec heat-shock at 42°C and 2 min on ice to cool down, 120 µl SOC medium was added and the bacteria were incubated for 1 h at 30°(for lentiviral vectors) or 37°C with shaking. 80-100 µl of transformed bacteria were plated on LB-agar plates with the corresponding antibiotics and incubated at 30°(for lentiviral vectors) or 37°C ON.

4.2.6 Plasmid DNA purification from transformed bacteria

To screen for positive colonies containing the expected plasmid DNA, at least three colonies were picked and grew in 3 ml LB-medium with the corresponding antibiotics overnight at 37°C in an horizontal shaker. Then, plasmid DNA was isolated from 2 ml of the growing culture with the QiaPrep mini kit according to manufacturers instructions and analyzed by restriction digestion. Once a positive colony was found, 150 ml of selection LB-medium was inoculated with 1 ml of the growing culture and incubated at 30°(for lentiviral vectors) or 37°C in an horizontal shaker ON. Plasmid DNA was prepared with the endoFree Plasmid Midi/Maxi kit according to manufacturer's instructions and eluted with 80-100 µl TE buffer pH 8.0.

4.2.7 Agarose gel electrophoresis

DNA gel electrophoresis was performed to separate DNA fragments by size. 1.2 % agarose gel was prepared by heating v/w agarose in 1x TAE buffer and 2 µl ethidium bromide. DNA samples mixed with 6x loading dye were subjected to electrophoresis at 70-90 V for 40 min. According to the expected DNA fragment size, 1-Kb or 100 bp DNA ladder were simultaneously loaded. DNA bands were detected by UV-light. To purify expected DNA fragments, bands were cut and transferred into a 1.5 ml reaction tube. DNA was extracted from the agarose gel using the QIAquick Gel Extraction Kit according to the manufacturer's protocol.

4.2.8 RNA Isolation

RNA was isolated from confluent mammalian cells (approximately 1x10^6 cells) grown in 6-well plates using the RNeasy Mini Kit. Culture medium was removed and cells were

washed twice with ice-cold 1xPBS. Subsequently, cells were lysed with 2-mercaptoethanol-containing RLT lysis buffer and treated according to the manufacturer's instructions. RNA was eluted with 40µl Nuclease-free water and stored at -80°C. RNA was quantified by a wave length of 260 nm with a Nanophotometer. To evaluate RNA quality, samples were measured with the Agilent Bioanalyzer (performed by Ute Ungethuem, Laboratory for Functional Genomics Charité).

4.3 Cell biology methods

4.3.1 Culture of mammalian cell lines

Cell lines were kept in 75 cm^2 flasks under the culture conditions described in the subsection 4.1.10. Once cells reached 80-90% confluence, medium was removed and they were rinsed once with 1x PBS and trypsinized with 2 ml trypsin/EDTA solution at 37°C until cells detached from the bottom. The reaction was stopped with 8 ml of fresh medium followed by suspension by pipetting. Then, cells were pelleted by centrifugation at 800 rpm for 5 min and resuspended with 10 ml fresh complete medium and seeded in a ratio 1:10.

4.3.2 Thawing of cell lines

Cryovials containing frozen cells were fast thawed in a water bath at 37°C by gently shaking. Next, cells were carefully transferred to a 15-ml tube and 10 ml fresh complete medium were dropwise added and mixed by gently tapping. To remove preservation medium, cells were centrifuged at 800 rpm for 5 min and resuspended with 10 ml fresh medium. The cell suspension was seeded in a 75 cm^2 flask and incubated at 37°C and 5% CO_2.

4.3.3 Cryopreservation of cell lines

Cells grown at 70% confluence were trypsinized as described (subsection 4.3.1). Cell pellets containing approximately $1x10^6$ cells were resuspended in 2 ml of culture medium with 10% DMSO and transferred to cryovial tubes. To avoid cell death, cryovials were frozen gradually in isopropanol-filled container and stored at -80°C overnight. Finally, cryovials were kept in the gas phase over liquid nitrogen until use.

4.3.4 Proliferation assay

To measure cell growth, a proliferation assay based on the cell metabolic activity was used. This colorimetric assay is based on the reduction of the tetrazolium dye XTT to the orange-colored and soluble formazan by mitochondrial oxidoreductases. 1000 208F cells/well in 100 µl culture medium were seeded in 96-well plates in triplicate for each time point and incubated at 37°C and 5% CO_2 overnight. Blank wells containing only culture medium were simultaneously prepared for each time point to obtain a background absorbance value. Then, 50 µl XTT solution containing the labeling and an

electron coupling reagent were added to each well and incubated for at least 4 h before measurement. Absorbance was quantified in an ELISA plate reader at a wavelength of 490 nm with a reference wavelength of 690 nm. The final cell growth value was obtained by subtracting the blank value from each sample mean.

4.3.5 Soft agar assay

In order to evaluate the anchorage-independent growth ability of 208F cells carrying PTPN11 or BRAF mutations, cells were grown in soft agar. 208F fibroblasts in logarithmic growth phase were trypsinized and resuspended in 10 ml D10 culture medium (see subsection 4.3.1). Cells were counted using a Neubauer cell chamber and prepared in two dilutions (100 and 1000 cells) in duplicate in 1 ml D10 medium pipetting several times to prepare homogeneous single-cell suspensions. 25 cm^2 culture flasks were filled with 25 ml 37°C pre-warmed 2x D10 medium, followed by 25 ml of 45°C pre-warmed 0.3% agar noble solution and 1 ml of the corresponding cell suspension. After gently mixing the suspension, the culture flasks were placed on ice for 10-15 min to cool down and harden the agar. Finally, the cells were incubated vertically at 37°C and 5% CO_2 for up to 4 weeks without refreshing the medium and visually monitored for growing colonies. Visible colonies were quantified for each dilution.

4.3.6 Trasient tansfection of cells

MCF10A, 208F and Cos7 cells were transfected using the following transfection reagents according to the manufacturer's protocol: Lipofectamine2000, PEI, Fugene6 and Effectene. Briefly, 2x10^4 cells were seeded in 6-well plates and incubated for at least 16 h at 37°C and 5% CO_2. Then, two separate solutions were prepared: 1). 2 µg plasmid DNA were mixed with 250 µl Optimem and 2). 3 µl transfection reagent diluted 250 µl Optimem. 5 min incubation at room temperature both solutions were dropwise mixed while gently shaking the reaction tube and incubated 20 min at room temperature. Finally, the transfection suspension was added dropwise over the cells. After 16 h incubation, old medium was replaced by fresh culture medium.

Amaxa nucleofection

Additional to the classical chemical-based transfection methods, the gene transfer by electroporation, or nucleofection, was also tested. 2x10^6 cells were used to gene transfer 2 µl DNA with the Amaxa nucleofection kit according to the manufacturer's protocol. 80% confluent cells were tripsinized (see subsection 4.3.1), quantified and 10^6 cells pelleted in 1.5 ml reaction tubes. Cell pellets were shortly resuspended in 100 µl Nucleofector solution and transfered into a sterile cuvette. After samples were subjected to the nucleofection with the program T20 in the Nucleofector I Device, 500 µl were added and cells were tranfered into 6-well plates previuosly filled with 1.5 ml fresh medium. The following day cell viability was monitored by microscopy and culture medium was replaced.

4.3.7 Production of lentiviral particles

The production of lentiviral particles was carried out under biosafety level 2 conditions in HEK293T cells in 75-cm^2 culture flasks, to harvest approximately 20 ml lentiviral supernatant or 200 µl of concentrated lentiviral particles. 70% confluent HEK293T cells were trasiently co-transfected with 8.4 µg of the lentiviral expression plasmid, 6 µg of the packaging psPAX plasmid and 3.6 µg of the envelope pMD2G plasmid using the CalPhos transfection kit. To prepare the transfection reaction, plasmids were diluted with 526 µl of the supplied H_2O and 74 µl of 2M Calcium solution in a 1.5 ml reaction tube. Then, this solution was added dropwise into a 15 ml reaction tube containing 600 µl 2x HBS. After 20 min incubation time at room temperature, 1.2 ml of the transfection solution was added dropwise to the cells and incubated at 37 °C ON. The next morning, culture media was replaced. Lentivirus-containing supernatant were harvested 48h and 72h after transfection. To remove remaining cell debris, the supernatant was centrifuged at 4100xg for 15 min at 4 °C and passed through a 0.45 µm filter. To concentrate the lentiviral particles, 1-volume of 5x PEG-it solution was gently mixed with the filtered supernatant and incubated ON at 4°C. After 30 min centrifugation by 3070 rpm at 4°C, the supernatant was carefully discharged and the white pellet containing the lentiviral particles was resuspended in DMEM a dilution factor 1/100 from the starting volume (in this case, 200 µl of DMEM). Lentiviral particles were stored at -80 °C.

4.3.8 Lentiviral transduction

2x10^5 cells were seeded in 6-well plates and incubated overnight at normal cell culture conditions (see subsection 4.1.10). After medium was replaced with fresh medium containing 8 µg/ml protamin sulfate, cells were transduced with 15 µl of the corresponding concentrated lentiviral particles and incubated overnight under biosafety level 2 conditions. Then, culture medium was carefully replaced after washing the cells twice with 1x PBS. Cell viability and morphology was supervised under the light microscope. Ectopic protein expression was evaluated 48h to 72h after transduction. To generate stable cell populations, transduced cells were selected with puromycin 48h after infection (see subsection 4.3.9).

4.3.9 Generation of stable transduced cell populations

To generate stable cell lines after lentiviral transduction, cells were cultured and transduced as described in 4.3.8. 48h after infection, cells were trypsinized and seeded into a 75-cm^2 culture flask containing a final volume of 10 ml culture medium with 10 µg/ml puromycin. Cell populations were monitored daily for viability and morphology under the microscope. Culture medium was replaced every 3rd day until cells were confluent. After two weeks of culture with selection medium, ectopic protein over-expression was verified by western blot and positive cell populations were frozen in liquid nitrogen (subsection 4.3.3). For subsequent experiments, cells were always kept in selection medium.

4.3.10 Generation of stable dox-inducible T-REx-HEK293 isogenic cell lines

T-REx HEK293 cells were used to generate stable isogenic cell populations that expressed the tagged protein after doxycycline induction. This cell line harbors a single stably integrated FRT site that allows the flp-mediated recombination of the expression vector containing the gene of interest. Two destination vector backbones, designed for the assays listed in table 4.9, were selected to generate expression clones using the gateway cloning strategy.

Table 4.9: Assays performed with T-REx-HEK293 cells

Vector backbone	Tag	Assay
pcDNA5-FRT-TO-N-TAP-EGFP-Hygro	N-ter TAP	Tandem Affinity Purification (TAP)
pcDNA5-FRT-TO-N-YFP-EGFP-Hygro	N-ter YFP	Reverse Phase Protein Array (RPPA) and Illumina microarrays

One day before co-transfection, 3x10^5 cells were seeded in 6-well culture plates with D10 high glucose containing 15 µg/ml blasticidin and 100 µg/ml zeocin and incubated at 37°C and 5% CO_2. After replacing the medium with D10 high glucose 1 h prior to transfection, the reaction was prepared as follows: 0.1 µg of the expression plasmid was mixed with 0.9 µg pOG44 plasmid in 100 µl Optimem. Then, 3 µl of PEI solution was diluted in 100 µl Optimem. This PEI-mix was gently combined with the plasmid DNA-mix and incubated for 15 min at room temperature. The transfection mix was added dropwise to the culture wells and cells were incubated ON at 37°C and 5% CO_2. 24 h after transfection, the medium was replaced with D10 high glucose without rinsing the cells with PBS to avoid cell detachment. 48 h after transfection, cells were trypsinized and resuspended in 2 ml final volume of D10 high glucose, from which 1 ml was seeded in a 75-cm^2 culture flask and 1 ml in a 10-cm^2 culture dish with D10 high glucose containing 15 µg/ml blasticidin and 100 µg/ml hygromycin for selection of the stable cell clones and posterior immunobloting for protein expression, respectively. Cells grown for selection were kept in culture for 2 weeks, replacing the selection medium twice a week, until the clones were visible and expanded for freezing cell aliquots. To test for tagged protein expression, cells grown on the 10-cm^2 culture dishes were induced with 50 µg/ml doxycycline for 48 h. YFP-tag protein expressing cells were monitored by both fluorescence microscopy and immunoblot. TAP-tagged protein expression was evaluated by western blot.

4.4 Protein biochemistry methods

4.4.1 Whole cell protein extraction

Protein lysates were prepared from confluent cell cultures grown in 10-cm culture dishes. Cells were washed twice with ice-cold 1xPBS and lysed with 200 μl M-Per lysis buffer containing phosSTOP and complete EDTA-free (see 4.1.7) for at least 15 min at 4°C.

Then, cells were scraped from the dish surface and the cell lysate mix was transfered to a 1.5 cm reaction tube. To remove cell debris, the lysates were centrifuged 15 min at 13.000 rpm at 4°C. The supernatant containing the protein lysate was then transferred to a new reaction tube and stored at -80°C until analysis.

4.4.2 Determination of protein concentration

Protein concentration was determined by the bicinchoninic acid (BCA) assay. 5 µl of the sample lysate were added to 200 µl BCA solution (prepared in a 50:1 proportion, according to instructions) and incubated for 30 min at 37 °C. A standard concentration scale with BSA (0.5-10 µg/ml) was also measured. Then, the colorimetric reaction was quantified in an ELISA reader, and protein concentration was determined according to the BSA standard concentration.

4.4.3 SDS-polyacrylamid gel electrophoresis

Proteins were separated according to their size by SDS-polyacrylamid gel electrophoresis (SDS-PAGE). The SDS-polyacrylamid resolving gels were prepared according to the expected protein size as indicated in 4.1.7, and covered with 1 ml of isopropanol to obtain a flat surface. After polymerization, the isopropanol was removed entirely and the stacking gel was poured. At least 40 µg protein lysate were mixed with 2x SDS sample buffer and heat-denaturated for 5 min at 95 °C. Protein samples and 3 µl PageRuler Pre-stained Protein Ladder were then loaded onto the gel and run at 70 V for 30 min. Once the samples reached the resolving gel, the voltage was increased to 115 V.

4.4.4 Western blotting

After proteins were separated by SDS-PAGE, sample proteins were transfered to a nitrocellulose membrane using a semi-dry blotting chamber. For this, gel, nitrocellulose membrane and 6 sheets of Whatmann filter paper were rinsed for 5 min in 1x transfer buffer. Three layers of Whatmann paper were first put on the blotting chamber, followed by the membrane, the gel and three Whatmann paper sheets. For each gel to transfer, 100 mA were applied, and depending on the protein size, the transfer time varied between 30-80 min (for Ras 30 min, for proteins between 40-80 KDa 1 h and for Gab1 80 min). After blotting, the membrane was rinsed once in 1x PBS to eliminate traces of methanol and blocked with a 1:1 1xPBS:Licor blocking solution for 1 h at room temperature. After washing the membrane with 1x PBST for 5 min, the primary antibody solution was added and incubated at 4 °C overnight. Then, the membrane was washed four times each 5 min with 1x PBST previous to the incubation with the fluorescent second antibody solution for 1 h. Again, the membrane was washed four times each 5 min with 1x PBST and rinsed once in 1x PBS. Finally, the membrane was scanned and analyzed in the Odyssey Infrared Imaging System.

4.4.5 Reverse-phase protein array

To quantify protein expression of inducible YFP-T-REx HEK293 cells in a high-throughput manner, a reverse-phase protein array (RPPA) was performed. The RPPA assay was performed by Dr. Julia Starmann from the Cancer Genome Research group at the German Cancer Research Center (DKFZ, Heidelberg) within the framework of the Mutanom Consortium. T-REx HEK293 cells were seeded in 6-well plates in triplicate for three induction time points (0, 24 and 48 h) in different densities: $4x10^5$ (0 h), $3x10^5$ (24 h) and $2x10^5$ (48 h). For each time point, there was a control group of non-induced cells. After incubation overnight at 37 °C and 5% CO_2, culture medium was replaced and cells were induced with 50 µg/ml dox for the corresponding time. To prepare protein lysates, cells were rinsed with ice-cold 1x PBS and 50 µl of M-Per lysis buffer was added. Protein samples were then prepared and quantified as described (see subsections 4.4.1 and 4.4.2) and sent for RPPA to the DKFZ. Protein lysates were serially diluted with lysis buffer and printed onto nitrocellulose coated glass-slides. Slides were blocked overnight at 4 µC with a mix of Licor blocking buffer and PBS containing 1% BSA and 0.02 % NP40. Then, samples were incubated with the primary antibodies for 2 h and subsequently washed four times each 5 min with wash buffer (1xPBS, 0.02 % NP40 and 0.02 % SDS). Then, slides were incubated with secondary antibody for 30 min and washed again four times each 5 min with wash buffer. Finally, slides were rinsed with water and air-dried at room temperature (for further details, see Brase et al. (2011)). In order to compare protein expression against the control cell line N-YFP, median values were calculated and normalized against the housekeeping protein GAPDH. Then, each value was subjected to a second normalization against the control group (empty vector N-YFP) among the same time point and treatment type (induced or non-induced).

4.4.6 Tandem affinity purification

To identify new protein binding partners, a tandem affinity purification (TAP) assay was performed. The TAP purification was performed by Dr. Artur Muradyan from the Max Planck Institute for Molecular Genetics (Department of Vertebrate Genomics, Berlin) and the TAP assay was done by Dr. Gerard Joberty from Cellzome (Heidelberg) within the framework of the Mutanom Consortium. To obtain approximately protein, TAP-T-REx HEK293 cells were expanded to 100 15-cm culture dishes. For this, confluent cells were grown and expanded in thirty 75-cm^2 culture flasks until they reached 80 % confluency. Twenty 15-cm culture dishes were obtained from one culture flask with an approximate cell density of $2.5x10^6$ cells/dish. After 24h of incubation at 37 °C and 5% CO_2, cells were induced with 50 µg/ml dox. After 48 h of induction, cells were rinsed twice with ice-cold 1x PBS, harvested with 1xPBS and pelleted by centrifugation at 1000 rpm, 4 °C for 5 min. For the TAP purification, cell lysates were prepared and bound to IgG sepharose beads at 4 °C for 4 h. After cleavage with the tobacco etch virus protease (TEV) overnight, the samples were bound to calmodulin-sepharose beads. All the probes were then eluted from calmodulin beads twice with 40mM TRIS (pH 9) and

4 % SDS. Eluates were combined and precipitated with TCA/Acetone. Protein pellets were dissolved in 2x Laemmli buffer (4% SDS, 20% glycerol, 10% 2-mercaptoethanol, 0.004% bromphenol blue and 0.125 M Tris pH 6.8), boiled at 99 °C for 15 min and stored frozen. For the protein complex identification, samples were resolved in a denaturating polyacrylamid NuPAGE 4-12 % Bis-Tris gel. After protein fixation, bands were cut out and proteins were identified by mass spectrometry following isobaric tag for relative and absolut quantitation (iTRAQ) labelling. The Mascot 2.2 (Matrix Science) software was used to query peptide mass and fragmentation data. Then, the obtained data were compared against an internally curated version of the International Protein Index, and quantification was registered when at least four unique spectra were observed.

4.4.7 Yeast two-hybrid system assay

To identify possible protein-protein interactions of SHP2, a yeast two-hybrid screening (Y2H) was performed. The Y2H assay was done by Dr. Sean-Patrick Riechers from the Max Delbrück-Center for Molecular Medicine (Proteomics and Molecular Mechanisms of Neurodegenerative Diseases Group, Berlin) within the framework of the Mutanom Consortium. A prey library of approximately 16.000 unique full-length cDNAs was individually transformed in the L40ccα MATα yeast strain [MATα his3$\triangle$200 trp1-910 leu2-3,112 ade2 LYS2::(lexAop)4HIS3 URA3::(lexAop)$_8$-lacZ GAL4 gal80 can1 cyh2]. The prey plasmids (pACT4-DM derivatives) coded for a Gal4 activation domain fusion products. The yeast clones were inoculated in a 384-well format. After 2-3 days of incubation, the prey matrix was stamped onto SDI (-Leu) agar plates. The bait plasmids (pBTM116-D9 derivatives coding for LexA DNA binding domain fusions) were introduced intro a L40ccua MATa yeast strain [MATa his3$\triangle$200 trp1-901 leu2-3,112 LYS2::(lexAop)$_4$-HIS3 ura3::(lexAop)$_8$-lacZ ADE2::(lexAop)$_8$-URA3 GAL4 gal80 can1 cyh2]. Bait pools were made of eight bait strains per pool. To select the protein-protein interactions, diploid yeasts were spotted onto SDIV (-Leu-Trp-Ura-His) agar plates and nylon membranes placed on SDIV agar plates. After 5-6 days of incubation at 30 °C, digitalized images of both agar plates and nylon membranes were assessed for growth and β-galactosidase activity using the Visual Grid software (GPC Biotech). To confirm protein interactions, the eight baites from each pool were mated with the positive preys identified in the first mating screen, After 36 h of incubation, yeast strains were spotted onto SDII agar plates for selection of diploid cells expression both protein fusions. Yeast colonies that grew four days later were assayed on SDIV aar plates and nylon membranes. then, a Support Vector Machine (SVM) score for predicting protein-protein interactions was calculated. The SVM score considered true or false assumption between known interactions and random protein pairs in the seven dimensional scoring space: 1). the gene-atlas based co-expression scoring, 2). known orthologous protein-protein interaction scoring, 3). protein domain complementarity analysis, 4). and 5). biological process and cellular component GO term semantic similarity scoring, 6). and 7). shortest path analysis number and length scoring. Interaction protein pairs were classified into high confidence (HC), medium confidence (MC) or low confidence (LC), according to the SVM score.

4.4.8 Co-immunoprecipitation

To validate the data obtained from the TAP assay approach by precipitation of protein binding partners, a co-immunoprecipitation (co-IP) assay was performed after epidermal growth factor (EGF) stimulation. 2x10^6 YFP-TREx HEK293 cells were seeded in 10-cm culture dishes with 5 ml medium for five stimulation time points (0, 5, 10, 30 and 60 min) and incubated overnight at 37°C and 5% CO_2. Then, YFP-tag protein expression was induced with 50 µg/ml dox for 48 h. Subsequently, the culture medium was removed and cells were serum starved for approximately 18 h before EGF stimulation. After the cells were stimulated with 25 ng/ml human EGF for the indicated time, cells were carefully rinsed once with ice-cold 1xPBS, schock-frozen on dry ice. Protein lysates were prepared with 250 µl of M-Per lysis buffer and concentration was determined as described in 4.4.1 and 4.4.2. 1 mg of whole protein was gently mixed with 50 µl of Dynabeads Protein A overnight at 4 °C by continuous rotation. Then, the supernatant was removed and the rabbit SHP2 primary antibody diluted in PBST 1:100 was incubated with the magnetic beads for 3 h at 4 °C with gentle rocking. The protein-bead pellets were carefully washed three times with 100 µl of M-Per lysis buffer and eluted in 20 µl of 2x SDS sample buffer. After denaturation at 80°C for 10 min, protein samples were analysed by western blotting (see subsection 4.4.4). Additionally, a western blot with 40 µg whole protein was also performed.

4.5 Phenotypic characterization methods

4.5.1 Xenotransplantation

To evaluate the ability of SHP2 mutations to confer an oncogenic potential in 208F cells that lead to solid tumors in vivo, a xenotransplantation assay on nude mice was done. This assay was performed by Maria Stecklum (EPO GmbH, Berlin). 208F cells were seeded in a 75-cm^2 culture flasks and grown to confluency. From this initial inoculum, five 75-cm^2 culture flasks were prepared to obtain 5x10^7 cells. Then, the cells were trypsinized with 2 ml EDTA-trypsin solution and resuspended in 8 ml of D10 culture medium. For harvesting, cells were centrifuged for 5 min at 800 x g and resuspended in 500 µl 1x PBS. Cells were kept on ice until inoculation the same day of collection. For each group, three mice were subcutaneously (s.c.) inoculated with 1x10^7 cells/100 µl 1x PBS. Mice were supervised and tumor growth documented every week. After completion of the growth time, tumors were excised, shock-frozen and stored at -80°C. Tumor size was measured in two dimensions with a caliper. Individual tumor volume was calculated with the formula: Volume = 0.5x(length x $width^2$)

4.5.2 Immunohistochemistry

For immunohistological analysis 3 µm thick paraffin sections of tumor tissue from xenografts from nude mice were dewaxed at 70°C for 20 min and afterwards rehydrated as follows: three times for 5 min with xylol, twice for 5 min with 100 % ethanol and

for 3 min with each 96%, 90%, 80% and 70% ethanol and H_2O. For antigen retrieval the sections were incubated in citrate buffer at 100°C for 20 min followed by a slowly cooling down step for 15 min and incubation for 10 min in 3 % H_20_2 solution. Then, blocking was carried out with 150 µl Dako Real Peroxidase-Blocking Solution for 30 min in a wet chamber prior to incubation with the rat monoclonal anti-mouse primary antibody against the endothelial cell marker CD-31 (PECAM1) diluted 1:500 in Dako Antibody Diluent overnight at 4°C. Binding was detected with the rabbit anti-goat HRP conjugated secondary antibody (Invitrogen) diluted 1:350. The colored reaction was detected using the Dako Kit. Next, sections were incubated in haematoxylin for 10 sec and washed with H^2O. Subsequently, each section was covered with cover slides and sealed with 1:1 xylol:Vitro-Clud (Langenbrink, Germany) and evaluated under the light microscope.

4.6 Bioinformatic analysis

4.6.1 Microarray experiments and data analysis

To study the gene expression profile of dox-inducible stable SHP2 or BRAF expressing HEK-TRex cells, 500 ng of total RNA in 11 µl were labelled and hybridized on Illumina HumanHT-12 v3 Expression BeadChips (in cooperation with the Genomics deparment, MPI for molecular genetics and the Laboratory for Functional Genomics Charité). Following washing and staining, the 12-probe arrays were scanned using the BeadArray™Reader controlled by the Bead Array Scan Software (version 3.0).

4.6.1.1 Data pre-processing

Raw data was processed with the Illumina BeadStudio Software. Then, background was subtracted and normalized within each chip using the Bioconductor limma package in the R software (Smyth, 2004). The mean value of the raw data was calculated from all arrays, except for the arrays corresponding to BRAF-TREx^{K499E}, which were removed due to strong hybridization artifacts. The intensity values were adjusted by quantile normalization and the batch effect was removed. Next, a linear model was fitted to the expression data for each gene and empirical Bayes method was applied. Then, p-values were adjusted by a false discovery rate (FDR) correction. To check for possible batch effects, the top 1000 significantly expressed genes from each array were compared within the group and a cluster diagram was generated. Next, normalized data were log2-transformed and quantile-normalized. Differential expressed genes were selected after a q-value <0.05 and a threshold of <0.7 or >1.4 fold-change. To compare differential gene expression between wild-type and mutant groups, log2 fold change values were calculated by subtraction of the mutation-value from wild-type.

4.6.1.2 Gene Ontology and pathway analysis

To classify the regulated genes of the microarray data in relevant categories, a Gene Ontology (GO) analysis was performed using the Database for Annotation, Visualization and Integrated Discovery (DAVID) and the WEB-based Gene Set Analysis Toolkit (WebGestalt) with a Benjamini-Hochberg multiple test adjustment (adj. p-val <0.05) and a minimum of two genes for each category. Here, different categories were selected, according to the three main groups: molecular function (MF), biological process (BP) and cellular component (CC). As background, the complete list of Ilumina identifiers was used. To identify genes in a signaling pathway, the enriched Kyoto Encyclopedia of Genes and Genomes (KEGG) was used.

Appendices

A.1 RPPA assays

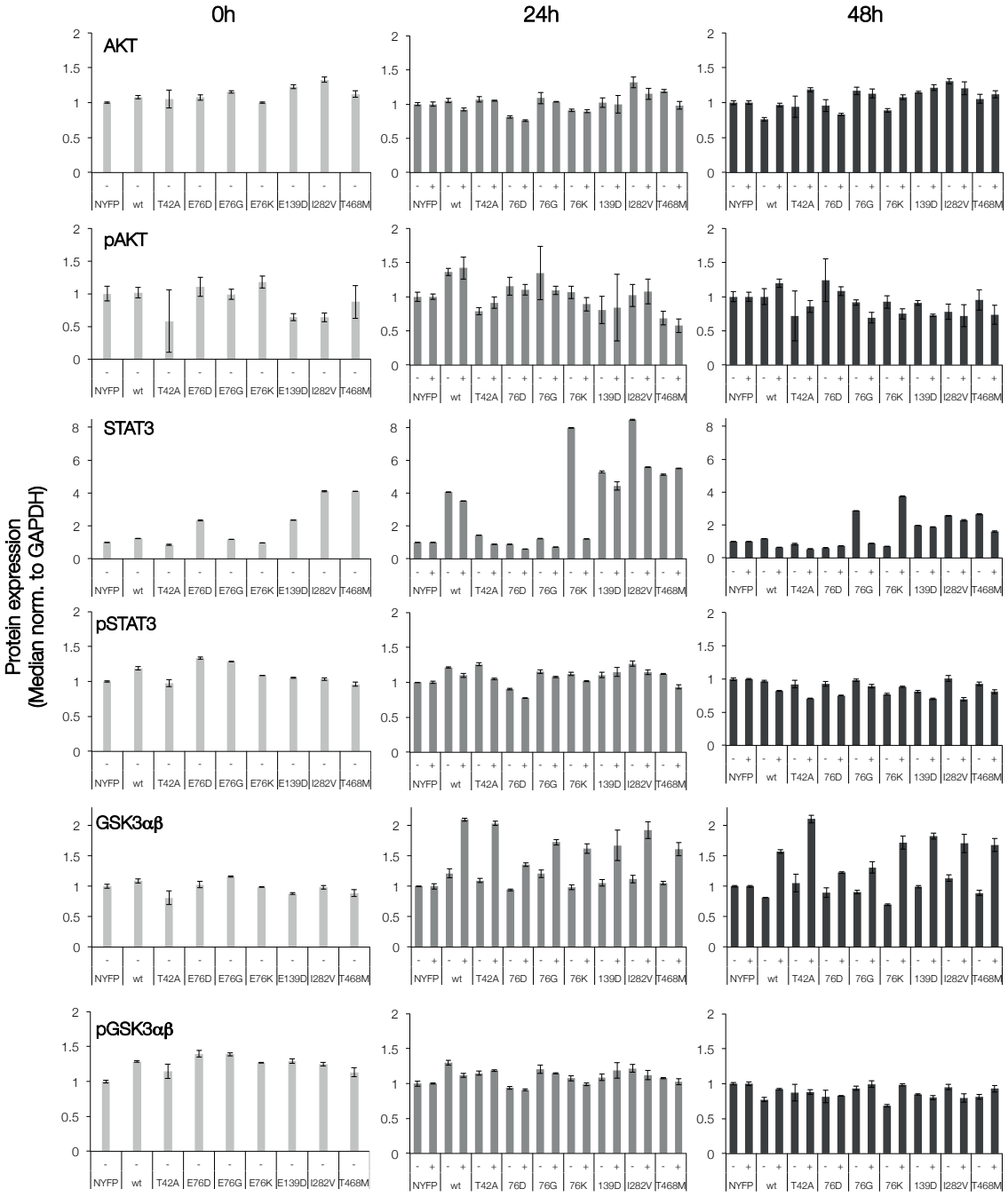

Figure A.1: RPPA analysis of AKT, STAT3 and GSK3α β in isogenic SHP2-TREx cells. Shown are the median values for 0, 24 and 48h of Dox induction after normalization to GAPDH for each time point and cell line.

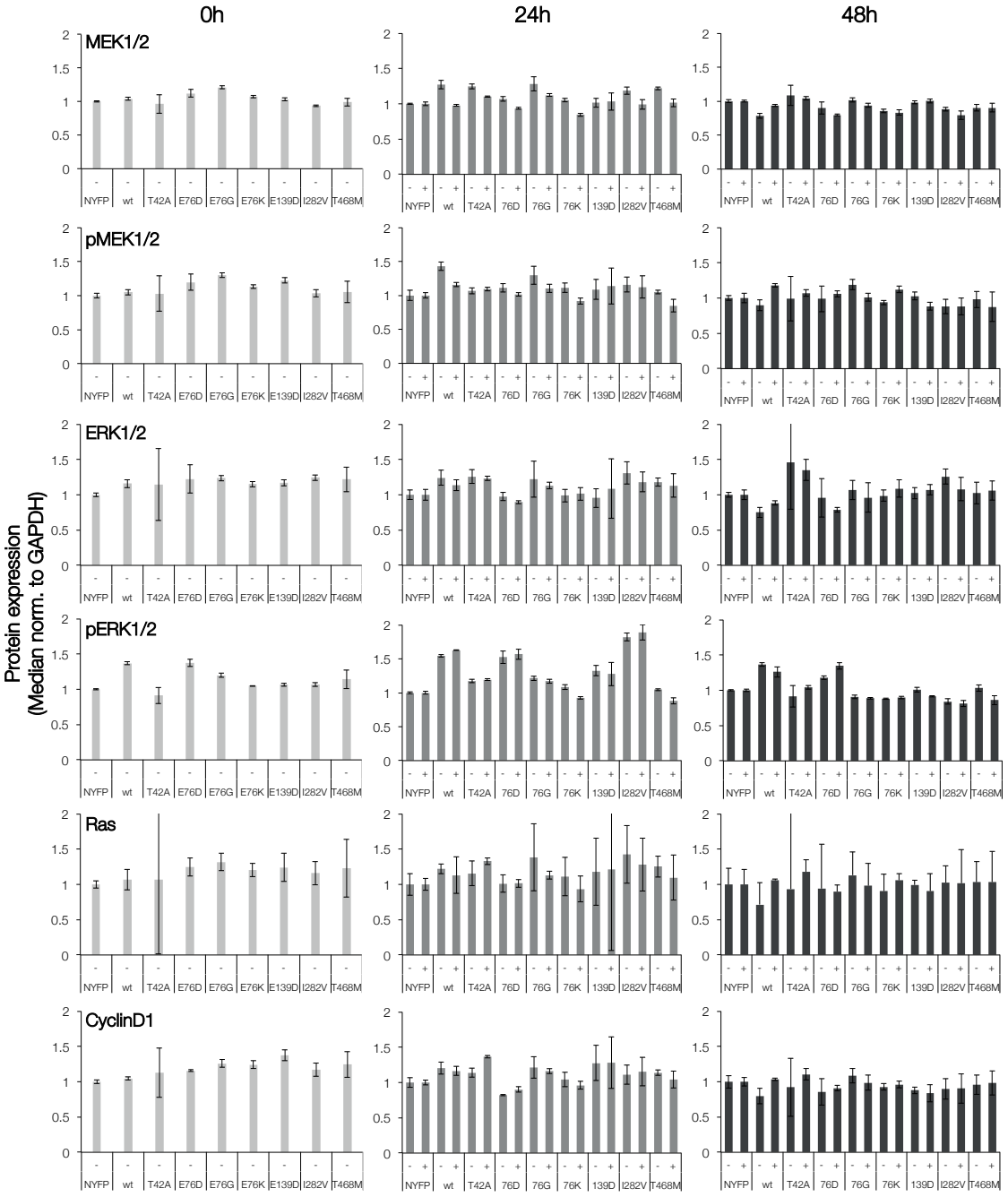

Figure A.2: RPPA analysis of MEK1/2, ERK1/2, Ras and cyclin D1 in isogenic SHP2-TREx cells. Shown are the median values for 0, 24 and 48h of Dox induction after normalization to GAPDH for each time point and cell line.

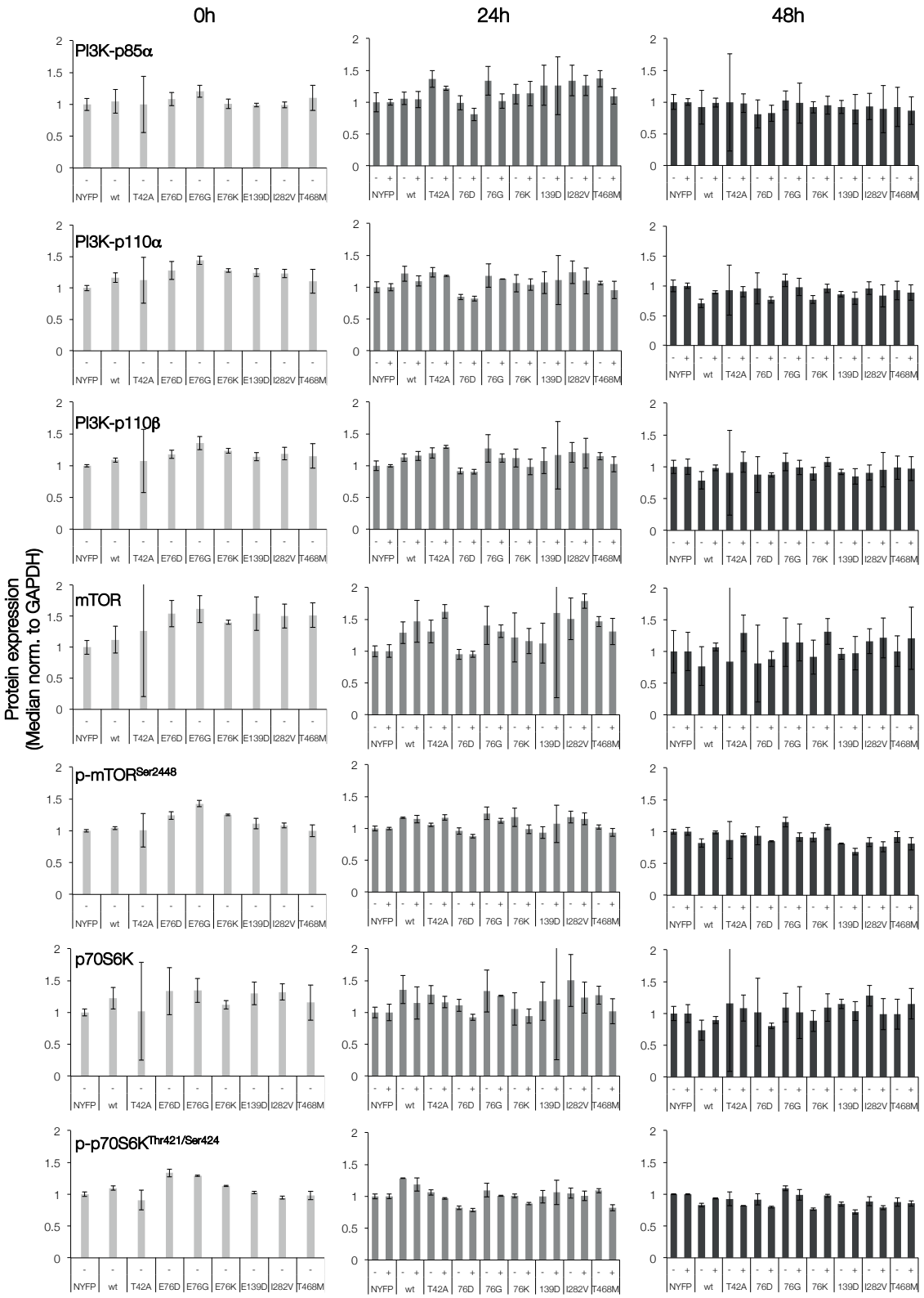

Figure A.3: RPPA analysis of PI3K-p85α/110α β, mTOR, and p70S6K in isogenic SHP2-TREx cells. Shown are the median values for 0, 24 and 48h of Dox induction after normalization to GAPDH for each time point and cell line.

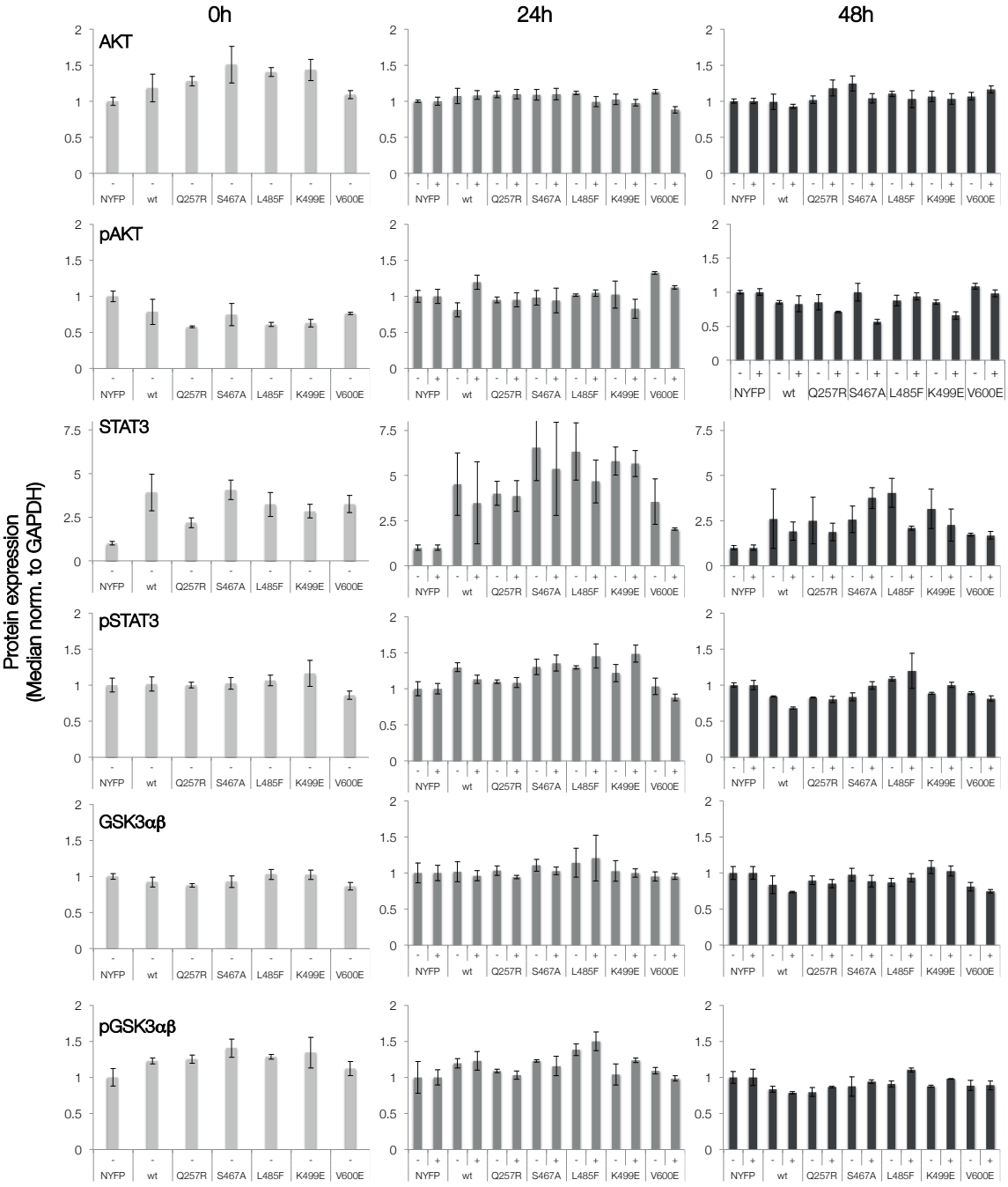

Figure A.4: RPPA analysis of AKT, STAT3 and GSK3α β in isogenic BRAF-TREx cells. Shown are the median values for 0, 24 and 48h of Dox induction after normalization to GAPDH for each time point and cell line.

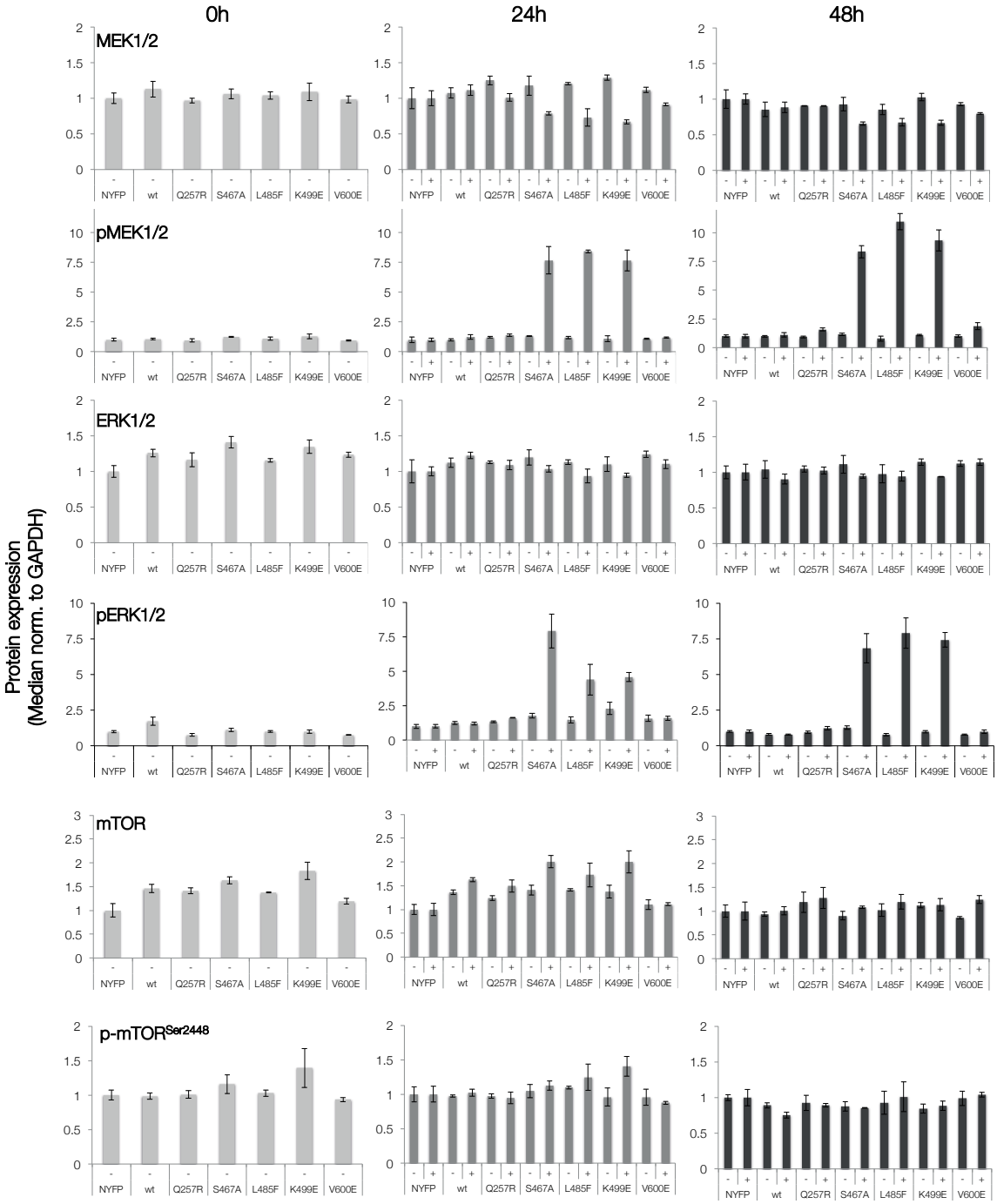

Figure A.5: RPPA analysis of MEK1/2, ERK1/2 and mTOR in isogenic BRAF-TREx cells. Shown are the median values for 0, 24 and 48h of Dox induction after normalization to GAPDH for each time point and cell line.

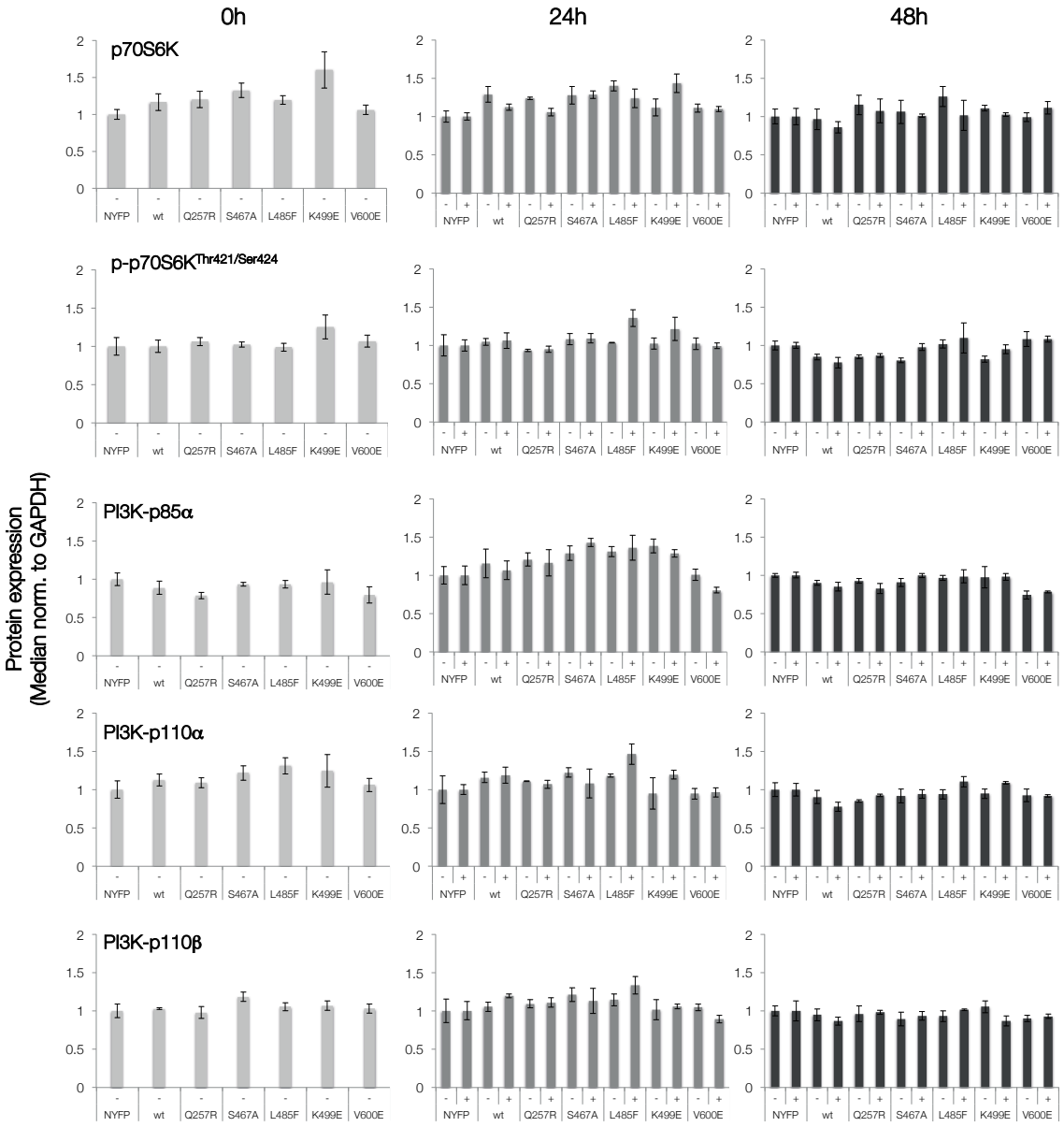

Figure A.6: RPPA analysis of p70S6K and PI3K-p85α/110$\alpha\beta$ in isogenic BRAF-TREx cells. Shown are the median values for 0, 24 and 48h of Dox induction after normalization to GAPDH for each time point and cell line.

A.2 Y2H assay

Table A.10: Literature search for SHP2 protein interaction partners.
Common binding targets found in both STRING and UniHI databases.

Gene ID	Gene symbol	Name
284	ANGPT1	angiopoietin 1
338	APOB	apolipoprotein B
558	AXL	AXL receptor tyrosine kinase
9564	BCAR1	breast cancer anti-estrogen resistance 1
613	BCR	breakpoint cluster region
151888	BTLA	B and T lymphocyte associated
847	CAT	catalase
857	CAV1	caveolin 1, caveolae protein, 22kDa
867	CBL	Cas-Br-M (murine) ecotropic retroviral transforming sequence
919	CD247	CD247 molecule
915	CD3D	CD3d molecule, delta (CD3-TCR complex)
916	CD3E	CD3e molecule, epsilon (CD3-TCR complex)
917	CD3G	CD3g molecule, gamma (CD3-TCR complex)
920	CD4	CD4 molecule
961	CD47	CD47 molecule
8832	CD84	CD84 molecule
942	CD86	CD86 molecule
1003	CDH5	cadherin 5, type 2 (vascular endothelium)
634	CEACAM1	carcinoembryonic antigen-related cell adhesion molecule 1
1398	CRK	v-crk sarcoma virus CT10 oncogene homolog (avian)
1399	CRKL	v-crk sarcoma virus CT10 oncogene hom (avian)-like
1437	CSF2	colony stimulating factor 2 (granulocyte-macrophage)
1438	CSF2RA	colony stimulating factor 2 receptor, alpha, low-affinity (granulocyte-macrophage)
1439	CSF2RB	colony stimulating factor 2 receptor, beta, low-affinity (granulocyte-macrophage)
1441	CSF3R	colony stimulating factor 3 receptor (granulocyte)
1445	CSK	c-src tyrosine kinase
1493	CTLA4	cytotoxic T-lymphocyte-associated protein 4
1499	CTNNB1	catenin (cadherin-associated protein), beta 1, 88kDa
7852	CXCR4	chemokine (C-X-C motif) receptor 4
1630	DCC	deleted in colorectal carcinoma
1950	EGF	epidermal growth factor
1956	EGFR	epidermal growth factor receptor
1969	EPHA2	EPH receptor A2
2057	EPOR	erythropoietin receptor
2064	ERBB2	v-erb-b2 erythroblastic leukemia viral oncogene homolog 2, neuro/glioblastoma derived oncogene homolog (avian)
2065	ERBB3	v-erb-b2 erythroblastic leukemia viral oncogene homolog 3 (avian)
2213	FCGR2B	Fc fragment of IgG, low affinity IIb, receptor (CD32); Fc fragment of IgG, low affinity IIc, receptor for (CD32)
3667	IRS1	insulin receptor substrate 1
8660	IRS2	insulin receptor substrate 2
8471	IRS4	insulin receptor substrate 4
3716	JAK1	Janus kinase 1
3717	JAK2	Janus kinase 2
3791	KDR	kinase insert domain receptor (a type III receptor tyrosine kinase)
3802	KIR2DL1	killer cell immunoglobulin-like receptor, two domains, long cytoplasmic tail, 2
3804	KIR2DL3	killer cell immunoglobulin-like receptor, two domains, long cytoplasmic tail, 3
3815	KIT	v-kit Hardy-Zuckerman 4 feline sarcoma viral oncogene homolog
4254	KITLG	KIT ligand
3821	KLRC1	killer cell lectin-like receptor subfamily C, member 1
3845	KRAS	v-Ki-ras2 Kirsten rat sarcoma viral oncogene homolog
3903	LAIR1	leukocyte-associated immunoglobulin-like receptor 1
3932	LCK	lymphocyte-specific protein tyrosine kinase
3953	LEPR	leptin receptor
3977	LIFR	leukemia inhibitory factor receptor alpha
11006	LILRB4	leukocyte immunoglobulin-like receptor, subfamily B (with TM and ITIM domains), member 4
8543	LMO4	LIM domain only 4
4063	LY9	lymphocyte antigen 9
4067	LYN	v-yes-1 Yamaguchi sarcoma viral related oncogene homolog
5595	MAPK3	mitogen-activated protein kinase 3
4233	MET	met proto-oncogene (hepatocyte growth factor receptor)
9019	MPZL1	myelin protein zero-like 1
4893	NRAS	neuroblastoma RAS viral (v-ras) oncogene homolog
9423	NTN1	netrin 1
55824	PAG1	phosphoprotein associated with glycosphingolipid microdomains 1
5133	PDCD1	programmed cell death 1
5155	PDGFB	platelet-derived growth factor beta polypeptide
5159	PDGFRB	platelet-derived growth factor receptor, beta polypeptide
5290	PIK3CA	phosphoinositide-3-kinase, catalytic, alpha polypeptide
5291	PIK3CB	phosphoinositide-3-kinase, catalytic, beta polypeptide
5294	PIK3CG	phosphoinositide-3-kinase, catalytic, gamma polypeptide
5295	PIK3R1	phosphoinositide-3-kinase, regulatory subunit 1 (alpha)
5296	PIK3R2	phosphoinositide-3-kinase, regulatory subunit 2 (beta)
8503	PIK3R3	phosphoinositide-3-kinase, regulatory subunit 3 (gamma)
29992	PILRA	paired immunoglobin-like type 2 receptor alpha
29990	PILRB	paired immunoglobin-like type 2 receptor beta

Gene ID	Gene symbol	Name
2321	FLT1	fms-related tyrosine kinase 1 (vascular endothelial growth factor/vascular permeability factor receptor)
2322	FLT3	fms-related tyrosine kinase 3
10818	FRS2	fibroblast growth factor receptor substrate 2
10817	FRS3	fibroblast growth factor receptor substrate 3
2534	FYN	FYN oncogene related to SRC, FGR, YES
2549	GAB1	GRB2-associated binding protein 1
9846	GAB2	GRB2-associated binding protein 2
139716	GAB3	GRB2-associated binding protein 3
2690	GHR	growth hormone receptor
2885	GRB2	growth factor receptor-bound protein 2
2904	GRIN2B	glutamate receptor, ionotropic, N-methyl D-aspartate 2B
3127	HLA-DRB5	major histocompatibility complex, class II, DR beta 5
3265	HRAS	v-Ha-ras Harvey rat sarcoma viral oncogene homolog
3448	IFNA14	interferon, alpha 14
3449	IFNA16	interferon, alpha 16
3440	IFNA2	interferon, alpha 2
3442	IFNA5	interferon, alpha 5
3443	IFNA6	interferon, alpha 6
3445	IFNA8	interferon, alpha 8
3454	IFNAR1	interferon (alpha, beta and omega) receptor 1
3456	IFNB1	interferon, beta 1, fibroblast
3458	IFNG	interferon, gamma
3459	IFNGR1	interferon gamma receptor 1
3460	IFNGR2	interferon gamma receptor 2
3480	IGF1R	insulin-like growth factor 1 receptor
3562	IL3	interleukin 3 (colony-stimulating factor, multiple)
3563	IL3RA	interleukin 3 receptor, alpha (low affinity)
3566	IL4R	interleukin 4 receptor
3567	IL5	interleukin 5 (colony-stimulating factor, eosinophil)
3568	IL5RA	interleukin 5 receptor, alpha
3569	IL6	interleukin 6 (interferon, beta 2)
3570	IL6R	interleukin 6 receptor
3572	IL6ST	interleukin 6 signal transducer (gp130, oncostatin M receptor)
3635	INPP5D	inositol polyphosphate-5-phosphatase, 145kDa
3643	INSR	insulin receptor
3394	IRF8	interferon regulatory factor 8
5335	PLCG1	phospholipase C, gamma 1
5518	PPP2R1A	protein phosphatase 2 (formerly 2A), regulatory subunit A, alpha isoform
5617	PRL	prolactin
5618	PRLR	prolactin receptor
5747	PTK2	PTK2 protein tyrosine kinase 2
2185	PTK2B	PTK2B protein tyrosine kinase 2 beta
5777	PTPN6	protein tyrosine phosphatase, non-receptor type 6
5829	PXN	paxillin
2889	RAPGEF1	Rap guanine nucleotide exchange factor (GEF) 1
5979	RET	ret proto-oncogene
6464	SHC1	SHC (Src homology 2 domain contain)transforming protein 1
114132	SIGLEC11	sialic acid binding Ig-like lectin 11
140885	SIRPA	signal-regulatory protein alpha
27240	SIT1	signaling threshold regulating transmembrane adaptor 1
6504	SLAMF1	signaling lymphocytic activation molecule family member 1
114836	SLAMF6	SLAM family member 6
8651	SOCS1	suppressor of cytokine signaling 1
9021	SOCS3	suppressor of cytokine signaling 3
6654	SOS1	son of sevenless homolog 1 (Drosophila)
10253	SPRY2	sprouty homolog 2 (Drosophila)
6714	SRC	v-src sarcoma (Schmidt-Ruppin A-2) viral oncogene homolog (avian)
6772	STAT1	signal transducer and activator of transcription 1, 91kDa
6773	STAT2	signal transducer and activator of transcription 2, 113kDa
6774	STAT3	signal transducer and activator of transcription 3 (acute-phase response factor)
6776	STAT5A	signal transducer and activator of transcription 5A
6777	STAT5B	signal transducer and activator of transcription 5B
7010	TEK	TEK tyrosine kinase, endothelial
8764	TNFRSF14	tumor necrosis factor receptor superfamily, member 14
28755	TRAC	T cell receptor alpha constant
340205	TREML1	triggering receptor expressed on myeloid cells-like 1
7297	TYK2	tyrosine kinase 2
7311	UBA52	ubiquitin A-52 residue ribosomal protein fusion product 1
7314	UBB	ubiquitin B
7316	UBC	ubiquitin C
8633	UNC5C	unc-5 homolog C (C. elegans)
7525	YES1	v-yes-1 Yamaguchi sarcoma viral oncogene homolog 1

Table A.11: Preys obtained after yeast-two-hybrid with SHP2 wild-type as bait.

Gene ID		Protein name	Co-expression	Domain	Sem sim bp	Sem sim cc	Topo x	Topo y	Svm score	Category
Bait	Prey									
5781	22921	MSRB2	0.01	0	0.16	0.92	0.54	0.2	1.19	HC
5781	375133	PI4KAP2	0.01	0	0.71	0.74	0.2	0.54	1.15	HC
5781	673	BRAF_1799TA	0.01	1	0.72	0.65	0.2	0.2	1.02	HC
5781	7297	TYK2	0.01	0.96	0.7	0.4	0.99	0.2	1.02	HC
5781	118932	ANKRD22	0.01	0.46	0.54	0.74	0.54	0.2	1	HC
5781	51701	NLK	0.01	0.96	0.61	0.53	0.38	0.2	0.98	HC
5781	26579	MYEOV	0.01	0	0.54	0.74	0.54	0.2	0.97	HC
5781	202500	TCTE1	0.01	0	0.54	0.74	0.54	0.2	0.97	HC
5781	5800	PTPRO	0	0.96	1	0.01	0.99	0.2	0.96	HC
5781	84969	TOX2	0.01	0.46	0.43	0.51	0.54	0.2	0.94	HC
5781	150365	MEI1	0.01	0	0.48	0.74	0.54	0.2	0.94	HC
5781	11019	LIAS	0.01	0	0.36	0.73	0.54	0.2	0.84	HC
5781	3064	HTT	0.01	0.46	0.5	0.52	0.83	0.2	0.84	HC
5781	343263	MYBPHL	0.01	0.76	0	0	0.54	0.2	0.46	HC
5781	23436	CELA3B	0.01	0.46	0.51	0	0.54	0.2	0.37	HC
5781	999	CDH1_1108GC	0.01	0	0.54	0.39	0.92	0.2	0.37	HC
5781	29934	SNX12	0.01	0	0.02	0.74	0.38	0.2	0.31	HC
5781	23769	FLRT1	0.01	0	0.03	0.01	0.54	0.2	0.24	HC
5781	10227	MFSD10	0.01	0	0.05	0.02	0.54	0.2	0.19	HC
5781	5519	PPP2R1B	0.01	0.46	0.54	0.74	0.2	0.2	0.16	HC
5781	3845	KRAS2_C467A	0.01	0.46	0.71	0.36	0.2	0.2	0.03	MC
5781	64396	GMCL1L	0.01	0	0.76	0.36	0.54	0.2	0.02	MC
5781	6788	STK3	0.01	0.96	0.65	0.63	0.54	0.38	-0.03	MC
5781	8061	FOSL1	0.01	0.46	0.53	0.62	0.38	0.38	-0.12	LC
5781	4763	NF1_2033del_c	0.01	0.46	0.61	0.35	0.83	0.38	-0.26	LC
5781	6754	SSTR4	0.01	0.46	0.72	0.01	0.38	0.54	-0.3	LC
5781	284001	CCDC57	0.01	0	0.54	0.74	0.2	0.2	-0.31	LC
5781	6122	RPL3	0.01	0.46	0.45	0.65	0.2	0.2	-0.35	LC
5781	89874	SLC25A21	0.01	0	0.04	0.43	0.54	0.2	-0.43	LC
5781	26009	ZZZ3	0.01	0	0.43	0.51	0.54	0.2	-0.49	LC
5781	166793	ZBTB49	0.01	0	0.54	0.47	0.54	0.2	-0.51	LC
5781	10794	ZNF460	0.01	0	0.47	0.49	0.54	0.2	-0.55	LC
5781	374899	ZNF829	0.01	0	0.47	0.49	0.54	0.2	-0.55	LC
5781	3816	KLK1	0.01	0.46	0.42	0.74	0.38	0.54	-0.55	LC
5781	3188	HNRNPH2	0.01	0.46	0.21	0.47	0.2	0.2	-0.73	LC
5781	23466	CBX6	0.01	0	0.46	0.4	0.54	0.2	-0.92	LC
5781	4118	MAL	0	0	0.54	0.33	0.54	0.2	-0.96	LC
5781	64114	TMBIM1	0.01	0	0.54	0.02	0.54	0.2	-0.97	LC
5781	81501	TM7SF4	0.01	0	0.58	0.01	0.54	0.2	-0.97	LC
5781	135927	C7orf34	0.01	0	0.54	0	0.2	0.54	-0.98	LC
5781	5805	PTS	0	0	0.39	0.84	0.54	0.38	-0.99	LC
5781	2189	FANCG	0.01	0	0.66	0.73	0.89	0.38	-0.99	LC
5781	271	AMPD2	0.01	0	0.26	0	0.2	0.38	-1	LC
5781	10169	SERF2	0.01	0	0.54	0.74	0.38	0.38	-1	LC
5781	6697	SPR	0.01	0	0.08	0.75	0.38	0.38	-1	LC
5781	8431	NR0B2	0.01	0	0.6	0.73	0.96	0.38	-1	LC
5781	26574	AATF	0.01	0	0.48	0.49	0.92	0.38	-1	LC
5781	10480	EIF3M	0.01	0	0.44	0.6	0.76	0.38	-1	LC
5781	55658	RNF126	0.01	0	0.54	0.74	0.66	0.38	-1	LC
5781	51621	KLF13	0.01	0	0.43	0.49	0.54	0.38	-1	LC
5781	391104	VHLL	0.01	0	0.55	0.51	0.2	0.38	-1.01	LC
5781	89866	SEC16B	0.01	0	0.02	0.3	0.2	0.38	-1.01	LC
5781	3792	KEL	0.01	0	0.44	0.01	0.38	0.38	-1.01	LC
5781	892	CCNC	0.01	0	0.43	0.51	0.76	0.38	-1.01	LC
5781	8883	NAE1	0.01	0	0.39	0.49	0.76	0.38	-1.01	LC
5781	11282	MGAT4B	0.01	0	0.3	0.18	0.38	0.38	-1.01	LC
5781	6598	SMARCB1	0.01	0	0.41	0.38	0.2	0.2	-1.01	LC
5781	2628	GATM	0	0	0.55	0.57	0.38	0.38	-1.02	LC
5781	3887	KRT81	0.01	0	0.54	0.49	0.2	0.38	-1.02	LC
5781	55048	VPS37C	0.01	0	0	0.2	0.38	0.38	-1.02	LC
5781	8493	PPM1D	0.01	0	0.4	0.51	0.38	0.38	-1.02	LC
5781	55718	POLR3E	0.01	0	0.32	0.51	0.2	0.38	-1.03	LC
5781	468	ATF4	0.01	0.46	0.44	0.32	0.2	0.2	-1.03	LC
5781	10099	TSPAN3	0	0	0.54	0.02	0.2	0.38	-1.04	LC
5781	10899	JTB	0.01	0	0.54	0.23	0.2	0.38	-1.05	LC
5781	28973	MRPS18B	0.01	0	0.5	0.61	0.38	0.38	-1.06	LC
5781	4688	NCF2	0.01	0.91	0.17	0.56	0.76	0.38	-1.07	LC
5781	7541	ZFP161	0.01	0	0.46	0.49	0.2	0.38	-1.08	LC
5781	7745	ZNF192	0.01	0	0.35	0.58	0.54	0.54	-1.14	LC
5781	9367	RAB9A	0.01	0.46	0.26	0.26	0.2	0.38	-1.4	LC

Biological process GO term semantic similarity scoring (Sem sim bp), cellular component GO term semantic similarity scoring (Sem sim cc), the shortest path length scoring (Topo x), the shortest path length scoring (Topo y), scoring vector machine (svm). HC: high confidence; MC: medium confidence; LC: low confidence.

A.3 Tandem affinity purification

Table A.12: Tandem affinity purification assay of SHP2-HEK-TRex cells.

1st TAP			
Protein name	qusm	*Fold change*	
		T42A	E76G
ACTB	9	0.9	1.3
CLTC	5	1.3	1.3
DHX9	43	0.6	1.7
FABP5	4	1.6	1.7
GAB1	**27**	**7.0**	**2.8**
HIST1H1C	7	1.0	3.7
HNRNPA2B1	19	0.7	2.2
HNRNPA3	6	0.8	2.1
HNRNPC	4	0.7	1.8
HNRNPU	37	0.8	2.7
HNRPA1L-2	14	0.8	2.7
HSPA5	12	1.2	1.1
LRPPRC	4	0.7	1.4
MFAP4	5	1.0	0.7
MPZL1	15	1.7	2.2
MRPS22	7	1.0	1.3
MRPS9	5	0.8	1.7
NCL	7	0.9	4.6
NPM1	6	0.7	7.6
PTPN11	1338	1.0	1.0
RPL11	7	0.5	3.1
RPL12	5	0.5	3.1
RPL23A	8	0.4	4.2
RPL24	5	0.4	6.6
RPL26	8	0.5	3.6
RPL30	4	0.5	3.6
RPLP0-LIKE	8	0.7	4.4
RPS10	11	0.6	2.2
RPS11	8	0.4	3.2
RPS13	15	0.4	2.8
RPS15	8	0.5	2.9
RPS15A	8	0.4	2.3
RPS16	6	0.6	2.7
RPS19	23	0.7	2.1
RPS20	5	0.8	2.0
RPS25	8	0.4	2.7
RPS3	12	0.5	2.2
RPS3A	7	0.5	2.6
RPS4X	9	0.5	4.0
RPS7	11	0.4	2.7
USP11	9	1.2	1.7

2nd TAP			
Protein name	qusm	*Fold change*	
		T42A	E76G
CAD	37	1.3	3.7
CALM1	6	1.2	1.0
CAPNS1	34	1.2	1.4
CUL7	101	1.0	2.2
CUL9	4	0.8	2.1
DDB1	17	1.1	2.0
DHX9	4	0.9	2.7
DLG5	10	1.3	0.7
EDD1	9	0.9	1.7
EEF2	5	1.4	3.9
EFTUD2	4	1.0	2.4
EPPK1	18	2.0	1.6
FASN	4	0.9	2.3
FBXW8	6	1.3	2.4
FLNA	5	1.6	2.2
GAB1	**9**	**8.8**	**7.4**
HNRNPA2B1	5	1.2	1.5
HNRNPU	7	1.2	2.0
HSPA5	5	1.1	1.3
IRS4	10	1.2	2.8
MAN2C1	84	1.5	1.6
NIN	5	0.7	1.7
NISCH	8	1.3	2.6
OBSL1	5	1.2	3.4
PNMA2	11	1.4	3.3
PPP2CA	10	1.0	2.8
PPP2R1A	12	1.3	3.3
PPP2R2A	13	1.3	3.0
PTPN11	893	1.0	1.0
RPS10	5	1.4	2.0
RPS19	8	1.2	1.8
RPS3	7	0.8	0.9
SIRT1	4	1.5	1.6
SNRNP200	12	1.0	2.1
TLN1	4	1.0	1.8
TUBA1A	11	1.1	3.9
UBR4	8	1.0	1.8
USP11	5	0.9	2.3
USP9X	14	1.3	3.1
VPS16	5	1.1	3.5
VPS18	13	1.1	4.4
VPS41	10	1.4	3.9

Fold change: represents the ratio mutant/wt. Protein below the threshold (0.8-1.4) are light-coloured. Qusm: quantified unique spectra.

A.4 Microarray analysis

Table A.13: Significant regulated genes in NS/LS-associated SHP2 mutants

Illumina ID	Gene symbol	logFC wt-mutant				
		T42A	E76G	E139D	I282V	T468M
ILMN_1732296	ID3	-1.00	-1.11	-0.92	-1.25	-1.75
ILMN_1704056	RPPH1	-0.79	-0.88	-0.78	-0.91	-1.08
ILMN_1788547	GCLM	-0.60	-0.59	-0.72	-0.59	-0.80
ILMN_1862013	NA	0.53	0.63	0.51	0.60	0.63
ILMN_1803945	HCP5	0.92	0.97	0.55	0.73	0.90
ILMN_1752299	RAB6B	0.66	0.60	0.61	0.62	0.77
ILMN_1770940	CDH1	0.85	0.80	0.62	0.65	0.74
ILMN_1704294	CDH3	0.87	0.86	0.70	0.77	1.04
ILMN_1680996	ALOX5	0.87	0.62	0.74	0.73	1.20
ILMN_1776157	SEPT4	0.91	0.73	0.77	0.76	1.13
ILMN_1674236	HSPB1	0.77	0.63	0.78	0.89	0.97
ILMN_1671703	ACTA2	1.03	0.72	0.79	0.97	1.35
ILMN_1672536	FBLN1	0.79	0.81	0.82	0.92	1.22
ILMN_1752199	LHPP	1.18	0.92	0.83	0.89	1.29
ILMN_2077952	GALNT16	1.07	0.70	0.88	0.96	1.06
ILMN_1895327	NA	0.88	0.89	0.90	0.94	1.39
ILMN_2305225	NDRG4	0.93	0.92	0.91	0.99	1.12
ILMN_1779071	FEZ1	1.07	0.92	0.98	1.11	1.49
ILMN_1803423	ARHGEF6	0.93	0.88	0.98	0.65	1.14
ILMN_1723480	BST2	1.18	0.92	0.99	0.95	1.55
ILMN_1740234	GSTO2	1.19	1.15	1.02	0.89	1.33
ILMN_1657111	AHNAK2	0.92	0.78	1.04	0.66	1.22
ILMN_1912171	NA	1.08	0.96	1.05	0.97	1.66
ILMN_2309534	RDM1	1.29	1.11	1.07	1.15	1.43
ILMN_1801246	IFITM1	1.14	0.79	1.07	1.00	1.28
ILMN_1666503	DENND2A	1.09	1.07	1.10	0.82	1.28
ILMN_1765446	EMP3	1.00	0.93	1.11	0.80	1.06
ILMN_1769520	UBE2L6	1.26	1.19	1.15	1.45	1.60
ILMN_1779015	ZNF467	1.13	0.95	1.15	1.13	1.32
ILMN_1708778	ASS1	1.16	0.76	1.21	1.01	1.86
ILMN_1709257	RIPPLY3	1.42	1.02	1.32	1.61	2.10

Each logFC value was obtained after subtraction from the corresponding gene in the wild-type group. For better understanding of the data, each value was multiplied by -1. All listed genes were selected with a fold-change of <0.7 and >1.4 (ratio <-0.5 and >0.5) with a adjusted p-val of <0.05.

Table A.14: Significant regulated genes in cancer- and CFC-associated BRAF mutants

Illumina Ids	Gene symbol	logFC wt-mutant			
		S467A	Q257R	L485F	V600E
ILMN_1757497	VGF	4.17	3.20	4.11	3.56
ILMN_1751607	FOSB	2.59	2.21	3.45	2.55
ILMN_1677402	C11orf96	4.01	2.87	3.25	2.47
ILMN_1762899	EGR1	3.03	2.78	2.91	2.33
ILMN_1711566	TIMP1	2.26	1.93	2.55	2.27
ILMN_1711120	ARC	2.37	1.78	2.56	2.19
ILMN_1687978	PHLDA1	2.19	1.39	1.75	1.78
ILMN_1669523	FOS	1.50	1.51	1.99	1.55
ILMN_1703123	CSRNP1	2.31	1.57	2.02	1.49
ILMN_1714861	CD68	2.08	1.56	2.42	1.41
ILMN_1723978	LGALS1	1.60	1.13	1.94	1.37
ILMN_1659936	PPP1R15A	1.70	1.20	1.97	1.37
ILMN_1699931	HCST	1.60	1.08	1.63	1.30
ILMN_1699829	CTGF	1.14	1.12	1.75	1.29
ILMN_1736078	THBS4	1.37	0.96	0.81	1.29
ILMN_1689004	TNFRSF12A	2.04	1.66	1.69	1.28
ILMN_1743199	EGR2	1.96	1.60	1.90	1.16
ILMN_1686623	CSF1R	1.11	0.78	1.78	1.11
ILMN_1652185	IL4R	1.31	0.84	1.19	1.10
ILMN_1725271	GPR3	1.31	1.24	1.68	1.02
ILMN_1663042	SDC4	0.97	0.81	1.27	1.00
ILMN_1725726	DHRS2	0.77	0.86	1.68	0.99
ILMN_1658847	NRARP	1.71	0.96	1.39	0.99
ILMN_1666733	IL8	1.45	1.30	2.79	0.93
ILMN_1667239	INPP1	1.53	1.03	1.31	0.87
ILMN_1742332	KCTD12	1.59	1.31	1.96	0.84
ILMN_1662390	ASPHD1	1.13	0.69	1.08	0.79
ILMN_1677691	NA	0.88	0.74	0.92	0.77
ILMN_1661631	LILRA3	0.91	0.76	1.59	0.72
ILMN_1761762	NA	0.65	0.67	1.04	0.70
ILMN_1706579	SHBG	1.06	0.73	1.09	0.69
ILMN_1718960	SERPINB8	1.05	0.67	1.45	0.68
ILMN_1724782	NA	1.16	0.86	1.39	0.67
ILMN_1723953	NA	0.95	0.64	1.11	0.63
ILMN_1671263	CACNA1H	1.24	0.74	0.85	0.62
ILMN_1658569	NA	0.90	0.57	0.94	0.62
ILMN_1721922	NAB2	0.98	0.69	0.89	0.61
ILMN_1680139	MAFF	0.90	0.62	1.06	0.61
ILMN_1751615	COQ10B	1.10	0.70	0.92	0.61
ILMN_1699160	ITK	1.04	0.68	1.37	0.60
ILMN_1680856	MAMLD1	1.13	0.64	0.85	0.57
ILMN_1691364	STAT1	0.98	0.74	0.81	0.54
ILMN_1719543	MAF	0.87	0.63	0.77	0.54
ILMN_1729453	TSPAN9	0.77	0.57	0.67	0.52
ILMN_1752046	SH2B3	0.59	0.64	0.77	0.50
ILMN_1715424	KLHL10	0.92	0.58	1.00	0.49
ILMN_1659142	MDK	-0.90	-0.69	-0.76	-0.52
ILMN_1696099	ALDH4A1	-1.00	-0.62	-1.13	-0.52
ILMN_1674038	CTSD	-0.95	-0.56	-0.88	-0.54
ILMN_1715024	LSS	-0.67	-0.59	-0.86	-0.54
ILMN_1715384	B3GNT1	-0.80	-0.57	-1.16	-0.55
ILMN_1726410	APRT	-0.92	-0.66	-1.08	-0.56
ILMN_1712583	METRN	-1.10	-0.80	-1.31	-0.56
ILMN_1701966	FIRRE	-0.62	-0.52	-0.53	-0.56
ILMN_1714445	SLC6A9	-0.75	-0.68	-0.58	-0.57
ILMN_1660965	PRR22	-1.11	-0.55	-0.69	-0.58
ILMN_1742507	LRRC45	-0.99	-0.56	-0.75	-0.58
ILMN_1697812	MNX1	-0.83	-0.61	-1.01	-0.60
ILMN_1736575	TRIM28	-1.15	-0.76	-1.24	-0.60
ILMN_1730307	MED16	-0.98	-0.68	-1.11	-0.61
ILMN_1657968	MAP2K2	-0.95	-0.83	-1.17	-0.62
ILMN_1704672	NABP2	-1.37	-0.71	-0.95	-0.62
ILMN_1722898	SFRP2	-0.57	-0.53	-0.67	-0.62
ILMN_1722491	APRT	-1.11	-0.75	-1.14	-0.63
ILMN_1668960	MID1IP1	-0.65	-0.65	-0.87	-0.65
ILMN_1657347	PODXL2	-0.90	-0.63	-0.85	-0.67
ILMN_1754827	LRRC45	-0.91	-0.56	-0.85	-0.67
ILMN_1723971	SLC29A1	-1.19	-0.66	-1.09	-0.72
ILMN_1660288	ZNF503-AS2	-1.00	-0.62	-0.92	-0.79
ILMN_1669321	MATK	-0.74	-0.58	-0.84	-0.81
ILMN_1674785	COL2A1	-0.82	-0.67	-1.27	-0.81
ILMN_1691861	FASTK	-0.97	-0.73	-0.84	-0.82
ILMN_1708743	NT5DC2	-1.40	-0.76	-1.46	-0.84
ILMN_1755582	PCSK1N	-1.46	-0.83	-1.24	-0.88
ILMN_1682812	C21orf33	-0.90	-0.71	-1.18	-0.92
ILMN_1673681	SLC46A1	-1.13	-0.69	-0.67	-0.95
ILMN_1728645	STMN3	-1.59	-0.87	-1.51	-0.96
ILMN_1748124	TSC22D3	-2.07	-1.10	-1.61	-1.16
ILMN_1716237	ACOT2	-1.34	-0.91	-1.26	-1.18

Illumina Ids	Gene symbol	logFC wt-mutant			
		S467A	Q257R	L485F	V600E
ILMN_2188862	GDF15	4.37	3.34	3.56	3.32
ILMN_1780255	KLK6	1.94	1.55	3.45	2.65
ILMN_1798256	UPP1	3.02	1.94	2.70	2.10
ILMN_2086077	JUNB	3.09	2.05	2.39	2.03
ILMN_1867119	NA	2.70	1.77	2.75	1.95
ILMN_2232463	ARL14	2.00	1.69	2.07	1.85
ILMN_1769013	ASGR1	2.57	2.18	2.36	1.78
ILMN_1775708	SLC2A3	2.71	2.00	2.33	1.65
ILMN_2357134	SPHK1	1.70	1.30	2.05	1.55
ILMN_1775224	NOS3	1.53	1.25	1.94	1.33
ILMN_2157099	CCNA1	1.86	1.30	1.76	1.32
ILMN_2208903	CD52	2.18	1.21	2.36	1.24
ILMN_1884160	NA	1.24	1.23	2.81	1.21
ILMN_2384745	PSG4	1.17	1.30	2.25	1.15
ILMN_2355831	FHL2	1.11	0.83	1.05	1.12
ILMN_2367883	GEM	1.65	0.89	1.48	1.11
ILMN_1768534	BHLHE40	2.07	1.48	1.80	1.08
ILMN_1813704	CEMIP	0.80	0.78	1.05	1.02
ILMN_2211065	TMEM91	1.44	1.02	1.30	1.02
ILMN_2286014	CATSPER2	1.15	0.87	1.26	0.99
ILMN_1769299	MTMR11	1.06	0.84	1.46	0.97
ILMN_2188264	CYR61	1.34	0.82	1.06	0.94
ILMN_2121408	HBEGF	1.00	0.74	1.19	0.94
ILMN_1778136	ZMYND15	1.56	1.05	1.34	0.92
ILMN_2387090	CGGBP1	1.08	0.74	1.27	0.90
ILMN_1794017	SERTAD1	1.42	0.95	1.71	0.88
ILMN_1803429	CD44	0.98	0.97	1.57	0.84
ILMN_2397028	SERPINB8	1.01	0.64	1.50	0.75
ILMN_1904238	NA	0.88	0.73	1.41	0.74
ILMN_1777881	TSPAN17	1.11	0.65	1.16	0.73
ILMN_1771376	PEA15	0.99	0.71	1.13	0.72
ILMN_2368971	PSMD12	0.65	0.50	0.92	0.72
ILMN_1805192	ITPRIP	1.04	0.64	0.85	0.71
ILMN_2064860	NA	0.91	0.52	0.79	0.70
ILMN_2188119	ARL16	0.62	0.60	0.62	0.69
ILMN_2041190	F2RL1	0.84	0.69	0.82	0.67
ILMN_2349071	GPR64	1.02	0.65	0.85	0.66
ILMN_1788223	RSPH3	1.17	0.73	1.00	0.63
ILMN_2179083	LOXL4	1.04	0.83	0.97	0.62
ILMN_1788203	HEY1	0.96	0.69	0.79	0.62
ILMN_1789244	SOX8	1.18	0.61	0.86	0.60
ILMN_2220187	GFPT1	0.69	0.66	0.79	0.60
ILMN_1812070	ABCB1	0.89	0.78	1.31	0.60
ILMN_1795298	GPER1	0.75	0.79	1.14	0.59
ILMN_2219618	AOC4P	0.82	0.67	0.92	0.58
ILMN_2384056	GPER1	0.72	0.72	1.04	0.55
ILMN_1763265	CHMP1B	0.75	0.49	0.79	0.49
ILMN_1805807	SLC30A3	0.72	0.62	0.81	0.49
ILMN_1764970	JMJD1C	0.59	0.62	0.71	0.49
ILMN_2405991	TRAF7	-0.80	-0.59	-1.16	-0.52
ILMN_2345016	PTGES2	-0.87	-0.64	-0.73	-0.54
ILMN_2362126	AGAP3	-0.76	-0.55	-0.80	-0.55
ILMN_2075065	FADS2	-0.95	-0.66	-1.05	-0.57
ILMN_2338963	SLC29A1	-0.79	-0.55	-0.91	-0.58
ILMN_1785731	MAPK8IP2	-1.47	-0.76	-1.10	-0.60
ILMN_1780799	ENPP2	-1.10	-0.76	-1.01	-0.61
ILMN_2131936	NA	-0.69	-0.56	-0.61	-0.62
ILMN_1769702	GPAA1	-0.95	-0.62	-1.04	-0.64
ILMN_2144401	GLB1L2	-1.18	-0.68	-1.17	-0.65
ILMN_1813671	SLC25A1	-1.04	-0.68	-1.22	-0.66
ILMN_1783444	DVL1	-0.81	-0.66	-0.97	-0.66
ILMN_2295620	MAZ	-1.37	-0.79	-1.77	-0.71
ILMN_2346769	FAM189B	-1.19	-0.70	-1.29	-0.77
ILMN_1804522	CCDC47	-1.10	-0.77	-0.93	-0.82
ILMN_2248725	TYSND1	-1.09	-0.75	-1.00	-0.83
ILMN_2399523	JAG2	-1.15	-0.89	-1.48	-0.84
ILMN_2386205	C21orf33	-0.80	-0.61	-1.04	-0.87
ILMN_2409793	MAZ	-1.61	-0.78	-1.65	-0.87
ILMN_1794595	GAMT	-1.23	-0.75	-1.29	-0.89
ILMN_2175317	CYP4X1	-1.93	-1.14	-1.92	-0.96
ILMN_2275803	LRRC45	-1.35	-0.78	-1.18	-0.97
ILMN_1765640	MAZ	-1.58	-0.84	-1.62	-1.10
ILMN_1779356	TP53	-1.75	-0.88	-1.53	-1.11
ILMN_2227968	NTHL1	-1.73	-0.99	-2.07	-1.14
ILMN_2276952	TSC22D3	-1.47	-1.06	-1.38	-1.21
ILMN_2376403	TSC22D3	-2.41	-1.32	-2.01	-1.52
ILMN_1805132	PCDH19	-2.30	-1.04	-1.96	-2.07

Each logFC value was obtained after subtraction from the corresponding gene in the wild-type group. For better understanding of the data, each value was multiplied by -1. All listed genes were selected with a fold-change of <0.7 and >1.4 (ratio <-0.5 and >0.5) with a adjusted p-val of <0.05.

Table A.15: Overlapping regulated genes between NS/LS-associated SHP2 mutations and BRAF^{V600E}

Illumina ID	Gene symbol	T468M
ILMN_1681679	TSPO	1.51
ILMN_2393296	GK	1.78
ILMN_1725471	GK	1.62
ILMN_2349658	TSPO	1.39
ILMN_2276952	TSC22D3	1.58
ILMN_1797668	INSM1	1.14
ILMN_2376403	TSC22D3	1.78
ILMN_1664861	ID1	-1.27
ILMN_2131293	ALG1L	0.97
ILMN_1668960	MID1IP1	0.75
ILMN_2260991	TSPO	0.85
ILMN_1748124	TSC22D3	1.59
ILMN_1862013	NA	0.63
ILMN_1765796	ENO2	0.86
ILMN_1789627	NA	1.07
ILMN_2131936	NA	-0.92
ILMN_1718972	MFSD3	0.77
ILMN_1660965	PRR22	-0.84
ILMN_2110908	MYC	1.10
ILMN_2319000	MATK	1.05
ILMN_1669321	MATK	0.82
ILMN_1729596	INF2	-0.76
ILMN_2120695	TSPAN7	0.88
ILMN_1901770	NA	-0.95
ILMN_1886846	NA	0.81
ILMN_1812976	DDX54	-0.87
ILMN_1902929	NA	-0.65
ILMN_2390853	CTSH	1.00
ILMN_1880982	NA	0.82
ILMN_2385173	U2AF2	-0.80
ILMN_1807719	CTNS	-0.90
ILMN_1690170	CRABP2	1.79
ILMN_2203588	MYL5	0.73
ILMN_1805807	SLC30A3	0.66
ILMN_1712774	IRS4	0.70
ILMN_1653432	HNRNPDL	0.79
ILMN_1701918	KLHDC9	0.50
ILMN_1809291	TSPAN7	0.81
ILMN_1659086	NEFL	0.52
ILMN_1813837	C9orf9	0.60
ILMN_1746948	MYL5	0.66
ILMN_1674038	CTSD	-0.72
ILMN_1716733	MYOM2	1.05

Illumina ID	Gene symbol	I282V
ILMN_1674785	COL2A1	1.40
ILMN_1789627	NA	1.18
ILMN_1765796	ENO2	0.84
ILMN_1862013	NA	0.60
ILMN_2108735	EEF1A2	0.92
ILMN_1690464	SLC35G1	-0.83
ILMN_1690170	CRABP2	1.84
ILMN_1734814	HSPA4	-0.72
		E139D
ILMN_2393296	GK	1.31
ILMN_1725471	GK	1.24
ILMN_1681679	TSPO	0.91
ILMN_1901770	NA	-1.03
ILMN_2349658	TSPO	0.81
ILMN_2276952	TSC22D3	1.03
ILMN_1789627	NA	0.98
ILMN_2227757	PCDHB2	0.63
ILMN_2131293	ALG1L	0.73
ILMN_1862013	NA	0.51
ILMN_2108735	EEF1A2	0.80
ILMN_1797668	INSM1	0.75
ILMN_1712774	IRS4	0.69
ILMN_1729596	INF2	-0.67
ILMN_2376403	TSC22D3	1.19
ILMN_1805807	SLC30A3	0.63
ILMN_1762899	EGR1	2.53
ILMN_2319000	MATK	0.87
ILMN_1660965	PRR22	-0.65
ILMN_1665425	RPRM	1.00
ILMN_1765796	ENO2	0.60
ILMN_1669321	MATK	0.64
		T42A
ILMN_1725471	GK	1.39
ILMN_2393296	GK	1.36
ILMN_1789627	NA	1.07
ILMN_2052373	RAB17	0.76
ILMN_1681679	TSPO	0.72
ILMN_2319000	MATK	1.03
ILMN_1666594	IRF8	0.81
ILMN_1901770	NA	-0.94
ILMN_1862013	NA	0.53

Illumina ID	Gene symbol	E76G
ILMN_2393296	GK	1.15
ILMN_2131936	NA	-1.05
ILMN_1725471	GK	1.05
ILMN_1862013	NA	0.63
ILMN_2120695	TSPAN7	0.95
ILMN_2184184	ANXA1	1.46
ILMN_2072622	ERVMER34-1	-0.72
ILMN_1729596	INF2	-0.75
ILMN_1809291	TSPAN7	0.86
ILMN_2052373	RAB17	0.64
ILMN_1805807	SLC30A3	0.66
ILMN_2390853	CTSH	0.96
ILMN_1849494	EFR3B	0.60
ILMN_1765796	ENO2	0.66
ILMN_2108735	EEF1A2	0.79
ILMN_1762899	EGR1	2.59
ILMN_1757467	H1F0	0.96
ILMN_1901770	NA	-0.82
ILMN_2371055	EFNA1	0.61
ILMN_1695311	HLA-DMA	0.62
ILMN_1754969	LMCD1	0.73
ILMN_2315979	LBH	0.75
ILMN_1664861	ID1	-0.80
ILMN_2349071	GPR64	0.71
ILMN_1687501	MOXD1	0.53
		E76D
ILMN_1681679	TSPO	1.03
ILMN_1725471	GK	1.11
ILMN_2393296	GK	1.12
ILMN_1862013	NA	0.64
		E76K
ILMN_1862013	NA	0.70
ILMN_2108735	EEF1A2	0.96

Each logFC value was obtained after subtraction from the corresponding gene in the wild-type group. For better understanding of the data, each value was multiplied by -1. All listed genes were selected with a fold-change of <0.7 and >1.4 (ratio <-0.5 and >0.5) with a adjusted p-val of <0.05.

Table A.16: GO analysis and heatmap of commonly regulated genes in CFC-associated and V600E BRAF HEK-TREx cells

Group	GO-ID	Name	Hits	Size	adj. P-val
BP	GO:0048513	organ development	41	2421	7.00E-04
	GO:0000003	reproduction	28	1475	2.80E-03
	GO:0022414	reproductive process	28	1470	2.80E-03
	GO:0009888	tissue development	27	1377	2.80E-03
	GO:0090196	regulation of chemokine secretion	3	8	3.40E-03
	GO:0050793	regulation of developmental process	26	1351	3.60E-03
	GO:0044702	single organism reproductive process	22	1066	4.20E-03
	GO:0032504	multicellular organism reproduction	15	588	4.60E-03
	GO:0048870	cell motility	19	869	4.60E-03
	GO:2000145	regulation of cell motility	12	407	4.60E-03
	GO:0007166	cell surface receptor signaling pathway	34	2194	4.60E-03
	GO:0050896	response to stimulus	71	6110	4.60E-03
	GO:0031325	positive regulation of cellular metabolic process	30	1795	4.60E-03
	GO:0002009	morphogenesis of an epithelium	11	357	7.00E-03
	GO:0030154	cell differentiation	37	2509	7.00E-03
	GO:0043009	chordate embryonic development	13	491	7.00E-03
	GO:1901342	regulation of vasculature development	7	156	8.50E-03
	GO:0016477	cell migration	17	804	8.50E-03
MF	GO:0003690	double-stranded DNA binding	7	142	9.90E-03
	GO:0008134	transcription factor binding	11	391	1.32E-02
	GO:0008083	growth factor activity	5	150	6.49E-02

Bibliography

Agazie, Y. M. and Hayman, M. J. 2003. Development of an efficient "substrate-trapping" mutant of src homology phosphotyrosine phosphatase 2 and identification of the epidermal growth factor receptor, gab1, and three other proteins as target substrates. *J Biol Chem*, 278(16):13952–8.

Ahearn, I. M., Haigis, K., Bar-Sagi, D., and Philips, M. R. 2012. Regulating the regulator: post-translational modification of ras. *Nat Rev Mol Cell Biol*, 13(1):39–51.

Ahmad, S., Banville, D., Zhao, Z., Fischer, E. H., and Shen, S. H. 1993. A widely expressed human protein-tyrosine phosphatase containing src homology 2 domains. *Proc Natl Acad Sci U S A*, 90(6):2197–201.

Ahuja, D., Saenz-Robles, M. T., and Pipas, J. M. 2005. Sv40 large t antigen targets multiple cellular pathways to elicit cellular transformation. *Oncogene*, 24(52):7729–45.

Akagi, T., Sasai, K., and Hanafusa, H. 2003. Refractory nature of normal human diploid fibroblasts with respect to oncogene-mediated transformation. *Proc Natl Acad Sci U S A*, 100(23):13567–72.

Akslen, L. A., Puntervoll, H., Bachmann, I. M., Straume, O., Vuhahula, E., Kumar, R., and Molven, A. 2008. Mutation analysis of the egfr-nras-braf pathway in melanomas from black africans and other subgroups of cutaneous melanoma. *Melanoma Res*, 18 (1):29–35.

Anastasaki, C., Estep, A. L., Marais, R., Rauen, K. A., and Patton, E. E. 2009. Kinase-activating and kinase-impaired cardio-facio-cutaneous syndrome alleles have activity during zebrafish development and are sensitive to small molecule inhibitors. *Hum Mol Genet*, 18(14):2543–54.

Anastasaki, C., Rauen, K. A., and Patton, E. E. 2012. Continual low-level mek inhibition ameliorates cardio-facio-cutaneous phenotypes in zebrafish. *Dis Model Mech*, 5(4): 546–52.

Aoki, Y. and Matsubara, Y. 2013. Ras/mapk syndromes and childhood hemato-oncological diseases. *Int J Hematol*, 97(1):30–6.

Araki, T., Mohi, M. G., Ismat, F. A., Bronson, R. T., Williams, I. R., Kutok, J. L., Yang, W., Pao, L. I., Gilliland, D. G., Epstein, J. A., and Neel, B. G. 2004. Mouse

model of noonan syndrome reveals cell type- and gene dosage-dependent effects of ptpn11 mutation. *Nat Med*, 10(8):849–57.

Bennett, A. M., Tang, T. L., Sugimoto, S., Walsh, C. T., and Neel, B. G. 1994. Protein-tyrosine-phosphatase shptp2 couples platelet-derived growth factor receptor beta to ras. *Proc Natl Acad Sci U S A*, 91(15):7335–9.

Bisson, N., James, D. A., Ivosev, G., Tate, S. A., Bonner, R., Taylor, L., and Pawson, T. 2011. Selected reaction monitoring mass spectrometry reveals the dynamics of signaling through the grb2 adaptor. *Nat Biotechnol*, 29(7):653–8.

Bodnar, A. G., Ouellette, M., Frolkis, M., Holt, S. E., Chiu, C. P., Morin, G. B., Harley, C. B., Shay, J. W., Lichtsteiner, S., and Wright, W. E. 1998. Extension of life-span by introduction of telomerase into normal human cells. *Science*, 279(5349):349–52.

Brase, J. C., Mannsperger, H., Sultmann, H., and Korf, U. 2011. Antibody-mediated signal amplification for reverse phase protein array-based protein quantification. *Methods Mol Biol*, 785:55–64.

Brooks, A. R., Harkins, R. N., Wang, P., Qian, H. S., Liu, P., and Rubanyi, G. M. 2004. Transcriptional silencing is associated with extensive methylation of the cmv promoter following adenoviral gene delivery to muscle. *J Gene Med*, 6(4):395–404.

Chen, G. I. and Gingras, A. C. 2007. Affinity-purification mass spectrometry (ap-ms) of serine/threonine phosphatases. *Methods*, 42(3):298–305.

Cholay, M., Reverdy, C., Benarous, R., Colland, F., and Daviet, L. 2010. Functional interaction between the ubiquitin-specific protease 25 and the syk tyrosine kinase. *Exp Cell Res*, 316(4):667–75.

Churin, Y., Al-Ghoul, L., Kepp, O., Meyer, T. F., Birchmeier, W., and Naumann, M. 2003. Helicobacter pylori caga protein targets the c-met receptor and enhances the motogenic response. *J Cell Biol*, 161(2):249–55.

Crouin, C., Arnaud, M., Gesbert, F., Camonis, J., and Bertoglio, J. 2001. A yeast two-hybrid study of human p97/gab2 interactions with its sh2 domain-containing binding partners. *FEBS Lett*, 495(3):148–53.

Davies, H., Bignell, G. R., Cox, C., Stephens, P., Edkins, S., Clegg, S., Teague, J., Woffendin, H., Garnett, M. J., Bottomley, W., Davis, N., Dicks, E., Ewing, R., Floyd, Y., Gray, K., Hall, S., Hawes, R., Hughes, J., Kosmidou, V., Menzies, A., Mould, C., Parker, A., Stevens, C., Watt, S., Hooper, S., Wilson, R., Jayatilake, H., Gusterson, B. A., Cooper, C., Shipley, J., Hargrave, D., Pritchard-Jones, K., Maitland, N., Chenevix-Trench, G., Riggins, G. J., Bigner, D. D., Palmieri, G., Cossu, A., Flanagan, A., Nicholson, A., Ho, J. W., Leung, S. Y., Yuen, S. T., Weber, B. L., Seigler, H. F., Darrow, T. L., Paterson, H., Marais, R., Marshall, C. J., Wooster, R., Stratton, M. R., and Futreal, P. A. 2002. Mutations of the braf gene in human cancer. *Nature*, 417 (6892):949–54.

Dawson, P. J., Wolman, S. R., Tait, L., Heppner, G. H., and Miller, F. R. 1996. Mcf10at: a model for the evolution of cancer from proliferative breast disease. *Am J Pathol*, 148 (1):313–9.

Delahaye, L., Rocchi, S., and Obberghen, E. V. 2000. Potential involvement of frs2 in insulin signaling. *Endocrinology*, 141(2):621–8.

Dhawan, P., Singh, A. B., Ellis, D. L., and Richmond, A. 2002. Constitutive activation of akt/protein kinase b in melanoma leads to up-regulation of nuclear factor-kappab and tumor progression. *Cancer Res*, 62(24):7335–42.

Digilio, M. C., Conti, E., Sarkozy, A., Mingarelli, R., Dottorini, T., Marino, B., Pizzuti, A., and Dallapiccola, B. 2002. Grouping of multiple-lentigines/leopard and noonan syndromes on the ptpn11 gene. *Am J Hum Genet*, 71(2):389–94.

Forbes, S. A., Bhamra, G., Bamford, S., Dawson, E., Kok, C., Clements, J., Menzies, A., Teague, J. W., Futreal, P. A., and Stratton, M. R. 2008. The catalogue of somatic mutations in cancer (cosmic). *Curr Protoc Hum Genet*, Chapter 10:Unit 10 11.

Fragale, A., Tartaglia, M., Wu, J., and Gelb, B. D. 2004. Noonan syndrome-associated shp2/ptpn11 mutants cause egf-dependent prolonged gab1 binding and sustained erk2/mapk1 activation. *Hum Mutat*, 23(3):267–77.

Franceschini, A., Szklarczyk, D., Frankild, S., Kuhn, M., Simonovic, M., Roth, A., Lin, J., Minguez, P., Bork, P., von Mering, C., and Jensen, L. J. 2013. String v9.1: protein-protein interaction networks, with increased coverage and integration. *Nucleic Acids Res*, 41(Database issue):D808–15.

Gallagher, S. J., Thompson, J. F., Indsto, J., Scurr, L. L., Lett, M., Gao, B. F., Dunleavey, R., Mann, G. J., Kefford, R. F., and Rizos, H. 2008. p16ink4a expression and absence of activated b-raf are independent predictors of chemosensitivity in melanoma tumors. *Neoplasia*, 10(11):1231–9.

Garner, E., Martinon, F., Tschopp, J., Beard, P., and Raj, K. 2007. Cells with defective p53-p21-prb pathway are susceptible to apoptosis induced by p84n5 via caspase-6. *Cancer Res*, 67(16):7631–7.

Gorlin, R. J., Anderson, R. C., and Blaw, M. 1969. Multiple lentigenes syndrome. *Am J Dis Child*, 117(6):652–62.

Griegel, S., Traub, O., Willecke, K., and Schafer, R. 1986. Suppression and re-expression of transformed phenotype in hybrids of ha-ras-1-transformed rat-1 cells and early-passage rat embryonic fibroblasts. *Int J Cancer*, 38(5):697–705.

Grossmann, K. S., Rosario, M., Birchmeier, C., and Birchmeier, W. 2010. The tyrosine phosphatase shp2 in development and cancer. *Adv Cancer Res*, 106:53–89.

Gutch, M. J., Flint, A. J., Keller, J., Tonks, N. K., and Hengartner, M. O. 1998. The caenorhabditis elegans sh2 domain-containing protein tyrosine phosphatase ptp-2 participates in signal transduction during oogenesis and vulval development. *Genes Dev*, 12(4):571–85.

Hahn, W. C. 2002. Immortalization and transformation of human cells. *Mol Cells*, 13 (3):351–61.

Hahn, W. C., Counter, C. M., Lundberg, A. S., Beijersbergen, R. L., Brooks, M. W., and Weinberg, R. A. 1999. Creation of human tumour cells with defined genetic elements. *Nature*, 400(6743):464–8.

Hamlet, M. R. J. and Perkins, L. A. 2001. Analysis of corkscrew signaling in the drosophila epidermal growth factor receptor pathway during myogenesis. *Genetics*, 159(3):1073–87.

Hanafusa, H., Torii, S., Yasunaga, T., Matsumoto, K., and Nishida, E. 2004. Shp2, an sh2-containing protein-tyrosine phosphatase, positively regulates receptor tyrosine kinase signaling by dephosphorylating and inactivating the inhibitor sprouty. *J Biol Chem*, 279(22):22992–5.

Hatakeyama, M. 2006a. The role of helicobacter pylori caga in gastric carcinogenesis. *Int J Hematol*, 84(4):301–8.

Hatakeyama, M. 2006b. Helicobacter pylori caga – a bacterial intruder conspiring gastric carcinogenesis. *Int J Cancer*, 119(6):1217–23.

Hayflick, L. and Moorhead, P. S. 1961. The serial cultivation of human diploid cell strains. *Exp Cell Res*, 25:585–621.

Heppner, G. H. and Wolman, S. R. 1999. Mcf-10at: A model for human breast cancer development. *Breast J*, 5(2):122–29.

Heuberger, J., Kosel, F., Qi, J., Grossmann, K. S., Rajewsky, K., and Birchmeier, W. 2014. Shp2/mapk signaling controls goblet/paneth cell fate decisions in the intestine. *Proc Natl Acad Sci U S A*.

Higashi, H., Tsutsumi, R., Muto, S., Sugiyama, T., Azuma, T., Asaka, M., and Hatakeyama, M. 2002. Shp-2 tyrosine phosphatase as an intracellular target of helicobacter pylori caga protein. *Science*, 295(5555):683–6.

Hix, L. M., Karavitis, J., Khan, M. W., Shi, Y. H., Khazaie, K., and Zhang, M. 2013. Tumor stat1 transcription factor activity enhances breast tumor growth and immune suppression mediated by myeloid-derived suppressor cells. *J Biol Chem*, 288(17): 11676–88.

Hof, P., Pluskey, S., Dhe-Paganon, S., Eck, M. J., and Shoelson, S. E. 1998. Crystal structure of the tyrosine phosphatase shp-2. *Cell*, 92(4):441–50.

Holderfield, M., Merritt, H., Chan, J., Wallroth, M., Tandeske, L., Zhai, H., Tellew, J., Hardy, S., Hekmat-Nejad, M., Stuart, D. D., McCormick, F., and Nagel, T. E. 2013. Raf inhibitors activate the mapk pathway by relieving inhibitory autophosphorylation. *Cancer Cell*, 23(5):594–602.

Holliday, R. 1996. Neoplastic transformation: the contrasting stability of human and mouse cells. *Cancer Surv*, 28:103–15.

Hopper, N. A. 2006. The adaptor protein soc-1/gab1 modifies growth factor receptor output in caenorhabditis elegans. *Genetics*, 173(1):163–75.

Hsu, S. H., Motiwala, T., Roy, S., Claus, R., Mustafa, M., Plass, C., Freitas, M. A., Ghoshal, K., and Jacob, S. T. 2013. Methylation of the ptpro gene in human hepatocellular carcinoma and identification of vcp as its substrate. *J Cell Biochem*, 114(8):1810–8.

Huang, Y. T., Li, F. F., Ke, C., Li, Z., Li, Z. T., Zou, X. F., Zheng, X. X., Chen, Y. P., and Zhang, H. 2013. Ptpro promoter methylation is predictive of poorer outcome for her2-positive breast cancer: indication for personalized therapy. *J Transl Med*, 11:245.

Huyer, G. and Ramachandran, C. 1998. The specificity of the n-terminal sh2 domain of shp-2 is modified by a single point mutation. *Biochemistry*, 37(9):2741–7.

Imielinski, M., Berger, A. H., Hammerman, P. S., Hernandez, B., Pugh, T. J., Hodis, E., Cho, J., Suh, J., Capelletti, M., Sivachenko, A., Sougnez, C., Auclair, D., Lawrence, M. S., Stojanov, P., Cibulskis, K., Choi, K., de Waal, L., Sharifnia, T., Brooks, A., Greulich, H., Banerji, S., Zander, T., Seidel, D., Leenders, F., Ansen, S., Ludwig, C., Engel-Riedel, W., Stoelben, E., Wolf, J., Goparju, C., Thompson, K., Winckler, W., Kwiatkowski, D., Johnson, B. E., Janne, P. A., Miller, V. A., Pao, W., Travis, W. D., Pass, H. I., Gabriel, S. B., Lander, E. S., Thomas, R. K., Garraway, L. A., Getz, G., and Meyerson, M. 2012. Mapping the hallmarks of lung adenocarcinoma with massively parallel sequencing. *Cell*, 150(6):1107–20.

Jarvis, L. A., Toering, S. J., Simon, M. A., Krasnow, M. A., and Smith-Bolton, R. K. 2006. Sprouty proteins are in vivo targets of corkscrew/shp-2 tyrosine phosphatases. *Development*, 133(6):1133–42.

Jiang, J., Jin, M. S., Kong, F., Wang, Y. P., Jia, Z. F., Cao, D. H., Ma, H. X., Suo, J., and Cao, X. Y. 2013. Increased expression of tyrosine phosphatase shp-2 in helicobacter pylori-infected gastric cancer. *World J Gastroenterol*, 19(4):575–80.

Jonsson, G., Staaf, J., Olsson, E., Heidenblad, M., Vallon-Christersson, J., Osoegawa, K., de Jong, P., Oredsson, S., Ringner, M., Hoglund, M., and Borg, A. 2007. High-resolution genomic profiles of breast cancer cell lines assessed by tiling bac array comparative genomic hybridization. *Genes Chromosomes Cancer*, 46(6):543–58.

Jopling, C., van Geemen, D., and den Hertog, J. 2007. Shp2 knockdown and noonan/leopard mutant shp2-induced gastrulation defects. *PLoS Genet*, 3(12):e225.

Juneja, R., Agulnik, S. I., and Silver, L. M. 1998. Sequence divergence within the sperm-specific polypeptide tcte1 is correlated with species-specific differences in sperm binding to zona-intact eggs. *J Androl*, 19(2):183–8.

Kadota, M., Yang, H. H., Gomez, B., Sato, M., Clifford, R. J., Meerzaman, D., Dunn, B. K., Wakefield, L. M., and Lee, M. P. 2010. Delineating genetic alterations for tumor progression in the mcf10a series of breast cancer cell lines. *PLoS One*, 5(2):e9201.

Kalathur, R. K., Pinto, J. P., Hernandez-Prieto, M. A., Machado, R. S., Almeida, D., Chaurasia, G., and Futschik, M. E. 2014. Unihi 7: an enhanced database for retrieval and interactive analysis of human molecular interaction networks. *Nucleic Acids Res*, 42(Database issue):D408–14.

Keilhack, H., Muller, M., Bohmer, S. A., Frank, C., Weidner, K. M., Birchmeier, W., Ligensa, T., Berndt, A., Kosmehl, H., Gunther, B., Muller, T., Birchmeier, C., and Bohmer, F. D. 2001. Negative regulation of ros receptor tyrosine kinase signaling. an epithelial function of the sh2 domain protein tyrosine phosphatase shp-1. *J Cell Biol*, 152(2):325–34.

Keilhack, H., David, F. S., McGregor, M., Cantley, L. C., and Neel, B. G. 2005. Diverse biochemical properties of shp2 mutants. implications for disease phenotypes. *J Biol Chem*, 280(35):30984–93.

Kim, J. S., Shin, O. R., Kim, H. K., Cho, Y. S., An, C. H., Lim, K. W., and Kim, S. S. 2010. Overexpression of protein phosphatase non-receptor type 11 (ptpn11) in gastric carcinomas. *Dig Dis Sci*, 55(6):1565–9.

Kinch, M. S., Clark, G. J., Der, C. J., and Burridge, K. 1995. Tyrosine phosphorylation regulates the adhesions of ras-transformed breast epithelia. *J Cell Biol*, 130(2):461–71.

Kontaridis, M. I., Swanson, K. D., David, F. S., Barford, D., and Neel, B. G. 2006. Ptpn11 (shp2) mutations in leopard syndrome have dominant negative, not activating, effects. *J Biol Chem*, 281(10):6785–92.

Kontaridis, M. I., Yang, W., Bence, K. K., Cullen, D., Wang, B., Bodyak, N., Ke, Q., Hinek, A., Kang, P. M., Liao, R., and Neel, B. G. 2008. Deletion of ptpn11 (shp2) in cardiomyocytes causes dilated cardiomyopathy via effects on the extracellular signal-regulated kinase/mitogen-activated protein kinase and rhoa signaling pathways. *Circulation*, 117(11):1423–35.

Kratz, C. P., Rapisuwon, S., Reed, H., Hasle, H., and Rosenberg, P. S. 2011. Cancer in noonan, costello, cardiofaciocutaneous and leopard syndromes. *Am J Med Genet C Semin Med Genet*, 157C(2):83–9.

Kubota, Y., O'Grady, P., Saito, H., and Takekawa, M. 2011. Oncogenic ras abrogates mek sumoylation that suppresses the erk pathway and cell transformation. *Nat Cell Biol*, 13(3):282–91.

Lechleider, R. J., Sugimoto, S., Bennett, A. M., Kashishian, A. S., Cooper, J. A., Shoelson, S. E., Walsh, C. T., and Neel, B. G. 1993. Activation of the sh2-containing phosphotyrosine phosphatase sh-ptp2 by its binding site, phosphotyrosine 1009, on the human platelet-derived growth factor receptor. *J Biol Chem*, 268(29):21478–81.

Lee, I. O., Kim, J. H., Choi, Y. J., Pillinger, M. H., Kim, S. Y., Blaser, M. J., and Lee, Y. C. 2010. Helicobacter pylori caga phosphorylation status determines the gp130-activated shp2/erk and jak/stat signal transduction pathways in gastric epithelial cells. *J Biol Chem*, 285(21):16042–50.

Lemmon, M. A. and Schlessinger, J. 2010. Cell signaling by receptor tyrosine kinases. *Cell*, 141(7):1117–34.

Li, C. W., Xia, W., Huo, L., Lim, S. O., Wu, Y., Hsu, J. L., Chao, C. H., Yamaguchi, H., Yang, N. K., Ding, Q., Wang, Y., Lai, Y. J., LaBaff, A. M., Wu, T. J., Lin, B. R., Yang, M. H., Hortobagyi, G. N., and Hung, M. C. 2012. Epithelial-mesenchymal transition induced by tnf-alpha requires nf-kappab-mediated transcriptional upregulation of twist1. *Cancer Res*, 72(5):1290–300.

Li, X. C. and Schimenti, J. C. 2007. Mouse pachytene checkpoint 2 (trip13) is required for completing meiotic recombination but not synapsis. *PLoS Genet*, 3(8):e130.

Makita, Y., Narumi, Y., Yoshida, M., Niihori, T., Kure, S., Fujieda, K., Matsubara, Y., and Aoki, Y. 2007. Leukemia in cardio-facio-cutaneous (cfc) syndrome: a patient with a germline mutation in braf proto-oncogene. *J Pediatr Hematol Oncol*, 29(5):287–90.

Mannell, H., Hellwig, N., Gloe, T., Plank, C., Sohn, H. Y., Groesser, L., Walzog, B., Pohl, U., and Krotz, F. 2008. Inhibition of the tyrosine phosphatase shp-2 suppresses angiogenesis in vitro and in vivo. *J Vasc Res*, 45(2):153–63.

Marin, T. M., Clemente, C. F., Santos, A. M., Picardi, P. K., Pascoal, V. D., Lopes-Cendes, I., Saad, M. J., and Franchini, K. G. 2008. Shp2 negatively regulates growth in cardiomyocytes by controlling focal adhesion kinase/src and mtor pathways. *Circ Res*, 103(8):813–24.

Miller, A. D., Hoeven, N. S. V., and Liu, S. L. 2004. Transformation and scattering activities of the receptor tyrosine kinase ron/stk in rodent fibroblasts and lack of regulation by the jaagsiekte sheep retrovirus receptor, hyal2. *BMC Cancer*, 4:64.

Miyamoto, D., Miyamoto, M., Takahashi, A., Yomogita, Y., Higashi, H., Kondo, S., and Hatakeyama, M. 2008. Isolation of a distinct class of gain-of-function shp-2 mutants with oncogenic ras-like transforming activity from solid tumors. *Oncogene*, 27(25): 3508–15.

Morales, L. D., Pavon, E. A. C., Shin, J. W., Garcia, A., Capetillo, M., Kim, D. J., and Lieman, J. H. 2014. Protein tyrosine phosphatases ptp-1b, shp-2, and pten facilitate rb/e2f-associated apoptotic signaling. *PLoS One*, 9(5):e97104.

Morrison, D. K. and Cutler, R. E. 1997. The complexity of raf-1 regulation. *Curr Opin Cell Biol*, 9(2):174–9.

Neri, G., Sabatino, G., Bertini, E., and Genuardi, M. 1987. The cfc syndrome–report of the first two cases outside the united states. *Am J Med Genet*, 27(4):767–71.

Niihori, T., Aoki, Y., Narumi, Y., Neri, G., Cave, H., Verloes, A., Okamoto, N., Hennekam, R. C., Gillessen-Kaesbach, G., Wieczorek, D., Kavamura, M. I., Kurosawa, K., Ohashi, H., Wilson, L., Heron, D., Bonneau, D., Corona, G., Kaname, T., Naritomi, K., Baumann, C., Matsumoto, N., Kato, K., Kure, S., and Matsubara, Y. 2006. Germline kras and braf mutations in cardio-facio-cutaneous syndrome. *Nat Genet*, 38(3):294–6.

Nishida, K., Yoshida, Y., Itoh, M., Fukada, T., Ohtani, T., Shirogane, T., Atsumi, T., Takahashi-Tezuka, M., Ishihara, K., Hibi, M., and Hirano, T. 1999. Gab-family adapter proteins act downstream of cytokine and growth factor receptors and t- and b-cell antigen receptors. *Blood*, 93(6):1809–16.

Noonan, J. A. and Nadas, A. S. 1958. The hypoplastic left heart syndrome; an analysis of 101 cases. *Pediatr Clin North Am*, 5(4):1029–56.

O'Gorman, S., Fox, D. T., and Wahl, G. M. 1991. Recombinase-mediated gene activation and site-specific integration in mammalian cells. *Science*, 251(4999):1351–5.

Pandit, B., Sarkozy, A., Pennacchio, L. A., Carta, C., Oishi, K., Martinelli, S., Pogna, E. A., Schackwitz, W., Ustaszewska, A., Landstrom, A., Bos, J. M., Ommen, S. R., Esposito, G., Lepri, F., Faul, C., Mundel, P., Siguero, J. P. L., Tenconi, R., Selicorni, A., Rossi, C., Mazzanti, L., Torrente, I., Marino, B., Digilio, M. C., Zampino, G., Ackerman, M. J., Dallapiccola, B., Tartaglia, M., and Gelb, B. D. 2007. Gain-of-function raf1 mutations cause noonan and leopard syndromes with hypertrophic cardiomyopathy. *Nat Genet*, 39(8):1007–12.

Paredes, J., Correia, A. L., Ribeiro, A. S., Milanezi, F., Cameselle-Teijeiro, J., and Schmitt, F. C. 2008. Breast carcinomas that co-express e- and p-cadherin are associated with p120-catenin cytoplasmic localisation and poor patient survival. *J Clin Pathol*, 61(7):856–62.

Perkins, L. A., Larsen, I., and Perrimon, N. 1992. corkscrew encodes a putative protein tyrosine phosphatase that functions to transduce the terminal signal from the receptor tyrosine kinase torso. *Cell*, 70(2):225–36.

Perkins, L. A., Johnson, M. R., Melnick, M. B., and Perrimon, N. 1996. The nonreceptor protein tyrosine phosphatase corkscrew functions in multiple receptor tyrosine kinase pathways in drosophila. *Dev Biol*, 180(1):63–81.

Piali, L., Hammel, P., Uherek, C., Bachmann, F., Gisler, R. H., Dunon, D., and Imhof, B. A. 1995. Cd31/pecam-1 is a ligand for alpha v beta 3 integrin involved in adhesion of leukocytes to endothelium. *J Cell Biol*, 130(2):451–60.

Pickering, M. T. and Kowalik, T. F. 2006. Rb inactivation leads to e2f1-mediated dna double-strand break accumulation. *Oncogene*, 25(5):746–55.

Prescott, M., Nowakowski, S., Nagley, P., and Devenish, R. J. 1999. The length of polypeptide linker affects the stability of green fluorescent protein fusion proteins. *Anal Biochem*, 273(2):305–7.

Princen, F., Bard, E., Sheikh, F., Zhang, S. S., Wang, J., Zago, W. M., Wu, D., Trelles, R. D., Bailly-Maitre, B., Kahn, C. R., Chen, Y., Reed, J. C., Tong, G. G., Mercola, M., Chen, J., and Feng, G. S. 2009. Deletion of shp2 tyrosine phosphatase in muscle leads to dilated cardiomyopathy, insulin resistance, and premature death. *Mol Cell Biol*, 29(2):378–88.

Qin, J. Y., Zhang, L., Clift, K. L., Hulur, I., Xiang, A. P., Ren, B. Z., and Lahn, B. T. 2010. Systematic comparison of constitutive promoters and the doxycycline-inducible promoter. *PLoS One*, 5(5):e10611.

Qiu, W., Wang, X., Romanov, V., Hutchinson, A., Lin, A., Ruzanov, M., Battaile, K. P., Pai, E. F., Neel, B. G., and Chirgadze, N. Y. 2014. Structural insights into noonan/leopard syndrome-related mutants of protein-tyrosine phosphatase shp2 (ptpn11). *BMC Struct Biol*, 14(1):10.

R. M. Freeman, J., Plutzky, J., and Neel, B. G. 1992. Identification of a human src homology 2-containing protein-tyrosine-phosphatase: a putative homolog of drosophila corkscrew. *Proc Natl Acad Sci U S A*, 89(23):11239–43.

Rangarajan, A., Hong, S. J., Gifford, A., and Weinberg, R. A. 2004. Species- and cell type-specific requirements for cellular transformation. *Cancer Cell*, 6(2):171–83.

Rauen, K. A. 2013. The rasopathies. *Annu Rev Genomics Hum Genet*, 14:355–69.

Rauen, K. A., Banerjee, A., Bishop, W. R., Lauchle, J. O., McCormick, F., McMahon, M., Melese, T., Munster, P. N., Nadaf, S., Packer, R. J., Sebolt-Leopold, J., and Viskochil, D. H. 2011. Costello and cardio-facio-cutaneous syndromes: Moving toward clinical trials in rasopathies. *Am J Med Genet C Semin Med Genet*, 157C(2):136–46.

Ren, L., Chen, X., Luechapanichkul, R., Selner, N. G., Meyer, T. M., Wavreille, A. S., Chan, R., Iorio, C., Zhou, X., Neel, B. G., and Pei, D. 2011. Substrate specificity of protein tyrosine phosphatases 1b, rptpalpha, shp-1, and shp-2. *Biochemistry*, 50(12): 2339–56.

Reynolds, J. F., Neri, G., Herrmann, J. P., Blumberg, B., Coldwell, J. G., Miles, P. V., and Opitz, J. M. 1986. New multiple congenital anomalies/mental retardation syndrome with cardio-facio-cutaneous involvement–the cfc syndrome. *Am J Med Genet*, 25(3): 413–27.

Roberts, P. J. and Der, C. J. 2007. Targeting the raf-mek-erk mitogen-activated protein kinase cascade for the treatment of cancer. *Oncogene*, 26(22):3291–310.

Rocchi, S., Tartare-Deckert, S., Murdaca, J., Holgado-Madruga, M., Wong, A. J., and Obberghen, E. V. 1998. Determination of gab1 (grb2-associated binder-1) interaction with insulin receptor-signaling molecules. *Mol Endocrinol*, 12(7):914–23.

Rodriguez, F. J., Lewis-Tuffin, L. J., and Anastasiadis, P. Z. 2012. E-cadherin's dark side: possible role in tumor progression. *Biochim Biophys Acta*, 1826(1):23–31.

Rodriguez-Viciana, P., Tetsu, O., Tidyman, W. E., Estep, A. L., Conger, B. A., Cruz, M. S., McCormick, F., and Rauen, K. A. 2006. Germline mutations in genes within the mapk pathway cause cardio-facio-cutaneous syndrome. *Science*, 311(5765):1287–90.

Sarkozy, A., Digilio, M. C., and Dallapiccola, B. 2008. Leopard syndrome. *Orphanet J Rare Dis*, 3:13.

Sarkozy, A., Carta, C., Moretti, S., Zampino, G., Digilio, M. C., Pantaleoni, F., Scioletti, A. P., Esposito, G., Cordeddu, V., Lepri, F., Petrangeli, V., Dentici, M. L., Mancini, G. M., Selicorni, A., Rossi, C., Mazzanti, L., Marino, B., Ferrero, G. B., Silengo, M. C., Memo, L., Stanzial, F., Faravelli, F., Stuppia, L., Puxeddu, E., Gelb, B. D., Dallapiccola, B., and Tartaglia, M. 2009. Germline braf mutations in noonan, leopard, and cardiofaciocutaneous syndromes: molecular diversity and associated phenotypic spectrum. *Hum Mutat*, 30(4):695–702.

Saxton, T. M., Henkemeyer, M., Gasca, S., Shen, R., Rossi, D. J., Shalaby, F., Feng, G. S., and Pawson, T. 1997. Abnormal mesoderm patterning in mouse embryos mutant for the sh2 tyrosine phosphatase shp-2. *EMBO J*, 16(9):2352–64.

Schaeper, U., Gehring, N. H., Fuchs, K. P., Sachs, M., Kempkes, B., and Birchmeier, W. 2000. Coupling of gab1 to c-met, grb2, and shp2 mediates biological responses. *J Cell Biol*, 149(7):1419–32.

Schaper, F., Gendo, C., Eck, M., Schmitz, J., Grimm, C., Anhuf, D., Kerr, I. M., and Heinrich, P. C. 1998. Activation of the protein tyrosine phosphatase shp2 via the interleukin-6 signal transducing receptor protein gp130 requires tyrosine kinase jak1 and limits acute-phase protein expression. *Biochem J*, 335 (Pt 3):557–65.

Schubbert, S., Shannon, K., and Bollag, G. 2007. Hyperactive ras in developmental disorders and cancer. *Nat Rev Cancer*, 7(4):295–308.

Seo, J. S., Ju, Y. S., Lee, W. C., Shin, J. Y., Lee, J. K., Bleazard, T., Lee, J., Jung, Y. J., Kim, J. O., Shin, J. Y., Yu, S. B., Kim, J., Lee, E. R., Kang, C. H., Park, I. K., Rhee, H., Lee, S. H., Kim, J. I., Kang, J. H., and Kim, Y. T. 2012. The transcriptional landscape and mutational profile of lung adenocarcinoma. *Genome Res*, 22(11):2109–19.

Shinohara, M., Mikhailov, A. V., Aguirre-Ghiso, J. A., and Rieder, C. L. 2006. Extracellular signal-regulated kinase 1/2 activity is not required in mammalian cells during late g2 for timely entry into or exit from mitosis. *Mol Biol Cell*, 17(12):5227–40.

Sithanandam, G., Kolch, W., Duh, F. M., and Rapp, U. R. 1990. Complete coding sequence of a human b-raf cdna and detection of b-raf protein kinase with isozyme specific antibodies. *Oncogene*, 5(12):1775–80.

Smyth, G. K. 2004. Linear models and empirical bayes methods for assessing differential expression in microarray experiments. *Stat Appl Genet Mol Biol*, 3:Article3.

Song, G., Ouyang, G., and Bao, S. 2005. The activation of akt/pkb signaling pathway and cell survival. *J Cell Mol Med*, 9(1):59–71.

Soule, H. D., Maloney, T. M., Wolman, S. R., W. D. Peterson, J., Brenz, R., McGrath, C. M., Russo, J., Pauley, R. J., Jones, R. F., and Brooks, S. C. 1990. Isolation and characterization of a spontaneously immortalized human breast epithelial cell line, mcf-10. *Cancer Res*, 50(18):6075–86.

Spurrier, B., Ramalingam, S., and Nishizuka, S. 2008. Reverse-phase protein lysate microarrays for cell signaling analysis. *Nat Protoc*, 3(11):1796–808.

Stahl, J. M., Sharma, A., Cheung, M., Zimmerman, M., Cheng, J. Q., Bosenberg, M. W., Kester, M., Sandirasegarane, L., and Robertson, G. P. 2004. Deregulated akt3 activity promotes development of malignant melanoma. *Cancer Res*, 64(19):7002–10.

Sykes, S. M., Lane, S. W., Bullinger, L., Kalaitzidis, D., Yusuf, R., Saez, B., Ferraro, F., Mercier, F., Singh, H., Brumme, K. M., Acharya, S. S., Scholl, C., Tothova, Z., Attar, E. C., Frohling, S., DePinho, R. A., Armstrong, S. A., Gilliland, D. G., and Scadden, D. T. 2011. Akt/foxo signaling enforces reversible differentiation blockade in myeloid leukemias. *Cell*, 146(5):697–708.

Tang, T. L., R. M. Freeman, J., O'Reilly, A. M., Neel, B. G., and Sokol, S. Y. 1995. The sh2-containing protein-tyrosine phosphatase sh-ptp2 is required upstream of map kinase for early xenopus development. *Cell*, 80(3):473–83.

Tartaglia, M. and Gelb, B. D. 2005. Germ-line and somatic ptpn11 mutations in human disease. *Eur J Med Genet*, 48(2):81–96.

Tartaglia, M., Mehler, E. L., Goldberg, R., Zampino, G., Brunner, H. G., Kremer, H., van der Burgt, I., Crosby, A. H., Ion, A., Jeffery, S., Kalidas, K., Patton, M. A., Kucherlapati, R. S., and Gelb, B. D. 2001. Mutations in ptpn11, encoding the protein tyrosine phosphatase shp-2, cause noonan syndrome. *Nat Genet*, 29(4):465–8.

Tartaglia, M., Kalidas, K., Shaw, A., Song, X., Musat, D. L., van der Burgt, I., Brunner, H. G., Bertola, D. R., Crosby, A., Ion, A., Kucherlapati, R. S., Jeffery, S., Patton, M. A., and Gelb, B. D. 2002. Ptpn11 mutations in noonan syndrome: molecular spectrum, genotype-phenotype correlation, and phenotypic heterogeneity. *Am J Hum Genet*, 70(6):1555–63.

Tartaglia, M., Cotter, P. D., Zampino, G., Gelb, B. D., and Rauen, K. A. 2003. Exclusion of ptpn11 mutations in costello syndrome: further evidence for distinct

genetic etiologies for noonan, cardio-facio-cutaneous and costello syndromes. *Clin Genet*, 63(5):423–6.

Tartaglia, M., Zampino, G., and Gelb, B. D. 2010. Noonan syndrome: clinical aspects and molecular pathogenesis. *Mol Syndromol*, 1(1):2–26.

Tchernitsa, O. I., Zuber, J., Sers, C., Brinckmann, R., Britsch, S. K., Adams, V., and Schafer, R. 1999. Gene expression profiling of fibroblasts resistant toward oncogene-mediated transformation reveals preferential transcription of negative growth regulators. *Oncogene*, 18(39):5448–54.

Teschendorf, C., K. H. Warrington, J., Siemann, D. W., and Muzyczka, N. 2002. Comparison of the ef-1 alpha and the cmv promoter for engineering stable tumor cell lines using recombinant adeno-associated virus. *Anticancer Res*, 22(6A):3325–30.

Tonks, N. K. 2006. Protein tyrosine phosphatases: from genes, to function, to disease. *Nat Rev Mol Cell Biol*, 7(11):833–46.

Tsutsumi, R., Takahashi, A., Azuma, T., Higashi, H., and Hatakeyama, M. 2006. Focal adhesion kinase is a substrate and downstream effector of shp-2 complexed with helicobacter pylori caga. *Mol Cell Biol*, 26(1):261–76.

Ugarte, N., Ladouce, R., Radjei, S., Gareil, M., Friguet, B., and Petropoulos, I. 2013. Proteome alteration in oxidative stress-sensitive methionine sulfoxide reductase-silenced hek293 cells. *Free Radic Biol Med*, 65:1023–36.

Urosevic, J., Sauzeau, V., Soto-Montenegro, M. L., Reig, S., Desco, M., Wright, E. M., Canamero, M., Mulero, F., Ortega, S., Bustelo, X. R., and Barbacid, M. 2011. Constitutive activation of b-raf in the mouse germ line provides a model for human cardio-facio-cutaneous syndrome. *Proc Natl Acad Sci U S A*, 108(12):5015–20.

van Den Berg, H. and Hennekam, R. C. 1999. Acute lymphoblastic leukaemia in a patient with cardiofaciocutaneous syndrome. *J Med Genet*, 36(10):799–800.

van Roy, F. 2014. Beyond e-cadherin: roles of other cadherin superfamily members in cancer. *Nat Rev Cancer*, 14(2):121–34.

Wan, P. T., Garnett, M. J., Roe, S. M., Lee, S., Niculescu-Duvaz, D., Good, V. M., Jones, C. M., Marshall, C. J., Springer, C. J., Barford, D., and Marais, R. 2004. Mechanism of activation of the raf-erk signaling pathway by oncogenic mutations of b-raf. *Cell*, 116(6):855–67.

Wang, D., Stockard, C. R., Harkins, L., Lott, P., Salih, C., Yuan, K., Buchsbaum, D., Hashim, A., Zayzafoon, M., Hardy, R. W., Hameed, O., Grizzle, W., and Siegal, G. P. 2008. Immunohistochemistry in the evaluation of neovascularization in tumor xenografts. *Biotech Histochem*, 83(3):179–89.

Wang, S., Yu, W. M., Zhang, W., McCrae, K. R., Neel, B. G., and Qu, C. K. 2009. Noonan syndrome/leukemia-associated gain-of-function mutations in shp-2 phosphatase (ptpn11) enhance cell migration and angiogenesis. *J Biol Chem*, 284(2):913–20.

Wellbrock, C. and Marais, R. 2005. Elevated expression of mitf counteracts b-raf-stimulated melanocyte and melanoma cell proliferation. *J Cell Biol*, 170(5):703–8.

Willecke, R., Heuberger, J., Grossmann, K., Michos, O., Schmidt-Ott, K., Walentin, K., Costantini, F., and Birchmeier, W. 2011. The tyrosine phosphatase shp2 acts downstream of gdnf/ret in branching morphogenesis of the developing mouse kidney. *Dev Biol*, 360(2):310–7.

Wilson, R., Vogelsang, E., and Leptin, M. 2005. Fgf signalling and the mechanism of mesoderm spreading in drosophila embryos. *Development*, 132(3):491–501.

Wojnowski, L., Zimmer, A. M., Beck, T. W., Hahn, H., Bernal, R., Rapp, U. R., and Zimmer, A. 1997. Endothelial apoptosis in braf-deficient mice. *Nat Genet*, 16(3): 293–7.

Worsham, M. J., Pals, G., Schouten, J. P., Miller, F., Tiwari, N., van Spaendonk, R., and Wolman, S. R. 2006. High-resolution mapping of molecular events associated with immortalization, transformation, and progression to breast cancer in the mcf10 model. *Breast Cancer Res Treat*, 96(2):177–86.

Yamada, M., Suzuki, K., Mizutani, M., Asada, A., Matozaki, T., Ikeuchi, T., Koizumi, S., and Hatanaka, H. 2001. Analysis of tyrosine phosphorylation-dependent protein-protein interactions in trkb-mediated intracellular signaling using modified yeast two-hybrid system. *J Biochem*, 130(1):157–65.

Yu, M., Lin, G., Arshadi, N., Kalatskaya, I., Xue, B., Haider, S., Nguyen, F., Boutros, P. C., Elson, A., Muthuswamy, L. B., Tonks, N. K., and Muthuswamy, S. K. 2012. Expression profiling during mammary epithelial cell three-dimensional morphogenesis identifies ptpro as a novel regulator of morphogenesis and erbb2-mediated transformation. *Mol Cell Biol*, 32(19):3913–24.

Yu, W. M., Hawley, T. S., Hawley, R. G., and Qu, C. K. 2003. Catalytic-dependent and -independent roles of shp-2 tyrosine phosphatase in interleukin-3 signaling. *Oncogene*, 22(38):5995–6004.

Yu, Z. H., Zhang, R. Y., Walls, C. D., Chen, L., Zhang, S., Wu, L., Liu, S., and Zhang, Z. Y. 2014. Molecular basis of gain-of-function leopard syndrome-associated shp2 mutations. *Biochemistry*, 53(25):4136–51.

Zhang, E. E., Chapeau, E., Hagihara, K., and Feng, G. S. 2004. Neuronal shp2 tyrosine phosphatase controls energy balance and metabolism. *Proc Natl Acad Sci U S A*, 101 (45):16064–9.

Zhang, H. H., Lipovsky, A. I., Dibble, C. C., Sahin, M., and Manning, B. D. 2006. S6k1 regulates gsk3 under conditions of mtor-dependent feedback inhibition of akt. *Mol Cell*, 24(2):185–97.

Zheng, L., Ren, J. Q., Li, H., Kong, Z. L., and Zhu, H. G. 2004. Downregulation of wild-type p53 protein by her-2/neu mediated pi3k pathway activation in human breast cancer cells: its effect on cell proliferation and implication for therapy. *Cell Res*, 14(6): 497–506.

Zimonjic, D., Brooks, M. W., Popescu, N., Weinberg, R. A., and Hahn, W. C. 2001. Derivation of human tumor cells in vitro without widespread genomic instability. *Cancer Res*, 61(24):8838–44.

Zito, C. I., Qin, H., Blenis, J., and Bennett, A. M. 2007. Shp-2 regulates cell growth by controlling the mtor/s6 kinase 1 pathway. *J Biol Chem*, 282(10):6946–53.

Zocchi, M. R., Ferrero, E., Leone, B. E., Rovere, P., Bianchi, E., Toninelli, E., and Pardi, R. 1996. Cd31/pecam-1-driven chemokine-independent transmigration of human t lymphocytes. *Eur J Immunol*, 26(4):759–67.

ABBREVIATIONS

ALL	Acute lymphoblastic leukemia
AML	Acute Myeloid Leukemia
A	Adenine
A - Ala	Alanine
ATCC	American Type Culture Collection
APS	ammonium persulfate
Amp	Ampicillin
aq. dest	aqua destillata
R - Arg	Arginine
D - Asp	Aspartic acid
bp	base pair
BCA	bicinchoninic acid
BP	biological process
BSA	bovine serum albumin
CIP	calf intestinal alkaline phosphatase
CFCS	Cardio-Facial-Cutaneous Syndrome
COSMIC	Catalogue of Somatic Mutations in Cancer
CC	cellular component
°C	Celsius grade
Cm	Chloramphenicol
CMML	chronic myelomonocytic leukemia
co-IP	co-immunoprecipitation
cDNA	complementary DNA
cDNA	copy DNA
CMV	cytomegalovirus
C	Cytosine
CagA	Cytotoxin Associated gene A
dNTP	Deoxynucleoside triphosphate
DNA	Deoxyribonucleic acid
DNA	deoxyribonucleic acid
DMSO	Dimethyl sulfoxide
D10	DMEM with FCS
dox	doxycycline
DMEM	Dulbecco's modified Eagles Medium

EF1a	elongation factor 1-alpha promoter
ECL	enhanced chemoluminescence
eGFP	enhanced green fluorescent protein
eYFP	enhanced yellow fluorescent protein
EDTA	Ethylenediaminetetraacetic acid
ERK	Extracellular signal-regulated kinase
FCS	Fetal calf serum
FAK	focal adhesion kinase
GeneID	gene identifier
GOI	gene of interest
GO	Gene Ontology
G418	Geniticin
E - Glu	Glutamic acid
Q - Gln	Glutamine
GAPDH	Glyceraldehyde 3-phosphate dehydrogenase
G - Gly	Glycine
g	gram
GAB1	GRB2-associated binding protein 1
G	Guanine
RasGEF	guanine nucleotide exchange factor
GTP	Guanosine triphosphate
H-Ras	Harvey rat sarcoma viral oncogene homolog
HRP	Horseradish peroxidase
h	hour
hFGF4	human fibrobroblast growth factor 4
ID	Identifier
IHC	Immunohistochemistry
ILMN ID	illumina identifier
IRES	internal ribosome entry site
IFS	invactivated fetal calf serum
I - Ile	Isoleucine
JMML	Juvenile Myelomonocytic Leukemia
kanr	kanamycin
LS	LEOPARD Syndrome
L - Leu	Leucine
LB	Luria Broth
K - Lys	Lysine
Tm	melting temperature
mRNA	messenger RNA
M	Methionine
μl	Microliter
ml	Milliliter

MEM-Alpha	minimal essential medium (MEM), Alpha modification
min	Minute
MAPK	Mitogen-activated protein kinase
MEK	Mitogen-activated protein kinase kinase
MF	molecular function
MCS	multiple cloning site
LEOPARD	Multiple lentigines, Electrocardiographic conduction abnormalities, Ocular hypertelorism, Pulmonic stenosis, Abnormal genitalia, Retardation of growth, and sensorineural Deafness
TEMED	N,N,N',N-Tetramethylethylenediamine
NS	Noonan Syndrome
norm.	normalized
OMIM	Online Mendelian Inheritance in Man
ORF	open reading frame
OD	Optical density
PFA	paraformaldehyde
F - Phe	Phenylalanine
PBS	Phosphate buffered saline
PI3K	Phosphatidylinositol-4,5-Bisphosphate 3-Kinase
PTP	Phosphotyrosine domain
PEI	Polyethylenimine
PCR	Polymerase chain reaction
PTM	Post-translational modification
SHP2	Protein encoded in gene PTPN11
PTPN11	protein tyrosine phosphatase, non-receptor type 11
Puro	puromycin
RTK	Receptor tyrosine kinase
rel.	relative
RPPA	reverse phase protein array
RNA	ribonucleic acid
RT	Room temperature
S - Ser	Serine
s.c.	subcutaneously
SDS	sodium dodecyl sulfate
SDS-PAGE	SDS-Polyacrylamide Gel Electrophoresis
sec	second
SH2	src-homology 2 region domain
STRING	Search Tool for the Retrieval of Interacting Genes/Proteins
SUMO	Small ubiquitin-like modifier
SVM	Support Vector Machine
SV40-ER	SV40-early region
TAP	Tandem Affinity Purification

T - Thr	Threonine
T	Thymine
TBS	Tris buffered Saline
TBST	Tris buffered Saline with Tween
TAE	Tris-acetate-EDTA buffer
TE	Tris-EDTA
Tyr	Tyrosine
EGFR	Tyrosine kinase epidermal growth factor receptor
UniHI	Unified Human Interactome
Akt	V-Akt Murine Thymoma Viral Oncogene
BRAF	v-raf murine sarcoma viral oncogene homolog B
V - Val	Valine
WB	Western blot
wt	wild-type
WPRE	woodchuck postranscriptional response element
XTT	Sodium 2,3-bis(2-methoxy-4-nitro-5-sulfophenyl)-5-[(phenyl-amino)carbonyl]-2H tetrazolium inner salt
Y2H	yeast-two-hybrid

SELBSTSTÄNDIGKEITSERKLÄRUNG

Hiermit erkläre ich, dass ich die vorliegende Arbeit selbständig und ohne unerlaubte Hilfe angefertigt und nur die angegebene Literatur und Hilfsmittel verwendet habe. Alle Stellen, die wörtlich oder sinngemäß aus Quellen entnommen wurden, sind mit der Quellenangabe versehen. Des Weiteren versichere ich, dass diese Dissertation nie Gegenstand eines früheren Promotionsverfahrens gewesen ist oder als ungenügend beurteilt wurde. Die Promotionsordnung der Lebenswissenschaftlichen Fakultät der Humboldt-Universität zu Berlin habe ich gelesen und akzeptiert.

Berlin, den 19.12.2014 Paula Medina-Pérez